10
Inlets, Nozzles, and Combustion Systems

10.1 Introduction to Inlets and Nozzles

The inlet and exhaust nozzle are the two engine components that directly interface with the internal airflow and the flow about the aircraft. In fact, integration of the engine and the airframe is one of the most complex problems and has a major impact on the performance of the aircraft system. Many technical books, reports, articles, etc., are available in open literature (public domain) that concentrate on only small parts of this major technical challenge. This chapter identifies the major design considerations of inlets and exhaust nozzles and presents basic analysis tools for their preliminary sizing and design.

The results of the engine performance analysis provide a wealth of information about the required performance of both the inlet and the exhaust nozzle. For example, the required full-throttle, corrected engine airflow vs both Mach number and altitude can be obtained from the engine performance analysis program PERF (see Figs. 8.21, 8.31, 8.50, and 8.74b). Likewise, the engine airflow at specific partial-throttle conditions (corresponding to cruise, loiter, etc.) and the assumed inlet total pressure ratio vs Mach number can be obtained. The design information defines the requirements of the inlet in terms of total pressure ratio and mass flow rate, and preliminary design of the inlet starts with this information.

The simplest and most powerful design tool available for preliminary design of these components is one-dimensional compressible flow. Both the inlet and the exhaust nozzle can be modeled as simple one-dimensional adiabatic flows or a series of these flows. The following sections of this chapter present the basic principles of operation for each component, the major design considerations, and the basic design tools. Starting at the front of the engine, we consider the inlet first.

10.2 Inlets

The inlet interchanges the organized kinetic and random thermal energies of the gas in an essentially adiabatic process. The perfect (no-loss) inlet would thus correspond to an isentropic process. The primary purpose of the inlet is to bring the air required by the engine from freestream conditions to the conditions required at the entrance of the fan or compressor with minimum total pressure loss. The fan or compressor works best with a uniform flow of air at a Mach

number of about 0.5. Also, because the installed engine performance depends on the inlet's installation losses (additive drag, forebody or cowl drag, bypass air, boundary-layer bleed air, etc.), the design of the inlet should minimize these losses. The performance of an inlet is related to the following characteristics: high total pressure ratio π_d, controllable flow matching of requirements, good uniformity of flow, low installation drag, good starting and stability, low signatures (acoustic, radar, etc.), and minimum weight and cost while meeting life and reliability goals. An inlet's overall performance must be determined by simultaneously evaluating all of these characteristics because improvement in one is often achieved at the expense of another.

The design and operation of subsonic and supersonic inlets differ considerably due to the characteristics of the flow. For the subsonic inlets, near-isentropic internal diffusion can be easily achieved, and the inlet flow rate adjusts to the demand. The internal aerodynamic performance of a supersonic inlet is a major design problem, because achieving efficient and stable supersonic diffusion over a wide range of Mach numbers is very difficult. In addition, the supersonic inlet must be able to capture its required mass flow rate, which may require variable geometry to minimize inlet loss and drag and provide stable operation. Because of these differences, in the following sections we consider the subsonic and supersonic inlets separately, beginning with the subsonic inlet.

10.3 Subsonic Inlets

Most subsonic aircraft have their engines placed in nacelles; thus, in this section we do not deal with the inlet alone but include the nacelle at subsonic Mach numbers. The cross section of a typical subsonic inlet and its geometric parameters are shown in Fig. 10.1. The inlet area A_1 is based on the flow cross section at the inlet highlight. Because the subsonic inlet can draw in airflow whose freestream area A_0 is larger than the inlet area A_1, variable inlet geometry

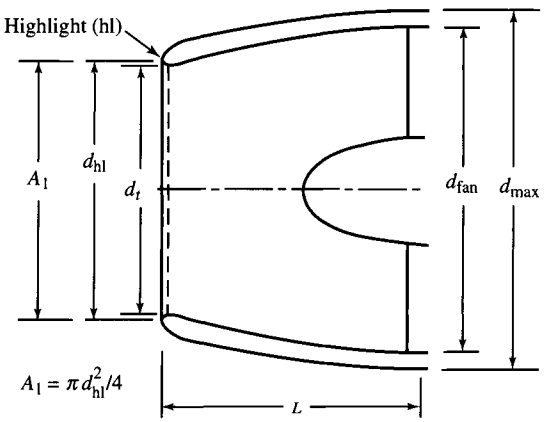

Fig. 10.1 Subsonic inlet nomenclature.

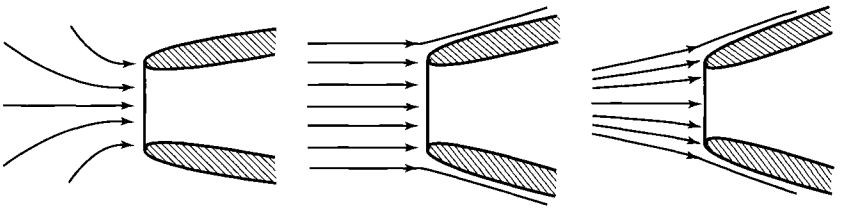

a) Static operation (or insufficient air for engine)

b) Low-speed operation (correct engine air)

c) High-speed operation (more air than the engine needs)

Fig. 10.2 Typical streamline patterns for subsonic inlet (Ref. 55).

is not required (except sometimes blow-in doors or auxiliary inlets are used to reduce installation drag during takeoff). The material in this section on subsonic inlets is based on a fixed-geometry inlet.

The operating conditions of an inlet depend on the flight velocity and mass flow demanded by the engine. Figure 10.2 shows the streamline pattern for three typical subsonic conditions. Figure 10.2a shows acceleration of the fluid external to the inlet that will occur when the inlet operates at a velocity lower than the design value or at a mass flow higher than the design value. Figure 10.2c shows deceleration of the fluid external to the inlet that will occur at a velocity higher than design or a mass flow lower than design.

A list of the major design variables for the inlet and nacelle includes the following:

1) Inlet total pressure ratio and drag at cruise
2) Engine location on wing or fuselage (avoidance of foreign-object damage, inlet flow upwash and downwash, exhaust gas reingestion, ground clearance)
3) Aircraft attitude envelope (angle of attack, yaw angle, cross-wind takeoff)
4) Inlet total pressure ratio and distortion levels required for engine operation
5) Engine-out windmilling airflow and drag (nacelle and engine)
6) Integration of diffuser and fan flow path contour
7) Integration of external nacelle contour with thrust reverser and accessories
8) Flowfield interaction between nacelle, pylon, and wing
9) Noise suppression requirements

Basic design tools for many of these items will be identified in this section. The reader is encouraged to research open literature (public domain) for a more in-depth analysis of any single item. Special attention is drawn to Refs. 54 and 55, which are textbooks on the aerodynamics of inlets.

10.3.1 Inlet Total Pressure Ratio π_d

In the cycle analysis used in the earlier chapters, the inlet total pressure ratio π_d was assumed to be constant for subsonic inlets and equal to $\pi_{d\max}$ (the total pressure ratio due to friction). Because of the complexity of the flow, we do not present a method for calculating the inlet total pressure ratio. However,

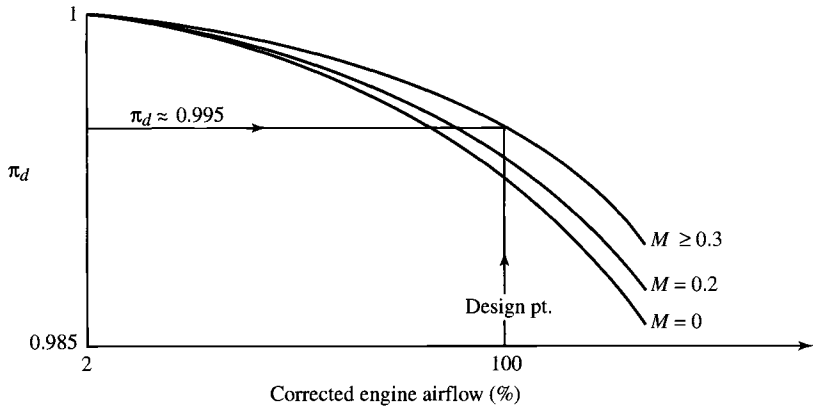

Fig. 10.3 Typical subsonic inlet total pressure ratio (after Younghans, Ref. 57).

Fig. 10.3 presents attainable π_d and its variation with flight Mach number and engine mass flow. The impact of the varying π_d on engine performance can be estimated by using this figure in concert with the performance analysis program and mission profile.

10.3.2 Inlet Sizing—Throat Diameter d_t

The diameter at the throat of the subsonic inlet is sized such that the Mach number at this location (based on one-dimensional flow) does not exceed 0.8. This will provide some margin for growth or error because the one-dimensional Mach number at the throat corresponding to actual inlet choke is about 0.9. The maximum corrected engine mass flow that the throat must pass will then correspond to this limiting Mach number, and the diameter is easily calculated by using

$$d_t = \sqrt{\frac{4}{\pi} A_{\text{th max}}} = \sqrt{\frac{4}{\pi}\left(\frac{\dot{m}_0\sqrt{T_{t0}}}{P_{t0}}\right)_{\max} \frac{1}{\text{MFP@}M = 0.8}}$$

which can be expressed in terms of the corrected mass flow as

$$d_t = \sqrt{\frac{4}{\pi}\frac{\sqrt{518.7}}{2116}\frac{\dot{m}_{c0\,\max}}{MFP@M = 0.8}}$$

and reduces to

$$d_t = 0.1636\sqrt{\dot{m}_{c0\,\max}} \qquad \text{or} \qquad d_t = 1.105\sqrt{A^*_{0\max}} \tag{10.1}$$

where $\dot{m}_{c0\,\max}$ has units of pound-mass per second, d_t has units of feet, and $A^*_{0\,\max}$ has units of square feet. Figure 10.4 is a representative output from

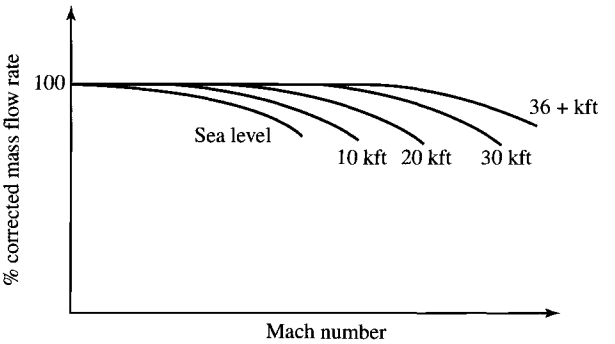

Fig. 10.4 Typical subsonic engine airflow requirements.

the engine performance computer program PERF of the corrected mass flow for a high-bypass-ratio turbofan engine. A figure like this can be used for selecting the point of maximum corrected mass flow that determines the throat diameter d_t.

10.3.3 Inlet Flow Distortion

Inlets operated with high angles of flow incidence are susceptible to flow separation from the inside contour of the inlet. This flow separation causes large regions of low total pressure, as shown in Fig. 10.5. The magnitude of

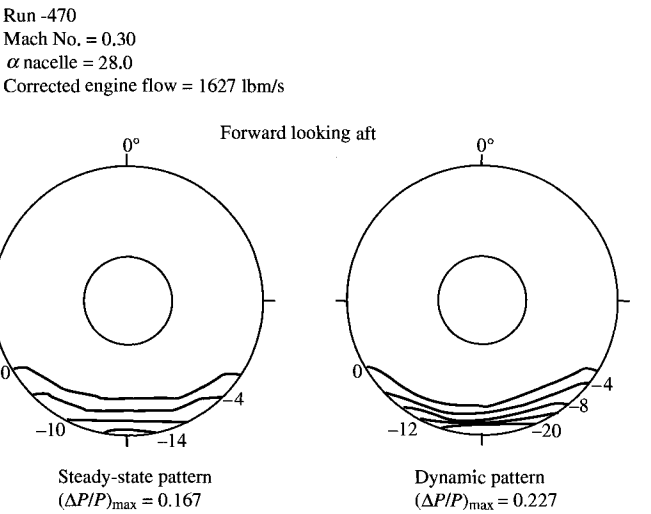

Fig. 10.5 Typical steady-state and dynamic total pressure distortion patterns (from Younghans, Ref. 56).

this distortion from the desired uniform flow is measured by the term called *inlet distortion* and is calculated by

$$\text{Inlet distortion} = \frac{P_{t\,\max} - P_{t\,\min}}{P_{t\,\text{av}}} \tag{10.2}$$

Both the instantaneous (dynamic) and time-averaged (steady-state) distortion levels are used to measure the quality of an inlet's flow. When Eq. (10.2) is used for calculation of the dynamic inlet distortion, the average total pressure in the denominator is the spatial average at an instant in time, and the maximum and minimum total pressures are for that same instant in time. Determination of the steady-state inlet distortion requires time-averaging of the total pressures in the inlet. The average total pressure $P_{t\,\text{av}}$ of Eq. (10.2) is the spatial average of the time-averaged total pressures.

The magnitude of the inlet distortion is a function of the inlet's geometry, mass flow rate, flight Mach number, and flow incidence angle. The effect of high distortion is to shift the fan or compressor surge line to values of higher mass flow rate, as shown in Fig. 10.6. This shift in surge line may result in compressor surge.

10.3.4 Inlet Drag

In Chapter 4, we looked at the additive drag that occurs when the area of the freestream air A_0 is different from the area of the entrance to the inlet A_1. Figure 4.5 shows a subsonic inlet at various flight Mach numbers and the use of "blow-in" doors at low Mach numbers to increase the inlet entrance area and thus reduce the additive drag. These blow-in doors were used in the turbofan-powered B-707 and in the early model of the B-747. Boeing deleted the use of

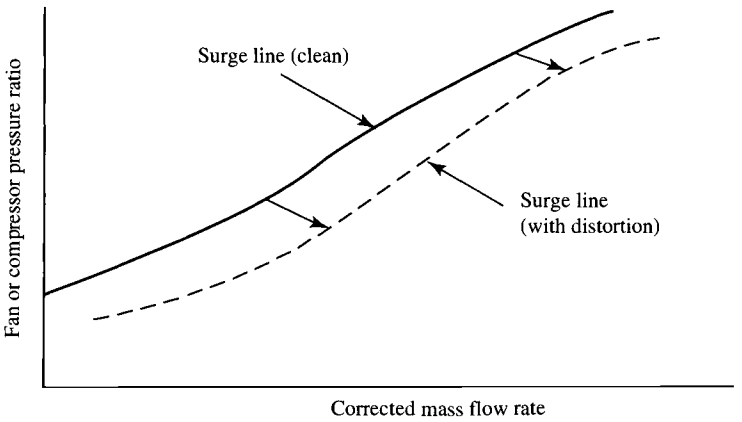

Fig. 10.6 Effect of inlet distortion on the fan or compressor.

blow-in doors in later models of the B-747 because of the nonuniform flow they created into the fan during takeoff and the resulting unacceptable fan noise. Elimination of blow-in doors required an increase in the entrance area, a more rounded lip, and a somewhat higher additive drag at cruise conditions. Most subsonic inlets operate as shown in Fig. 10.2c at cruise conditions.

At an engine inlet, flow separation can occur on the external surface of the nacelle due to local high velocities and subsequent deceleration. Flow separation can also occur on the internal surface of the inlet due to the flow deceleration, which causes an adverse pressure gradient (static pressure increase in the direction of flow). We will discuss the flow inside the inlet subsequently.

The size of the nacelle forebody [d_{h1}/d_{max} and L/d_{max} (see Fig. 10.1)] is a design compromise between the requirement of low cruise drag and avoiding catastrophes when one or more engines are out. The nacelle forebody size that gives minimum drag at cruise may not give good engine-out drag. In Chapter 4, the additive drag given by Eq. (4.8) was used as a conservative estimate of the inlet drag for engine sizing. A portion of the additive drag can be recovered along the forebody portion of the engine nacelle if the flow does not separate. This is indicated by the suction pressures near the lip of the nacelle in Fig. 10.7. The resulting pressure force on the outside of the nacelle forebody is called the *forebody drag*. The sum of the additive drag and the forebody drag is called the *inlet drag*.

Because flow around a curved surface accelerates the flow, then (at high subsonic Mach numbers) the local velocity can become supersonic adjacent to a nacelle. A shock then occurs, and a rise in static pressure across the shock reduces the negative pressure, thereby reducing the thrust component. This phenomenon is the same as that for an airfoil on which the local sonic velocity appears at the critical flight Mach number. At higher subsonic speeds, therefore, the curve of the inlet must be reduced in order to reduce the drag forces. The result is that for high subsonic Mach numbers, the inlet lip becomes very thin with little or no external curvature.

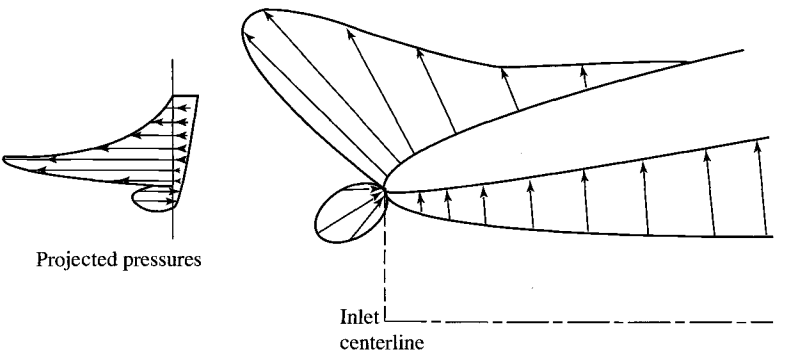

Fig. 10.7 Pressure distribution around a subsonic inlet lip (Ref. 57).

10.3.5 Nacelle and Interference Drag

The minimum drag for a nacelle does not necessarily occur when the inlet is designed for minimum inlet drag. The influences of the afterbody drag, interference drag, and aircraft trim drag need to be included in the integration and design of an engine nacelle. The inlet and afterbody drag of a typical nacelle is shown in Fig. 10.8 as a function of forebody diameter d_{h1}/d_{max} and flight Mach number. Note that the design value of d_{h1}/d_{max} corresponding to minimum inlet drag does not correspond to minimum inlet-plus-afterbody drag. Also note that the design value of d_{h1}/d_{max} corresponding to minimum inlet-plus-afterbody drag changes with flight Mach number. Thus the selection of d_{h1}/d_{max} for an inlet will depend on the design flight Mach number and may require the compromise of an individual component design goal to achieve the best overall system performance.

The engine location on the wing that provides the best integration of engine and airframe depends on the nacelle design, wing design, and resulting interference drag. Considerable analytical and experimental work is needed in the design of each installation. The resulting difference in best engine location on three aircraft is shown in Fig. 10.9.

10.3.6 Diffuser

The flow within the inlet is required to undergo diffusion in a divergent duct. This reduction in flow velocity creates an increase in static pressure that interacts with the boundary layer. If the pressure rise due to diffusion occurs more rapidly than turbulent mixing can reenergize the boundary layer, the boundary layer will

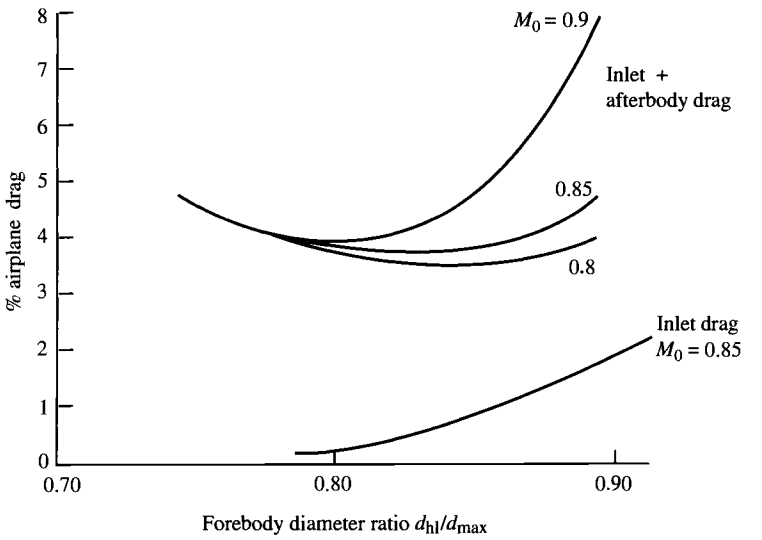

Fig. 10.8 Typical inlet and afterbody drag (from Younghans, Ref. 56).

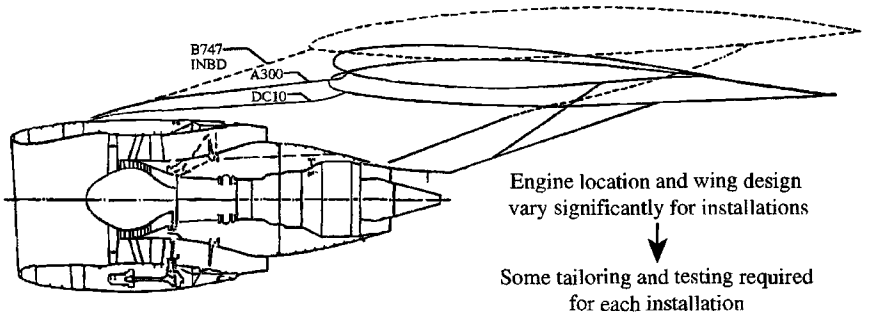

Fig. 10.9 The CF6-50 installation on three aircraft. (Courtesy of GE Aircraft Engines.)

assume the configurations shown in Fig. 10.10. If the flow in an inlet separates, the total and static pressures are reduced from their corresponding nonseparated flow values.

The rate of area increase in a diffuser has a direct effect on the behavior of flow in the diffuser, as shown in Fig. 10.11. If the rate of area increase is greater than that needed to keep the boundary layer energized and attached, the flow may be characterized by unsteady zones of stall. The turbulent mixing is no longer able to overcome the pressure forces at all points in the flow, and local separation occurs at some points. The total pressure decreases markedly due to the irreversible mixing of a fairly large portion of low-velocity fluid with the main flow. If the diffuser walls diverge rapidly, the flow will separate completely and behave much as a jet, as shown in Fig. 10.11d.

The rate of area increase without stall for a diffuser depends on the characteristics of the flow at the entrance and on the length of the divergent section. Figure 10.12a shows the results for two-dimensional straight-walled diffusers as presented by Kline in Ref. 58. Kline's results are for incompressible flow, and they do not give a qualitatively valid indication of the sensitivity of any diffuser to rapid divergence of flow area.

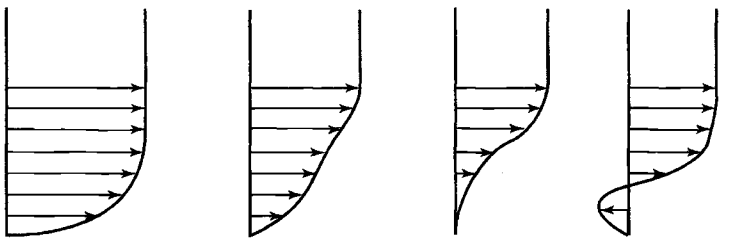

a) Turbulent **b) Intermediate** **c) Separation** **d) Reversed flow**

Fig. 10.10 Boundary layer with an adverse pressure gradient (Ref. 57).

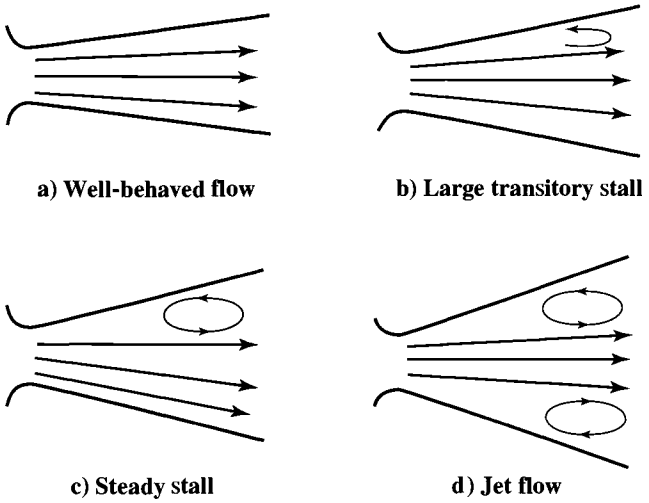

Fig. 10.11 Types of flow in straight-walled diffusers (Ref. 41).

For the design of an optimum diffuser, research has shown that the boundary-layer profile should maintain a constant shape, although the boundary-layer thickness will, of course, increase as the flow moves down the diffuser. The stipulation of a constant shape for the boundary-layer profile implies the assumption that mixing reenergizes the profile at the same rate as the static pressure depletes it.

In the presence of an adverse pressure gradient (static pressure increasing in the direction of flow), boundary layers tend to separate when the boundary layer is not reenergized rapidly enough by turbulent mixing. In Ref. 59, Taylor proposed the use of vortex generators as a mechanical mixing device to supplement the turbulent mixing. If vortices are generated by vortex generators in pairs, regions of inflow and outflow exist. These carry high-energy air into the boundary layer and low-energy air out. Figure 10.12b shows how vortex generators reenergize a boundary layer.

By using vortex generators together with a short, wide-angle diffuser, it may be possible to have a lower total pressure loss than with a long diffuser without vortex generators. Here, the reduced skin friction losses associated with flow

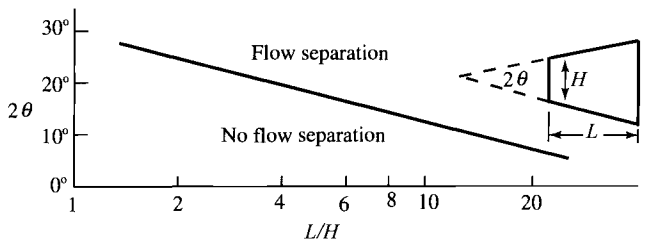

Fig. 10.12a Flow separation limits in two-dimensional straight-walled diffusers (Ref. 58).

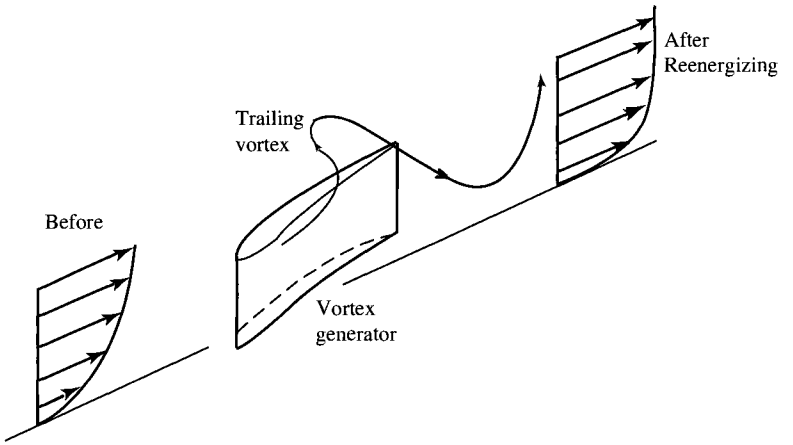

Fig. 10.12b Vortex generators reenergize a boundary layer.

separation are traded against vortex losses. The use of shorter diffusers may reduce weight and facilitate engine installation.

The rotating blades of an engine are a large source of an easily detected reflected radar signature. To reduce this signature, every effort is used to hide the engine face from direct (line-of-sight) view and thus reduce reflected radar. A serpentine-shaped diffuser with radar-absorbing material (RAM) can reduce the inlet's signature. Figure 10.13 shows some of the challenges facing designers—the energy transmission is at least a function of the shape of the duct (e.g., the number of reflections) and the wavelength-to-duct-width ratio. The F-117A Nighthawk stealth fighter uses a gridded inlet with 1.5-cm pitch between elements to keep out X-band and below radiation.[60]

10.4 Supersonic Inlets

The supersonic inlet is required to provide the proper quantity and uniformity of air to the engine over a wider range of flight conditions than the subsonic inlet is. In addition, the nature of supersonic flow makes this inlet more difficult to design and integrate into the airframe. In supersonic flight, the flow is decelerated by shock waves that can produce a total pressure loss much greater than, and in addition to, the boundary-layer losses. Indeed, at $M_0 = 3$, a simple pitot-type inlet preceded by a normal shock wave would have a total pressure recovery η_r of 0.32 due to the normal shock alone!

An engine overall compression ratio is the product of the engine's ram, diffuser, and compressor pressure ratios:

$$\text{Cycle compression ratio} \frac{P_{t3}}{P_0} = \pi_r \pi_d \pi_c \tag{10.3}$$

Because the product $\pi_r \pi_d$ is a major fraction of the cycle compression ratio at high supersonic Mach numbers, the engine thrust specific fuel consumption and

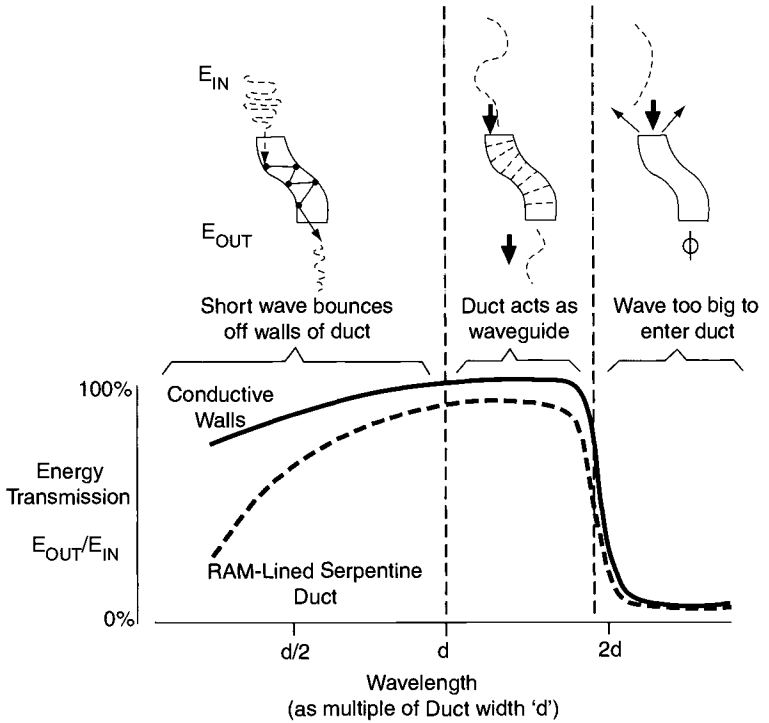

Fig. 10.13 Radar attenuation of engine inlet duct. (From Ref. 60. Copyright © 2001, McGraw-Hill Companies, Inc. Reproduced with permission.)

thrust per unit mass flow are very sensitive to the diffuser pressure ratio π_d. For supersonic cruise flight, therefore, the design of the inlet becomes of paramount importance. For this reason, we shall now examine the basic principles and operating characteristics of supersonic aircraft inlets (or diffusers).

The study of supersonic inlets is not new, and many excellent books and reports have been written for the benefit of students and practicing professionals (see Refs. 54–59 and 61–67). Special attention should be paid to Ref. 55, a textbook that covers the aerodynamics of inlets.

10.4.1 Basics of One-Dimensional Inlet Flow

First, we review some one-dimensional perfect gas flow ideas that are basic to understanding a supersonic diffuser operation.

10.4.1.1 Total and sonic state points and A/A^*. Consider the one-dimensional perfect gas flow of Fig. 10.14. The static state point of the gas at station 1 of the flow is designated as 1 in the T-s diagram of Fig. 10.14. Associated with static state point 1 at the same entropy are the total state point $t1$, where $M = 0$, and the sonic state point ^{*1}, where $M = 1$. The sonic and total state points can be attained by imagining a duct at station 1 decelerating the supersonic flow

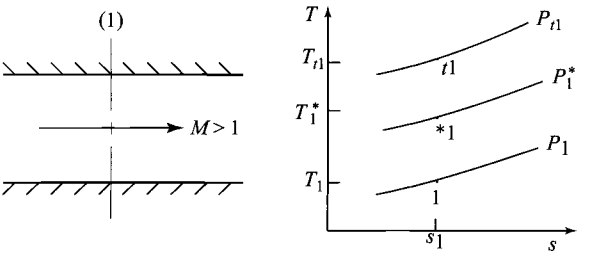

Fig. 10.14 States for supersonic flow.

isentropically to a sonic throat *1 followed by a subsonic deceleration to zero speed $t1$ in an infinitely large storage reservoir.

Treating station 1 as any general station in the flow with no subscripts, we can write the area ratio A/A^* as [Eq. (2.77)]

$$\frac{A}{A^*} = \frac{1}{M}\left[\frac{2}{\gamma+1}\left(1+\frac{\gamma-1}{2}M^2\right)\right]^{(\gamma+1)/[2(\gamma-1)]}$$

Since P and T in a given isentropic flow are also functions of the Mach number, this equation connects A to P, T, and other flow properties. In Fig. 10.15, A/A^*, P/P_t, and T/T_t are plotted vs the Mach number. Note that A/A^* varies from a minimum of 1 to 4.23 at $M = 3$. This large variation tends to complicate supersonic inlet design.

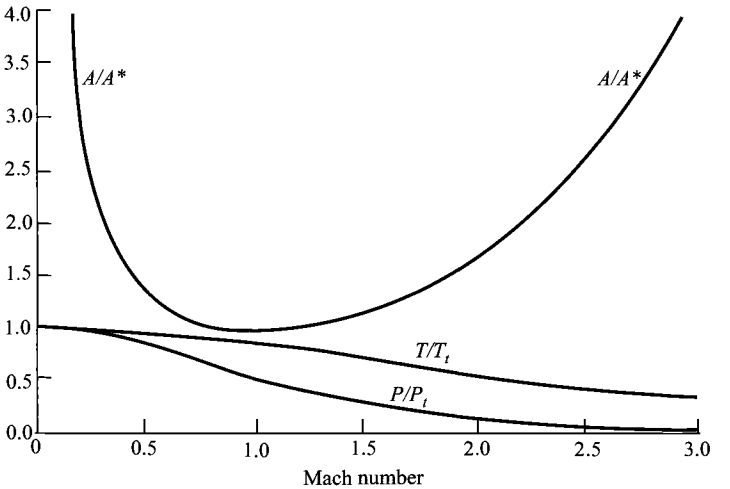

Fig. 10.15 Compressible flow functions vs Mach number.

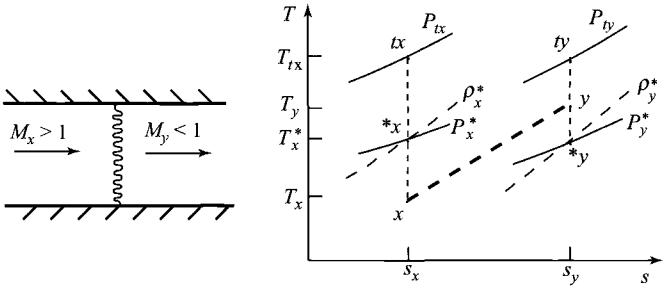

Fig. 10.16 Normal shock wave.

10.4.1.2 Normal shock wave. Consider the perfect gas flow through a normal shock wave depicted in Fig. 10.16, with subscripts x and y denoting shock upstream and downstream flow conditions, respectively. The static, sonic, and total state points of the gas entering and leaving the shock wave are shown in the T-s diagram of the figure with $s_y > s_x$ since the flow through a normal shock is irreversible and adiabatic at constant T_t. It follows that $T_x^* = T_y^*$, $P_{ty} < P_{tx}$, $V_x^* = V_y^*$, and $\rho_y^* < \rho_x^*$, as indicated in the T-s diagram.

Given the inlet conditions to a normal shock wave in a perfect gas, the exit conditions can be found since $P_y/P_x = f_1(M_x)$, $M_y = f_2(M_x)$, $P_{ty}/P_{tx} = f_3(M_x)$, etc. The total pressure ratio across a normal shock is of particular interest in supersonic diffuser studies and is plotted in Fig. 10.17 along with A/A^* from Fig. 10.15.

Suppose, now, that the flow of Fig. 10.16 passes through sonic throats of areas A_x^* and A_y^*, as in Fig. 10.18. What is the ratio of the area of the first throat to that of the second throat A_x^*/A_y^*? Conservation of mass and one-dimensional

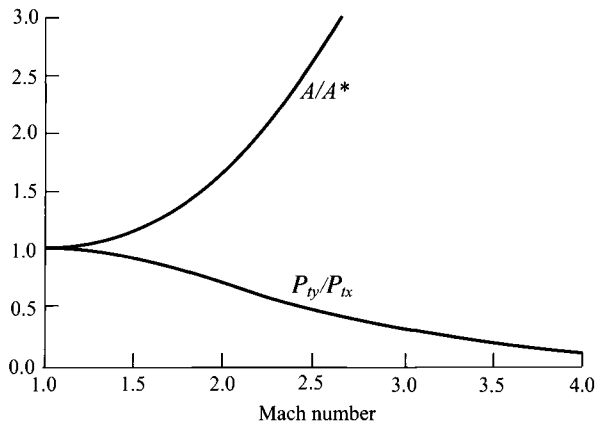

Fig. 10.17 A/A^* and P_{ty}/P_{tx} vs Mach number.

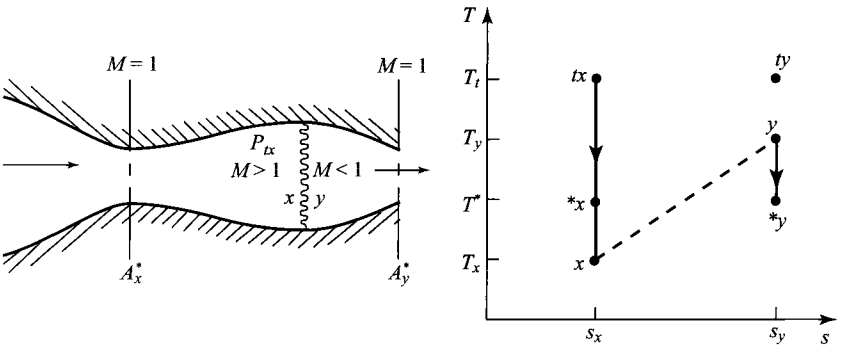

Fig. 10.18 A/A^* **and shock wave.**

flow give

$$(\rho VA)_x^* = (\rho VA)_y^*$$

Since in this equation $V_x^* = V_y^*$ and $\rho_x^* > \rho_y^*$, the second throat area must be larger than the first to compensate for the lower-density gas passing through it, and

$$\frac{A_x^*}{A_y^*} = \frac{\rho_y^*}{\rho_x^*}$$

With $T_x^* = T_y^*$, we can write

$$\frac{\rho_y^*}{\rho_x^*} = \frac{P_y^*}{P_x^*} = \frac{P_{ty}}{P_{tx}} \frac{(P^*/P_t)_y}{(P^*/P_t)_x} \quad \text{(the ratio equals 1)}$$

Therefore,

$$\frac{A_x^*}{A_y^*} = \frac{\rho_y^*}{\rho_x^*} = \frac{P_{ty}}{P_{tx}} \tag{10.4}$$

and the plot of P_{ty}/P_{tx} in Fig. 10.17 can also be interpreted as A_x^*/A_x^* or ρ_y^*/ρ_x^* vs Mach number.

Example 10.1

Let us illustrate the preceding ideas with an example involving a supersonic inlet. The stream tube of air captured by the ideal shock-free inlet in Fig. 10.19 has an area A_0 equal to the inlet capture area A_c. Since $A_0 = A_c$, no

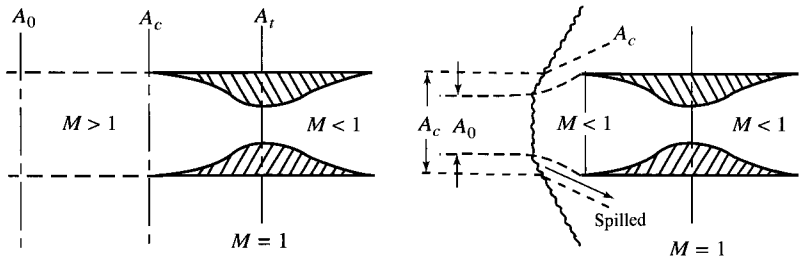

Fig. 10.19 Inlet spillage.

air is spilled by the inlet. The inlet on the right is preceded by a shock wave and capture air contained in a stream tube of area $A_0 < A_c$. The freestream airflow contained in the projected area A_c that does not enter the inlet is said to be spilled as shown. The fraction of air spilled is

$$\text{Fraction spilled} = \frac{(\rho V)_0 A_c - (\rho V)_0 A_0}{(\rho V)_0 A_c}$$

$$\text{Fraction spilled} = \frac{A_c - A_0}{A_c} = \frac{A_c/A_t - A_0/A_t}{A_c/A_t} \tag{10.5}$$

Consider a fixed-geometry inlet operating in a freestream flow with $M_0 = 2$ and with a normal shock, as in Fig. 10.19. If the inlet capture/throat area ratio is $A_c/A_t = 1.34$, determine the fraction of air spilled.

Solution: We have

$$\text{Fraction spilled} = \frac{A_c/A_t - A_0/A_t}{A_c/A_t} = \frac{1.34 - A_0/A_t}{1.34}$$

and so we must find A_0/A_t. Using y for the exit state of the normal shock, we have the flow state points and path line shown in the T-s diagram of Fig. 10.20. By using the sonic state points ^{*0} and $^*y$, we can find A_0/A_t thus. Since $A_t = A_y^*$,

$$\frac{A_0}{A_t} = \left(\frac{A}{A^*}\right)_0 \frac{A_0^*}{A_y^*}$$

From Eq. (10.4),

$$\frac{A_0^*}{A_y^*} = \frac{(\rho V)_y^*}{(\rho V)_0^*} = \frac{\rho_y^*}{\rho_0^*} = \frac{P_{ty}}{P_{t0}}$$

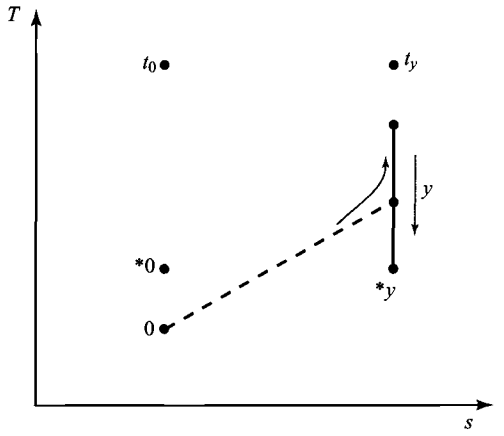

Fig. 10.20 Stages of inlet flow across shock.

where P_{ty}/P_{t0} is the total pressure ratio of a normal shock wave. Hence

$$\frac{A_0}{A_t} = \left[\left(\frac{A}{A^*}\right)\frac{P_{ty}}{P_{t0}}\right]_{M_0} \tag{10.6}$$

The right-hand side of this equation is the product of points lying on the two curves of Fig. 10.17 at a given M_0. Thus, at $M_0 = 2$, $A/A^* = 1.688$ and $P_{ty}/P_{t0} = 0.721$ (GASTAB), so that

$$\frac{A_0}{A_t} = (1.688)(0.721) = 1.218$$

and

$$\text{Fraction spilled} = \frac{1.34 - 1.218}{1.34} = 9.1\%$$

As M_0 increases above 2, the shock wave will move closer to the inlet and less air is spilled. Finally, when M_0 reaches the critical value M_{0c}, the shock is at the lip of the inlet and $A_0 = A_c$. (The shock is immediately swallowed by the inlet once it gets to the inlet lips because this is an unstable condition.)

10.4.2 Ideal One-Dimensional Internal Compression Inlet

One would think initially that a supersonic inlet could operate shock-free as a simple converging-diverging nozzle in reverse. Although this is feasible in principle, a starting problem arises that prevents the attainment of this condition in a constant-geometry inlet. To fix ideas in the arguments to follow, consider a

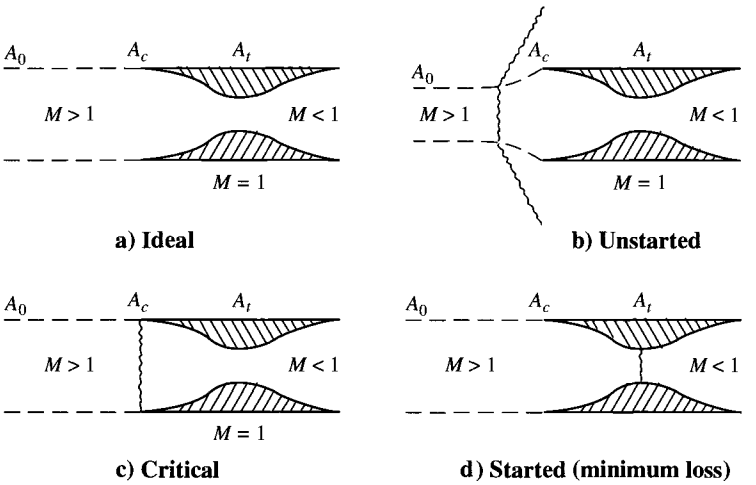

Fig. 10.21 Operation of ideal internal compression inlet.

supersonic inlet with a capture/throat area ratio of $A_0/A_t = 1.34$. Assuming no viscous boundary-layer losses, as we do throughout our treatment of inlets, this inlet could, in theory, operate free at $M_0 = 1.7$, corresponding to $A_0/A^* = A_c/A_t = 1.34$ with $A_0 = A_c$, as in Fig. 10.21a. This flow condition cannot be attained, however, by increasing M_0 from a lower value up to $M_0 = 1.7$ with a fixed-geometry inlet. This is the reason: $A_0/A^* < A_c/A_t$ if $M_0 < 1.7$ (Fig. 10.17), and in shock-free flow with $A_t = A_0^*$, it follows that $A_c > A_0$ so that the inlet captures more flow than the throat can pass. Consequently, air piles up in the inlet, causing, almost instantaneously, a shock to form ahead of the inlet, as in Fig. 10.21b). The excess airflow spills around the inlet in the subsonic flow behind the shock wave. To find the fraction of air spilled in the unstarted condition, we must find A_0/A_t in the expression

$$\text{Fraction spilled} = \frac{A_c - A_0}{A_c} = \frac{A_c/A_t - A_0/A_t}{A_c/A_t}$$

This can be done by using the identity

$$\frac{A_0}{A_t} = \frac{A_0}{A_0^*}\frac{A_0^*}{A_y^*}$$

Here, A_0^* is smaller than A_y^* because the mass flows through the two sonic throats *0 and *y (Fig. 10.22) are equal

$$(\rho A V)_0^* = (\rho A V)_y^*$$

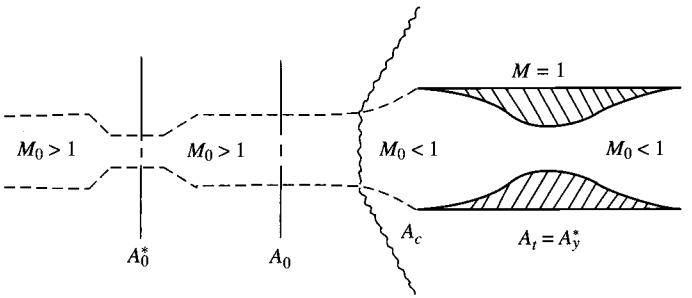

Fig. 10.22 Area relationships.

and $V_0^* = V_y^*$, but $\rho_x^* > \rho_y^*$. In fact, by Eq. (10.4),

$$\frac{A_0^*}{A_y^*} = \frac{\rho_y^*}{\rho_0^*} = \frac{P_{ty}}{P_{t0}}$$

hence

$$\frac{A_0}{A_t} = \left[\left(\frac{A}{A^*}\right)\frac{P_{ty}}{P_{t0}}\right]_{M_0} = f(M_0) \tag{10.7}$$

This ratio of actual captured stream-tube area to inlet throat area is plotted vs M_0 in Fig. 10.23. The curve of A_0/A_t in Fig. 10.23 is the product of the A/A^* and

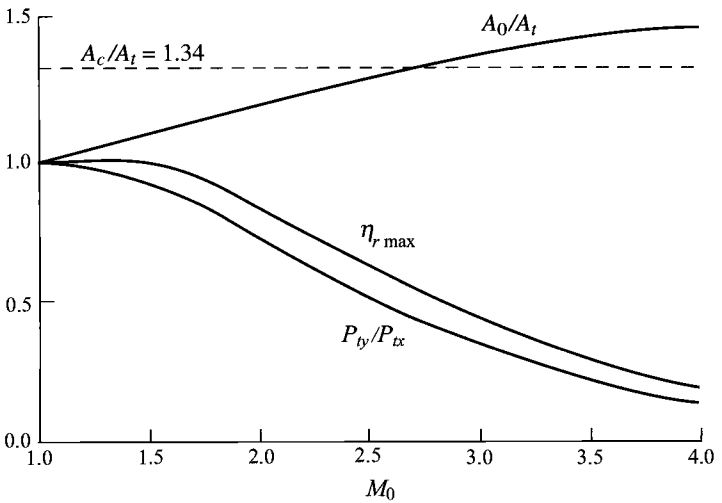

Fig. 10.23 Performance of ideal internal compression inlet.

P_{ty}/P_{t0} curves in accordance with Eq. (10.7). We show, in Fig. 10.23, a horizontal line representing $A_c/A_t = 1.34$. The vertical distance between this line and the A_0/A_t curve (to the left of their intersection) is proportional to the amount of air spilled by the inlet [Eq. (10.5)]. As M_0 is increased from $M_0 = 1$, this vertical distance decreases so that less and less air is spilled until at $M_{0c} = 2.66$, the shock is on the inlet lips. This is an unstable position, and the shock will move precipitously through the converging portion of the inlet if perturbed.

This can be explained as follows: The mass flow through the throat is proportional to ρ_y^*, which, in turn, is proportional to P_{ty}. If the shock moves into the inlet, M_x decreases so that P_{ty} and the throat mass flow increase. Because the flow at the lips continues to be at freestream conditions, the throat passes more air than is captured by the inlet. To make the throat mass flow equal to the flow captured, the density at the throat must decrease. This lower density is attained by the shock passing through the throat with supersonic flow at the throat as in the started condition of Fig. 10.16d. Once started, the inlet backpressure can be adjusted (e.g., by closing bypass doors downstream of the throat) to place the shock at the throat for minimum M_x and least total pressure loss.

The throat Mach number of a started inlet with area ratio $A_c/A_t = A_0/A_t$ is that corresponding to the value of $(A/A^*)_t$ obtained from

$$\left(\frac{A}{A^*}\right)_{M_t} = \left(\frac{A}{A^*}\right)_{M_0}\left(\frac{A_t}{A_0}\right)_{M_0} = \left(\frac{A}{A^*}\frac{1}{A_0/A_t}\right)_{M_0}$$

where A_0/A_t and A/A^* on the right-hand side of this equation are each a function of M_0 as given in Figs. 10.23 and 10.17, respectively. For example, at $M_0 = 2$

$$\left(\frac{A}{A^*}\right)_{M_t} = \left(\frac{A}{A^*}\frac{1}{A_0/A_t}\right)_{M_0} = \frac{1.688}{1.216} = 1.388$$

and

$$M_t = 1.75$$

The value of M_t corresponding to each flight Mach number can be found in this manner. Then, for each M_t, the corresponding normal shock total pressure loss can be determined to obtain the curve labeled $\eta_{r\max}$ in Fig. 10.23. For example, at $M_0 = 2$ and $M_t = 1.75$, the total pressure recovery of the inlet with a normal shock at the throat with $M_x = M_t = 1.75$ is $P_{ty}/P_{t0} = \eta_{r\max} = 0.835$.

Example 10.2

Design a fixed-area internal compression inlet that will start at $M_0 = 2.9$ for an aircraft that will cruise at $M_0 = 2.4$.

1) Determine the capture/throat area ratio A_c/A_t.

2) Determine both $\eta_{r\max}$ of the inlet after starting at $M_0 = 2.9$ and the shock located at the throat.

3) Determine $\eta_{r\max}$ of the inlet after starting at $M_0 = 2.4$ and the shock located at the throat.

4) Determine the Mach number at which the inlet will "unstart."

Solution:

1) Design an inlet to start at $M_0 = 2.9$. Thus $A_0 = A_c$ at $M_0 = 2.9$. Using Eq. (10.7), we have

$$\frac{A_c}{A_t} = \frac{A_0}{A_t}\left(\frac{A}{A^*}\frac{P_{ty}}{P_{tx}}\right)_{M_0} = 3.8498 \times 0.35773 = 1.377$$

Or, using Fig. 10.23, we read $A_c/A_t = 1.38$.

2) After starting, $A_c = A_0$; thus, we want to determine the area ratio A_t/A^* to get the Mach number at the throat and $\eta_{r\max}$ for $M_0 = 2.9$.

$$\frac{A_t}{A^*} = \frac{A_0/A^*}{A_c/A_t} = \frac{3.8498}{1.377} = 2.796$$

From GASTAB, $M_t = 2.56$. Then $P_{ty}/P_{tx} = \eta_{r\max} = 0.4754$. Or, using Fig. 10.23, we read $\eta_{r\max} = 0.48$.

3) For this inlet $A_c = A_0$,

$$\frac{A_t}{A^*} = \frac{A_0/A^*}{A_c/A_t} = \frac{2.4031}{1.377} = 1.745$$

From GASTAB, $M_t = 2.04$. Then $P_{ty}/P_{tx} = \eta_{r\max} = 0.702$.

4) The inlet will "unstart" when $M_t = 1$. We are looking for an M_0 whose A_0/A^* is equal to the inlet's A_c/A_t. For $A_0/A^* = 1.377$, $M_0 = 1.74$ from GASTAB or Fig. 10.17.

10.4.3 Inlet Types

As discussed in Chapter 4, supersonic inlets are classified into three basic types, characterized by the location of the supersonic compression wave system: internal compression, external compression, and mixed compression.

10.4.3.1 Internal compression inlet. The internal compression inlet shown in Fig. 10.24a achieves compression through a series of internal oblique shock waves followed by a terminal normal shock positioned downstream of the throat (its stable location). This type of inlet requires variable throat area to allow the inlet to swallow the normal shock (during starting). Fast reaction bypass doors are also required downstream of the throat to permit proper positioning of the normal shock under varying flight and engine conditions.

Figure 10.24a shows an internal compression inlet with an area contraction ratio A_1/A_t of 2.56 (corresponding to $M_1 = 2.5$ and $M_t = 1.2$) operating at design. With the terminal normal shock positioned downstream of the throat for stable operation, where the Mach number is 1.3, this inlet's ideal total

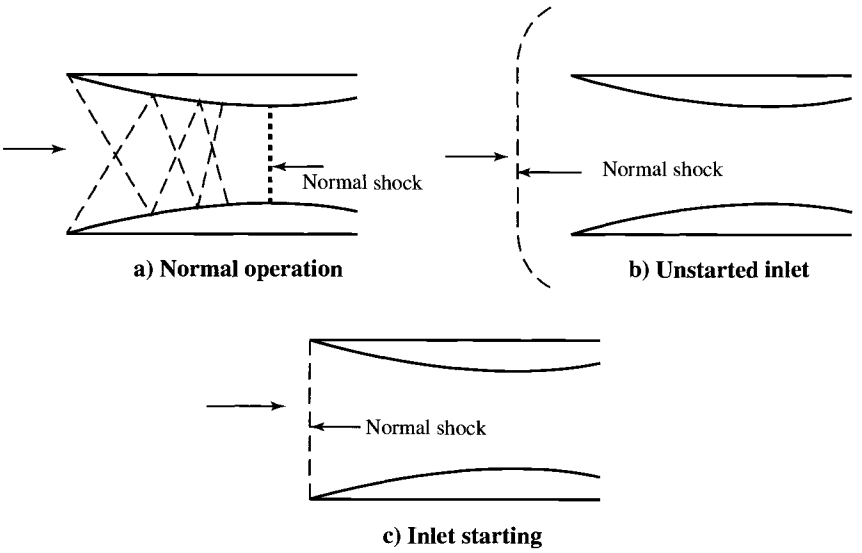

a) Normal operation

b) Unstarted inlet

c) Inlet starting

Fig. 10.24 Internal compression inlet.

pressure ratio (total pressure recovery η_r) corresponds to that across a normal shock at Mach 1.3, or $\eta_r = 0.9794$ when $\gamma = 1.4$. Reduction in the flight Mach number to 2.47 or movement of the terminal shock to the throat (which is an unstable location) will cause the total internal flow pattern to be completely disrupted (inlet unstarting), followed by formation of a normal shock ahead of the inlet and its associated low total pressure ratio (about 0.52), reduced mass flow through the inlet, high spillage drag, and possible engine flameout. The unstarted inlet is shown in Fig. 10.24b. This unstarted condition of the inlet can also be achieved by bringing the freestream Mach number from subsonic up to 2.5 without changing the throat area sufficiently to start the inlet (swallow the normal shock).

Starting of the inlet can be achieved when the area of the throat (flow is choked at the throat) is made large enough for the normal shock to move back and touch the inlet tip (critical operation), as shown in Fig. 10.24c. The ratio of the throat area required to start the inlet A_{ts} to the throat area required at normal operation A_{tr}, (corresponding to $M_t = 1.2$) is obtained from basic one-dimensional flow, plotted in Fig. 10.25 and expressed as

$$\frac{A_{ts}}{A_{tr}} = \frac{1}{1.030(P_{ty}/P_{tx})_{M_0}} \tag{10.8}$$

where 1.030 is the value of A/A^* corresponding to $M_t = 1.2$ and $(P_{ty}/P_{tx})_{M_0}$ is the total pressure ratio across a normal shock with upstream Mach number of M_0. As can be seen in Fig. 10.25, the internal compression inlet has a large throat area variation required to start the inlet at Mach numbers greater

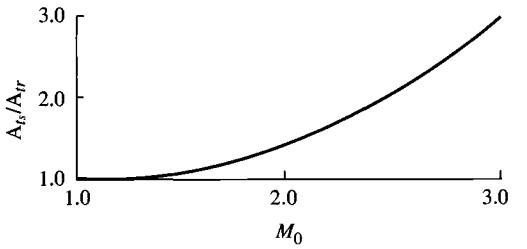

Fig. 10.25 Throat area variation required of an internal compression inlet.

than 2. For example, the throat area required to start an inlet at a Mach number of 2.4 is about 1.8 times the throat area required for normal operation. This large area variation, the problem of inlet upstart, the poor performance at angles of attack, and many other problems have led to the demise of the internal compression inlet.

10.4.3.2 External compression inlet. The compression of the external compression inlet (Fig. 10.26) is achieved through either one or a series of oblique shocks followed by a normal shock, or simply through one normal shock. As shown in Fig. 10.26, A_{0i}, A_{0e}, $A_{0\,\mathrm{bl}}$, and $A_{0\,\mathrm{bp}}$ are the freestream tube areas containing the inlet, engine, boundary-layer bleed, and bypass airflows, respectively.

The external compression inlet that achieves compression through only a single normal shock is called a *pitot inlet or normal shock inlet* and is shown in Fig. 10.27. The pitot inlet is simple, short, lightweight, and inexpensive. The total pressure recovery η_r of this inlet corresponds to the total pressure ratio across a normal shock, shown in Fig. 10.23. The total pressure recovery of this inlet is acceptable for flight Mach numbers up to about 1.6. Above this Mach number, the total pressure recovery of the inlet is too low and another, more efficient inlet design must be used.

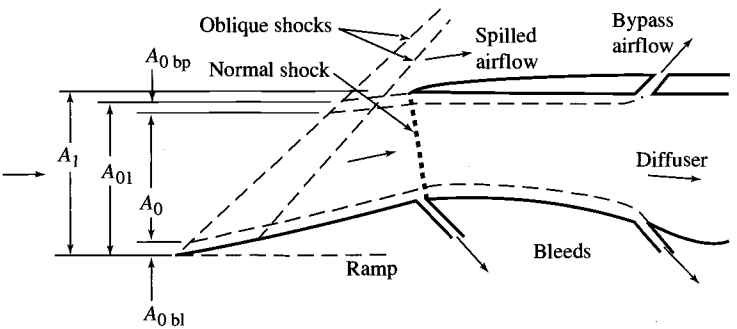

Fig. 10.26 External compression inlet and flow areas.

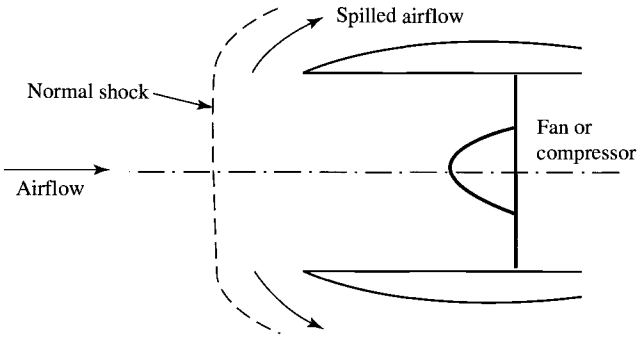

Fig. 10.27 Pilot or normal shock inlet.

The external compression inlet with one or more oblique shocks (Fig. 10.26) has its inlet throat at or very near the cowl leading edge. Desired operation of this inlet is with the normal shock positioned at or very near the cowl lip (critical operation).

The total pressure recovery η_r across n oblique shocks of equal strength (same total pressure ratio) followed by a normal shock is shown in Fig. 10.28. Increasing the number of oblique shocks increases η_r for any given freestream Mach number. However, the ramp of the external compression inlet turns the flow away from the axial direction; thus, the subsonic diffuser duct must turn the flow back to the axial direction, which may add weight and length to the inlet. Figure 10.29 shows the total turning angle of an external compression shock system that attains the total pressure recovery of MIL-E-5008B as a function of freestream Mach number. As the freestream Mach number increases, the

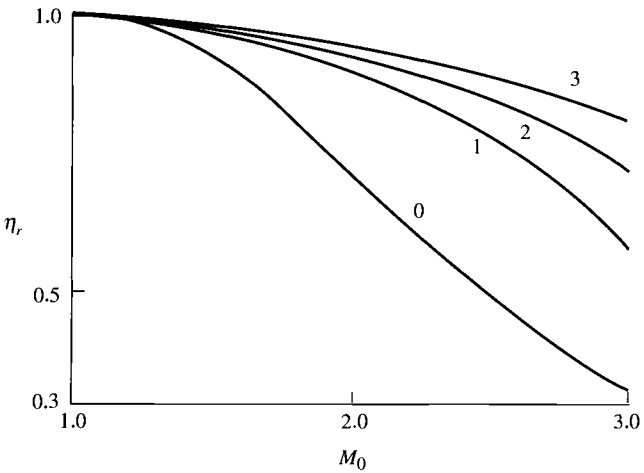

Fig. 10.28 Total pressure recovery of oblique shocks.

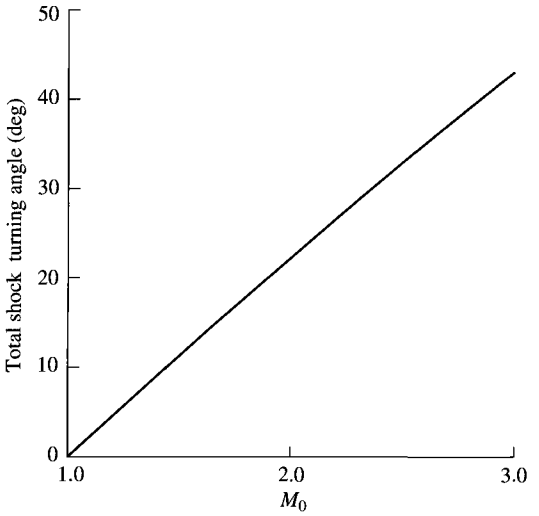

Fig. 10.29 Turning angle of external compression shock system (Ref. 61).

total shock-turning angle of the external ramp increases, resulting in increases in cowl angle and cowl drag. External compression inlets can maintain a balance between an acceptable total pressure ratio and cowl drag up to a flight Mach number of about 2.5.

10.4.3.3 Mixed compression inlet. At flight Mach numbers above 2.5, the mixed compression inlet is used to obtain an acceptable total pressure ratio (by utilizing the required number of oblique shocks) while obtaining acceptable cowl drag. The mixed compression inlet is more complex, heavier, and costlier than the external compression inlet. The typical mixed compression inlet (Fig. 10.30) achieves compression through the external oblique shocks, the internal reflected oblique shocks, and the terminal normal shock. The ideal location of the normal shock is just downstream of the inlet throat, to minimize total pressure loss while maintaining a stable operating location of this shock. Similar to the internal compression inlet, the mixed compression inlet requires

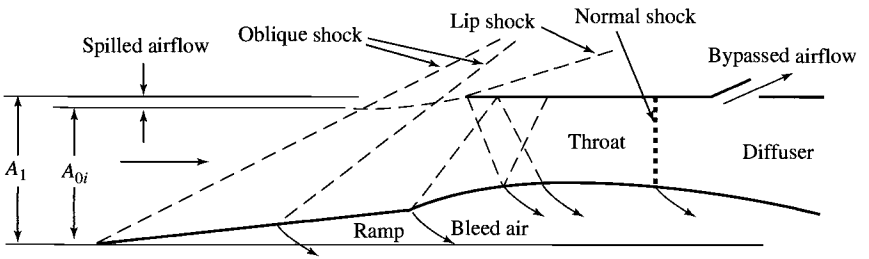

Fig. 10.30 Two-dimensional mixed compression inlet.

both fast-reacting bypass doors (to maintain the normal shock in a stable location) and variable throat area (to allow the inlet to start by swallowing the normal shock). However, the variation in inlet throat area of the mixed compression inlet is considerably less than that of the internal compression inlet because of the mixed compression inlet's external oblique shock system.

Supersonic inlets can also be classified further as *two-dimensional* (rectangular) and *axisymmetric* (circular or a portion of a circle). Figure 10.30 shows a typical two-dimensional mixed compression inlet. Axisymmetric inlets have a slight advantage over two-dimensional inlets with respect to weight and total pressure ratio. However, the two-dimensional inlets have an advantage in design simplicity and in providing a larger variation in inlet airflow. Furthermore, axisymmetric inlets have the added design problem of getting sufficient boundary-layer bleed air out from the centerbody through the support struts.

The improved performance of variable-geometry mixed compression inlets and external compression inlets at high Mach numbers comes with some reduced performance at low supersonic Mach numbers due to the increased frictional losses. Figures 10.31 and 10.32 show the total pressure recovery of past and current aircraft and the supersonic transport (SST) model. Note, in Fig. 10.32, the reduced total pressure recovery of the complex SST mixed compression inlet at subsonic and low supersonic Mach numbers when compared to the simple pitot intake. The message of these two figures is that a supersonic inlet can be designed for good performance at supersonic or subsonic flight Mach numbers, but not at both.

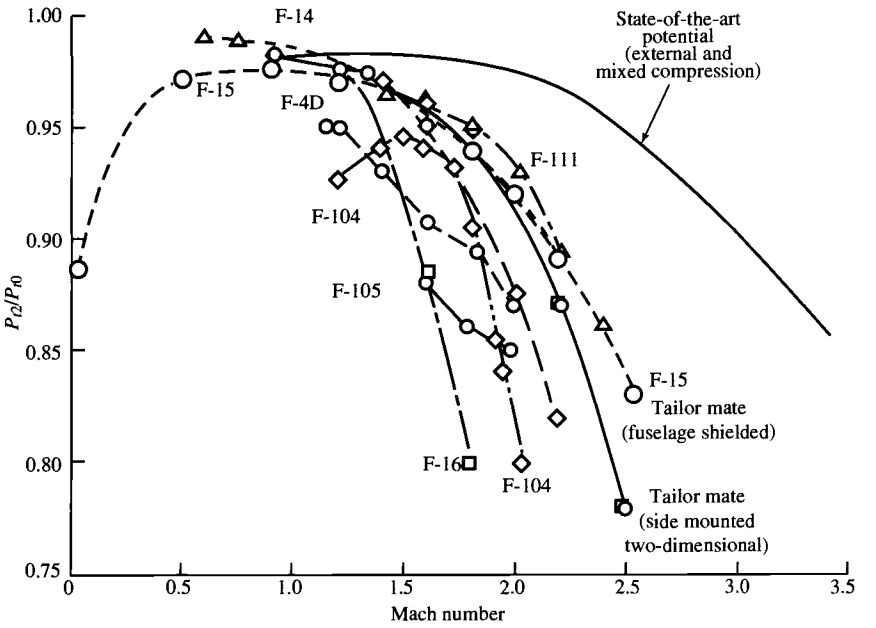

Fig. 10.31 Total pressure ratio survey (Refs. 62–64).

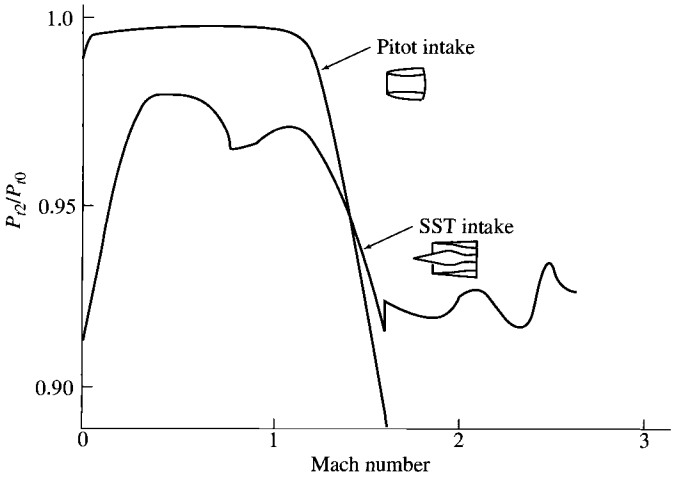

Fig. 10.32 Total pressure ratio—SST model (Ref. 63).

10.4.4 Total Pressure Recovery η_r

In the engine cycle analysis of this textbook, the total pressure recovery of the supersonic inlet was estimated by [Eq. (6.6)]

$$\eta_r = \begin{cases} 1 & M_0 \leq 1 \\ 1 - 0.075(M_0 - 1)^{1.35} & 1 < M_0 < 5 \\ \dfrac{800}{M_0^4 + 935} & 5 < M_0 \end{cases}$$

the ram recovery of military specification MIL-E-5008B. This design inlet total pressure recovery has been added to Fig. 10.28 to give Fig. 10.33, a very useful design tool for selection of inlet type and preliminary number of oblique shocks required. As an example, consider an inlet for flight at Mach 2.5. Equation (6.6) or Fig. 10.33 gives an allowable total pressure ratio for the shock system of 0.87. Figure 10.33 shows that more than two oblique shocks of equal strength followed by a normal shock are required. This could be obtained by an external compression inlet with three oblique shocks or a mixed compression inlet.

Example 10.3

Consider an external compression inlet (part 1). The total pressure recovery of the external compression inlet shown in Fig. 10.34 can be determined by using the normal and oblique shock tables of GASTAB. Applying the normal and oblique shock equations to this inlet with $\theta_a = \theta_b = 5$ deg yields the results

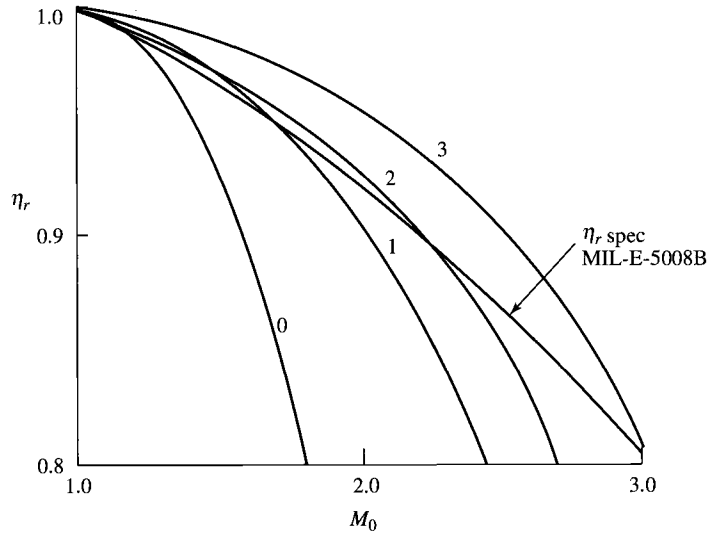

Fig. 10.33 Total pressure recovery required.

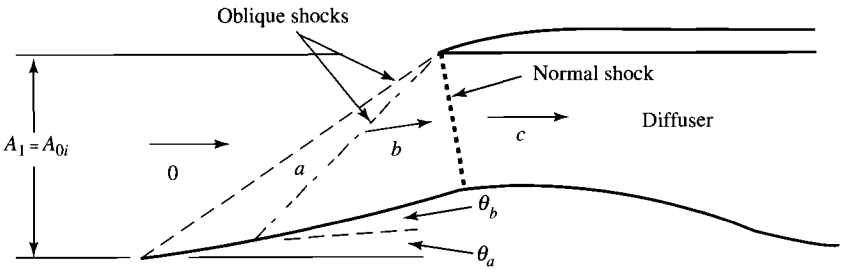

a) On-design operation

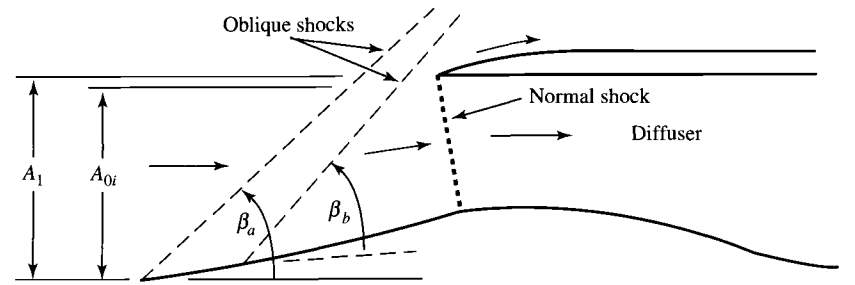

b) Off-design operation

Fig. 10.34 External compression inlet of Example 10.3.

shown in Table 10.1 and plotted in Fig. 10.35. The total pressure recovery η_r of the inlet is the product of the total pressure ratio across each shock. This inlet exceeds the total pressure recovery required by Eq. (6.6) at Mach 1.7 (0.9654 vs 0.9537) but not at Mach 1.8 (0.9396 vs 0.9445).

Note that for M_0 between 1.42 and 1.26, the second oblique shock becomes the terminal normal shock because its ramp angle θ is larger than θ_{max} for M_0 between 1.238 and 1.023. Likewise, the first oblique shock becomes the terminal normal shock for M_0 between 1.23 and 1.0. Also note that the total pressure recovery goes through local maxima and minima as these oblique shocks become normal shocks.

Table 10.1 External compression inlet of Fig. 10.34 with $\theta_a = \theta_b = 5$ deg

M_0	β_a	P_{ta}/P_{t0}	M_a	β_b	P_{tb}/P_{ta}	M_b	P_{tc}/P_{tb}	η_r
2.00	34.30	0.9979	1.821	37.95	0.9982	1.649	0.8765	0.8731
1.95	35.23	0.9980	1.773	39.09	0.9983	1.602	0.8945	0.8912
1.90	36.23	0.9981	1.725	40.34	0.9983	1.554	0.9117	0.9084
1.85	37.30	0.9982	1.677	41.70	0.9984	1.506	0.9278	0.9246
1.80	38.44	0.9982	1.628	43.19	0.9984	1.457	0.9428	0.9396
1.75	39.68	0.9983	1.579	44.84	0.9985	1.407	0.9563	0.9533
1.70	41.03	0.9984	1.529	46.69	0.9985	1.356	0.9684	0.9654
1.65	42.50	0.9984	1.480	48.78	0.9985	1.303	0.9788	0.9758
1.60	44.11	0.9985	1.429	51.21	0.9985	1.248	0.9873	0.9842
1.55	45.89	0.9985	1.378	54.11	0.9984	1.190	0.9937	0.9906
1.50	47.89	0.9985	1.325	57.77	0.9982	1.125	0.9980	0.9947
1.45	50.16	0.9985	1.272	63.05	0.9976	1.045	0.9999	0.9960
1.44	50.65	0.9985	1.261	64.59	0.9973	1.024	1	0.9958
1.43	51.16	0.9985	1.250	66.59	0.9969	0.9974	1	0.9953
1.42	51.68	0.9984	1.238	90	0.9886	0.8192	1	0.9870
1.41	52.22	0.9984	1.227	90	0.9899	0.8257	1	0.9884
1.40	52.78	0.9984	1.216	90	0.9912	0.8325	1	0.9896
1.35	55.93	0.9983	1.156	90	0.9963	0.8705	1	0.9946
1.30	59.96	0.9980	1.090	90	0.9992	0.9195	1	0.9972
1.29	60.95	0.9979	1.075	90	0.9995	0.9316	1	0.9974
1.28	62.04	0.9977	1.059	90	0.9998	0.9450	1	0.9975
1.27	63.26	0.9976	1.042	90	0.9999	0.9602	1	0.9975
1.26	64.69	0.9973	1.023	90	1	0.9782	1	0.9973
1.25	66.50	0.9969	0.9986	0	1	0.9986	1	0.9969
1.24	69.90	0.9957	0.9554	0	1	0.9554	1	0.9957
1.23	90	0.9896	0.8241	0	1	0.8241	1	0.9896
1.22	90	0.9907	0.8300	0	1	0.8300	1	0.9907
1.21	90	0.9918	0.8360	0	1	0.8360	1	0.9918
1.20	90	0.9928	0.8422	0	1	0.8422	1	0.9928
1.15	90	0.9967	0.8750	0	1	0.8750	1	0.9967
1.10	90	0.9989	0.9118	0	1	0.9118	1	0.9989
1.05	90	0.9999	0.9531	0	1	0.9531	1	0.9999

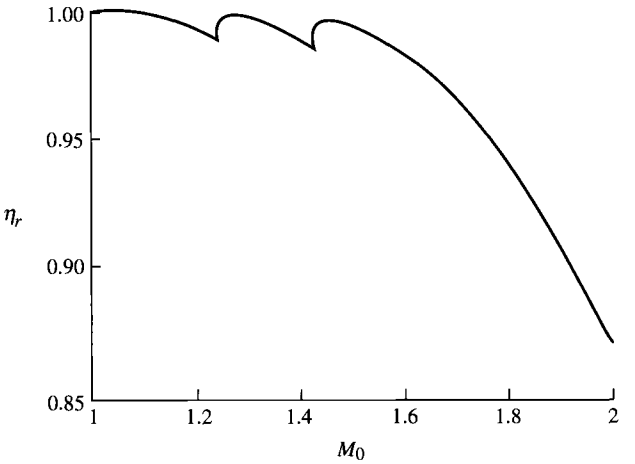

Fig. 10.35 Total pressure recovery η_r of external compression inlet (Fig. 10.36) with $\theta_a = \theta_b = 5$ deg.

10.4.5 Mass Flow Characteristics

The *inlet mass flow ratio* is the ratio of the actual mass flow rate of the inlet $\dot{m}_i$ to the mass flow rate that could be captured $\dot{m}_1$ by the inlet (see Fig. 10.36), and from the conservation of mass equation

$$\frac{\dot{m}_i}{\dot{m}_1} = \frac{\rho_0 V_0 A_{0i}}{\rho_0 V_0 A_1} = \frac{A_{0i}}{A_1} \tag{10.9}$$

which is the inlet area ratio. Thus the inlet mass flow ratio and the inlet area ratio are used interchangeably. The difference between $\dot{m}_i$ and $\dot{m}_1$ is the air that is spilled around the inlet. The *engine mass flow ratio* is defined similarly to that

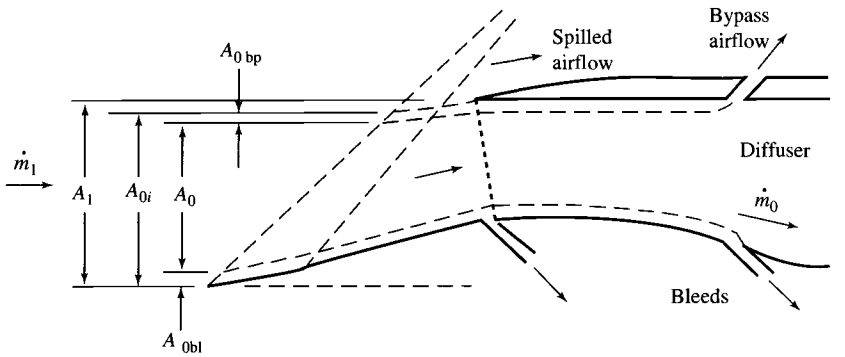

Fig. 10.36 Critical inlet operation.

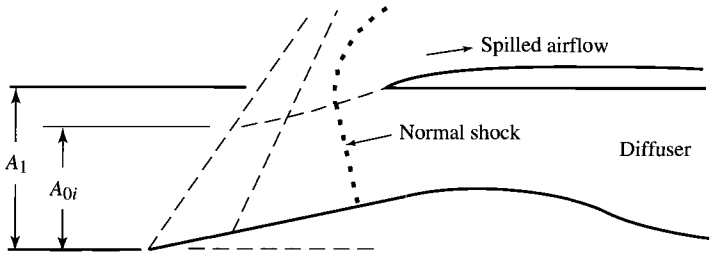

Fig. 10.37 Subcritical inlet operation.

of the inlet, as the ratio of the required engine mass flow rate $\dot{m}_0$ to the mass flow rate that the inlet could capture $\dot{m}_1$, or

$$\frac{\dot{m}_0}{\dot{m}_1} = \frac{\rho_0 V_0 A_0}{\rho_0 V_0 A_1} = \frac{A_0}{A_1} \tag{10.10}$$

The difference between $\dot{m}_i$ and $\dot{m}_0$ is the air that enters the inlet but is removed through boundary-layer bleed, the bypass system, or the secondary air system.

When the inlet can accept the mass flow rate of air required to position the terminal shock just inside the cowl lip (*critical* operation), the fraction of air spilled around the inlet is a minimum and the inlet is said to be *matched* to the engine. When the inlet is not matched, as shown in Fig. 10.37, the normal shock moves upstream (*subcritical* operation) and the fraction of air spilled is increased. This increase in air spillage has associated with it an increase in *spillage drag*, or drag due to the change in momentum of the spilled air and the pressure forces on its stream tube.

When the inlet cannot capture the mass flow rate required by the engine and the other systems, the terminal normal shock is sucked down into the diffuser (*supercritical* operation), as shown in Fig. 10.38, which strengthens the shock and increases the *corrected* mass flow rate to the engine. At a specific operating point on the fan or compressor map, the engine operates as a constant corrected mass flow device. Thus, when the inlet cannot provide the required corrected mass flow rate at critical operation, the engine causes supercritical

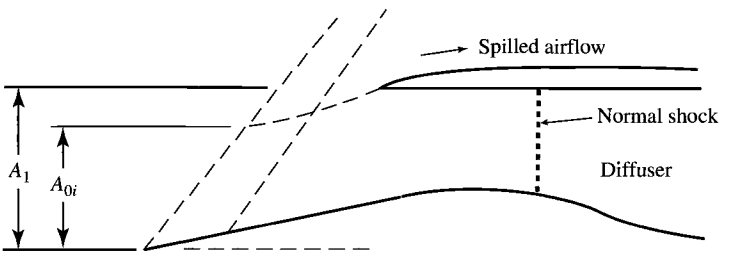

Fig. 10.38 Supercritical inlet operation.

operation and attains the required corrected mass flow rate. Note that supercritical operation has a lower inlet total pressure recovery associated with it, thus, a reduction in engine performance (lower thrust and higher specific fuel consumption). Supercritical operation of the inlet is to be avoided when possible because of poor engine performance.

A common way of presenting the mass flow rate characteristics of an inlet is through a map of the total pressure recovery vs the inlet mass flow ratio, as shown in Fig. 10.39. The performance of a typical external compression inlet is presented in Fig. 10.39 for a specific freestream Mach number. The critical operation point and the subcritical and supercritical operating regimes are also shown on this figure.

The engine mass flow ratio $\dot{m}_0/\dot{m}_1$ can be expressed in terms of corrected mass flow rates and the inlet total pressure ratio as

$$\frac{\dot{m}_0}{\dot{m}_1} = \frac{\dot{m}_{c0}}{\dot{m}_{c1}}\pi_d = \frac{\dot{m}_{c0}}{\dot{m}_{c1}}\eta_r \pi_{d\max} \tag{10.11}$$

where $\dot{m}_{c0}$ is the corrected mass flow rate of the engine and $\dot{m}_{c1}$ is the corrected mass flow rate based on the capture area, a constant for fixed capture area and flight condition. Variation in the engine corrected mass flow rate $\dot{m}_{c0}$ due to a change in engine throttle can be presented on the inlet mass flow map of Fig. 10.39 for the case where the boundary-layer bleed and bypass flows are essentially constant. A line of constant $\dot{m}_{c0}$ is shown on Fig. 10.39 along with the direction of increasing $\dot{m}_{c0}$. When the engine's requirement for air decreases below that required for critical inlet operation, the inlet operating point moves

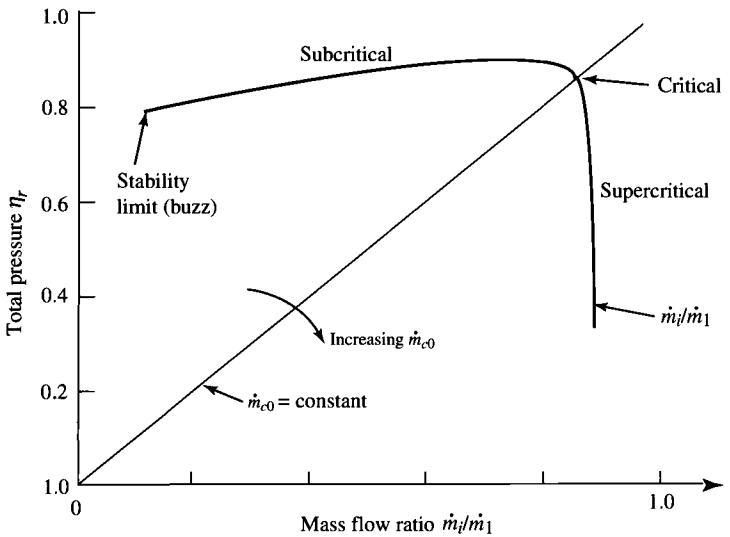

Fig. 10.39 External compression inlet performance characteristics.

into the subcritical region as the engine mass flow rate decreases and the fraction of air spilled increases. When the engine's requirement for air increases above that required for critical operation, the inlet operating point moves into the supercritical region as the engine mass flow ratio remains constant and the total pressure recovery of the inlet decreases with the strengthening of the terminal normal shock in the diffuser.

Two supersonic flow phenomena associated with the stability of the shock structure in external and mixed compression inlets require consideration at this point. One is called inlet *buzz*, and the other is associated with the location of the terminal normal shock.

Buzz is a low-frequency, high-amplitude pressure oscillation that is linked to shock/boundary layer and/or shock/shock interaction at relatively low inlet mass flow ratio. As an example of a flow condition leading to inlet buzz, consider the external compression inlet of Fig. 10.40. When this inlet is operated in the subcritical regime, the terminal normal shock will impinge on the boundary layer formed along the wall of the ramp, causing the boundary layer to separate. If the separated boundary layer produces a large enough low-velocity flow region, the inlet will choke, reducing the inlet mass flow rate and moving the normal shock forward along the ramp. The boundary layer at this forward location is thinner; its separated mass flow region does not choke the inlet. Thus the inlet mass flow increases, moving the normal shock back up the ramp toward its original location, to be repeated again and again, creating buzz. When buzz occurs on a mixed compression inlet, the inlet will "unstart" and engine flameout is possible.

The stability of the terminal normal shock in a mixed compression inlet is important during operation of the inlet near its design point. Design for stability of the terminal normal shock requires that the need for higher total pressure recovery be compromised, and the design throat Mach number be 1.2, with the normal shock positioned downstream where the Mach number is 1.3. Thus the mixed compression inlet is designed to operate in the supercritical regime. When the engine needs less air than provided by this inlet, the excess air must bypass the engine to maintain the terminal normal shock at its stable location and prevent the inlet from "unstarting" (expelling the normal shock). When the engine wants more air than the inlet can provide, the terminal normal shock is

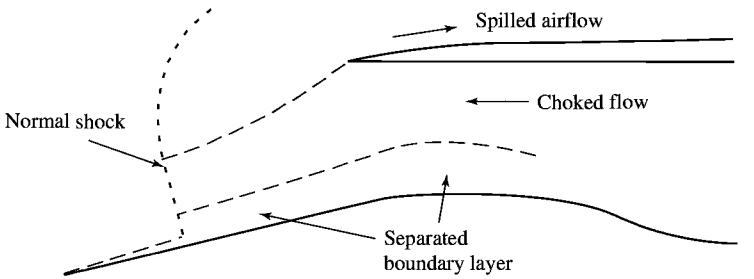

Fig. 10.40 Condition leading to inlet "buzz."

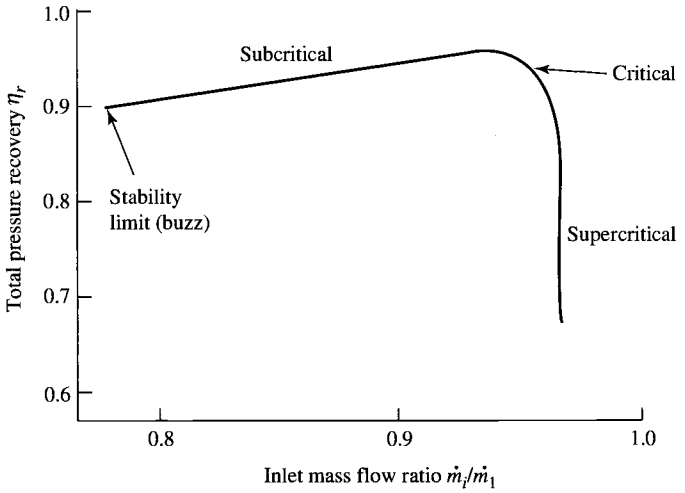

Fig. 10.41 Mixed compression inlet performance characteristics.

drawn downstream into the diffuser, strengthening the shock and increasing the corrected mass flow rate to the engine. When the normal shock is drawn downstream into the diffuser, flow separation and flow distortion become dominant design considerations. To limit this problem, the inlet needs to be designed to provide the required engine mass flow rate with the terminal normal shock positioned where the Mach number in the diffuser is 1.3.

The total pressure recovery vs mass flow ratio of a typical mixed compression inlet is shown in Fig. 10.41. Note that this inlet has a much smaller allowable variation in mass flow ratio before onset of buzz than does the external compression inlet of Fig. 10.39. This reduction in the range for the inlet mass ratio $\dot{m}_i/\dot{m}_1$ corresponds to a larger change in the amount of inlet air that is required to be bypassed $\dot{m}_{bp}$ to prevent buzz (maintain $\dot{m}_i/\dot{m}_1$ above the stability limit), with a corresponding smaller variation in the amount of air spilled.

10.4.6 Inlet Design and Sizing

The design and sizing for a supersonic inlet are considerably more difficult than for the subsonic inlet due mainly to differences in the nature of supersonic and subsonic flows. The supersonic inlet is designed to operate at both subsonic and supersonic flight Mach numbers. The capture and throat areas of the inlet must be large enough not to choke the airflow required by the engine, boundary-layer bleed system, etc. For supersonic flight conditions, the inlet's capture area A_1 is sized to capture the required airflow. Because this airflow varies with both flight Mach number and engine throttle setting, variable-geometry inlet design is sometimes needed to meet the total pressure recovery goal of military specification MIL-E-5008B and/or to keep the installation losses low (spillage drag and/or bypass air drag).

The required values of engine airflow $\dot{m}_0$ and the corresponding values of the freestream area A_0, calculated by the engine performance analysis of Chapter 8 and/or the associated engine performance computer program PERF, are based on the total pressure recovery given by military specification MIL-E-5008B, where

$$\eta_{r\,\text{spec}} = \begin{cases} 1 & M_0 \le 1 \\ 1 - 0.075(M_0 - 1)^{1.35} & 1 < M_0 < 5 \\ \dfrac{800}{M_0^4 + 935} & 5 < M_0 \end{cases} \tag{10.12}$$

This same reference inlet total pressure recovery is used by many others. [Note: Because the total pressure recovery η_r of an inlet design may be different from $\eta_{r\text{spec}}$ given by Eq. (10.12), the required values of engine airflow $\dot{m}_0$ and the corresponding values of freestream area A_0 will be different from those calculated in the engine performance analyses. Thus the values of $\dot{m}_0$ and A_0 determined by using the total pressure recovery of Eq. (10.12) will be referred to as $\dot{m}_{0\,\text{spec}}$ and $A_{0\,\text{spec}}$ respectively, from this point on.]

Inlet design and sizing begin with an analysis of airflow requirements. Figure 10.42 shows the typical variation in inlet airflow requirements at different altitudes from engine performance analyses $A_{0\,\text{spec}}$ with flight Mach number for an advanced supersonic engine. Variable boundary-layer bleed and a safety margin of 4% have been added to the maximum full-throttle engine airflow to obtain the required inlet airflow $A_{0i\,\text{spec}}$.

The engine airflow requirements ($\dot{m}_0$, A_0) for a given inlet design η_r can be estimated based on the engine airflow requirements ($\dot{m}_{0\,\text{spec}}$, $A_{0\,\text{spec}}$) obtained by using a known inlet total pressure recovery $\eta_{r\,\text{spec}}$. Because the engine operates essentially as a constant corrected mass flow device ($\dot{m}_{c2}$ = constant) when the

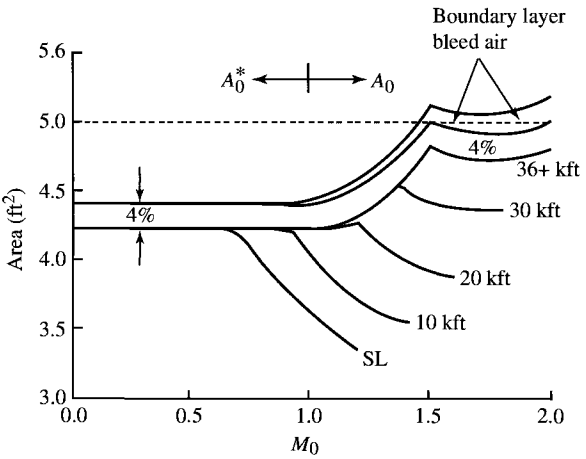

Fig. 10.42 Typical engine airflow requirements.

throttle and flight conditions are constant, then the required engine airflow $\dot{m}_0$ for a specific inlet design η_r can be determined from required engine airflow data ($\dot{m}_{0\,\text{spec}}$, $A_{0\,\text{spec}}$) based on a reference inlet total pressure recovery $\eta_{r\,\text{spec}}$ by using

$$\frac{\dot{m}_0}{\dot{m}_{0\,\text{spec}}} = \frac{A_0}{A_{0\,\text{spec}}} = \frac{\eta_r}{\eta_{r\,\text{spec}}} \tag{10.13a}$$

Likewise, for the inlet air

$$\frac{\dot{m}_i}{\dot{m}_{i\,\text{spec}}} = \frac{A_{0i}}{A_{0i\,\text{spec}}} = \frac{\eta_r}{\eta_{r\,\text{spec}}} \tag{10.13b}$$

10.4.6.1 Inlet performance. Consider the generalized inlet of Fig. 10.43 with capture area A_1 and area A_s at location s. The inlet mass flow ratio can be written as

$$\frac{A_{0i}}{A_1} = \frac{A_{0i}}{A_s}\frac{A_s}{A_1} \tag{10.14a}$$

where A_s/A_1 is determined by the geometry of the inlet. The shock system determines the area ratio A_{0i}/A_s as follows. Conservation of mass gives $\dot{m}_i = \dot{m}_s$ or $\rho_0 V_0 A_{0i} = \rho_s V_s A_s$; thus

$$\frac{A_{0i}}{A_s} = \frac{\dot{m}_s/A_s}{\dot{m}_i/A_{0i}} = \frac{\rho_s V_s}{\rho_0 V_0}$$

and for adiabatic flow in the inlet ($T_{ts} = T_{t0}$), the mass flow rate per unit area in the preceding equation can be written in terms of total pressure and mass flow parameter as

$$\frac{A_{0i}}{A_s} = \frac{P_{ts}}{P_{t0}}\frac{\text{MFP}(M_s)}{\text{MFP}(M_0)} \tag{10.14b}$$

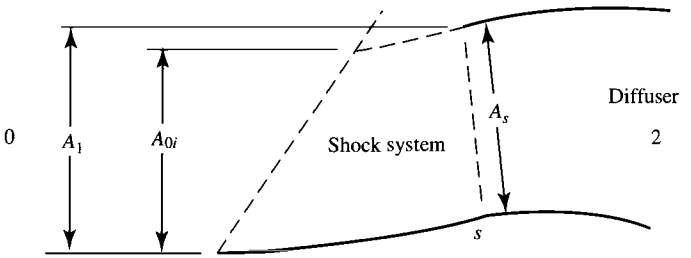

Fig. 10.43 External compression inlet.

Equations (10.14a) and (10.14b) provided the tools to estimate the inlet mass flow ratio A_{0i}/A_1 of an inlet. The area ratio A_s/A_1 is a geometric function of the inlet design, whereas the area ratio A_{0i}/A_s is a function of the flow properties at stations 0 and s. The previous section on total pressure recovery presented the analytical tools for determining both M_s and P_{ts}/P_{t0} of a general inlet, as shown in Example 10.3. Reference 54 contains exact solutions for one and two oblique shock inlets designed for critical operation.

10.4.6.2 Inlet size. The ratio of the inlet capture area A_1 to the engine's area at state 0* for the cycle reference point $A^*_{0\,\mathrm{ref}}$ is referred to as the *inlet size* $A_1/A^*_{0\,\mathrm{ref}}$, since this ratio is the size of the inlet relative to the engine. The required inlet size $(A_1/A^*_{0\,\mathrm{ref}})_{\mathrm{req}}$ at a flight condition can be calculated from the required inlet airflow $A_{0i\,\mathrm{req}}/A^*_{0\,\mathrm{ref}}$ and the inlet mass flow ratio $A^*_{0\,\mathrm{ref}}/A_1$ by using

$$\left(\frac{A_1}{A^*_{0\,\mathrm{ref}}}\right)_{\mathrm{req}} = \frac{(A_{0i}/A^*_{0\,\mathrm{ref}})_{\mathrm{req}}}{A_{0i}/A_1} \tag{10.15}$$

For an inlet with fixed capture area A_1, the flight condition requiring the largest inlet size $(A_1/A^*_{0\,\mathrm{ref}})_{\mathrm{req}}$ is used to size the inlet capture area A_1.

Care must be taken that the inlet does not choke the flow to the engine at subsonic flight conditions. This can be ensured by having the inlet capture area A_1 larger than the maximum required one-dimensional inlet area A^*_{0i} by about 4% ($A/A^* = 1.038$ at $M = 0.8$) and/or providing additional air inlet area for very low-velocity engine airflow requirements.

Example 10.4

Consider an external compression inlet (part 2). We consider the double-ramp external compression inlet of Fig. 10.34 with $\theta_a = \theta_b = 5$ deg to be used with the engine whose required airflow is plotted as $A_0/A^*_{0\,\mathrm{ref}}$ in Fig. 10.44. These data are based on the airflow requirements of Fig. 10.42 at 40-kft altitude and an $A^*_{0\,\mathrm{ref}}$ of 4.22 ft^2 at sea-level static conditions. The inlet is to be capable of operating up to Mach 2 at 40 kft with efficient operation ($\eta_r > \eta_{r\ \mathrm{spec}}$) at Mach numbers less than 1.7. The inlet size and mass flow characteristics of the inlet and engine are considered.

a) Inlet performance. The total pressure recovery of this inlet η_r is tabulated in Table 10.1, is plotted in Fig. 10.35, and meets the requirement for efficient total pressure recovery ($\eta_r > \eta_{r\ \mathrm{spec}}$) at Mach numbers less than 1.75. Analysis of the mass flow characteristics of the inlet and the engine is required before this inlet can be sized. As long as the normal shock between stations b and c touches the lip of the inlet, either station b or c of Fig. 10.34 can be equated to station s of Fig. 10.43. From Eq. (10.14b), we have

$$\frac{A_{0t}}{A_s} = \frac{P_{tb}}{P_{t0}}\frac{\mathrm{MFP}(M_b)}{\mathrm{MFP}(M_0)} = \frac{P_{tc}}{P_{t0}}\frac{\mathrm{MFP}(M_c)}{\mathrm{MFP}(M_0)} \tag{10.16a}$$

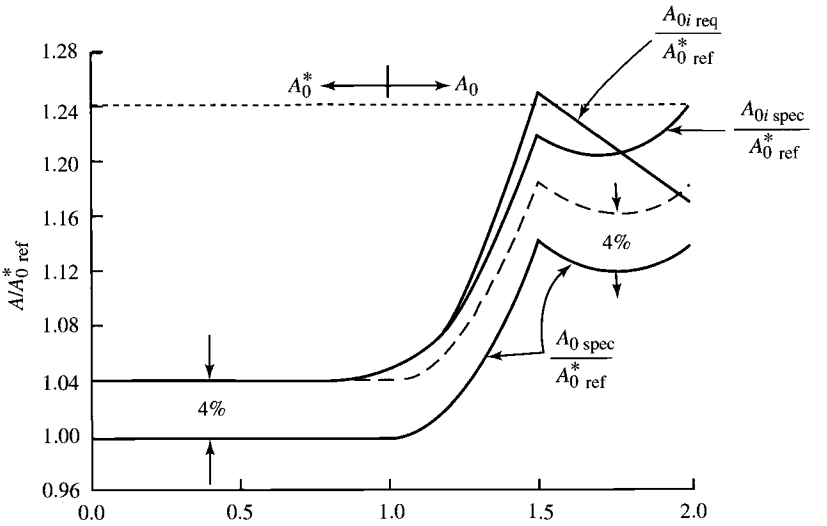

Fig. 10.44 Airflow requirement for example inlet at altitude.

and

$$\frac{P_{tc}}{P_{t0}} = \eta_r \quad \frac{P_{tb}}{P_{t0}} = \frac{\eta_r}{P_{tc}/P_{tb}} \tag{10.16b}$$

The area ratio A_{0t}/A_s can be calculated by using the results of Table 10.1, assuming that $M_s = M_b$ at subsonic values of M_b (no local flow acceleration or deceleration). For subsonic M_0, a reasonable approximation is for choked flow at station s; thus, $A^*_{0i} = A_s$.

The results of the area ratio A_{0i}/A_s calculations for this example inlet are plotted in Fig. 10.45. Note that this plot has a minimum value of 1 at $M_0 = 1$. Also note the jumps in value of A_{0i}/A_s corresponding to the transition between normal and oblique shocks at each ramp (these also correspond to the jumps in total pressure shown in Fig. 10.35).

The selected design point of an external compression inlet sets the value of A_s/A_1. Since $A_{0i} = A_1$ at an inlet's supersonic design point, then $A_s/A_1 = 1/(A_{0i}/A_s)$ evaluated at this design point. For this example, the inlet design point is the maximum M_0 of 2.0. Thus $A_s/A_1 = 0.7681$ and the resulting values of A_{0i}/A_1, from using Eq. (10.14a), are tabulated in Table 10.2.

b) Inlet size. Now that the mass flow ratio of the inlet has been determined, the inlet mass flow rate requirements must be established before it can be sized. By using these data, the maximum calculated value of the inlet size ($A_1/A^*_{0\ \text{ref}}$), from Eq. (10.15), sets the size of this fixed-geometry inlet. Comparison of Figs. 10.44 and 10.45 indicates that the two most demanding operating points will most likely be at $M_0 = 1.23$ and $M_0 = 1.42$. Sizing calculations at the two Mach

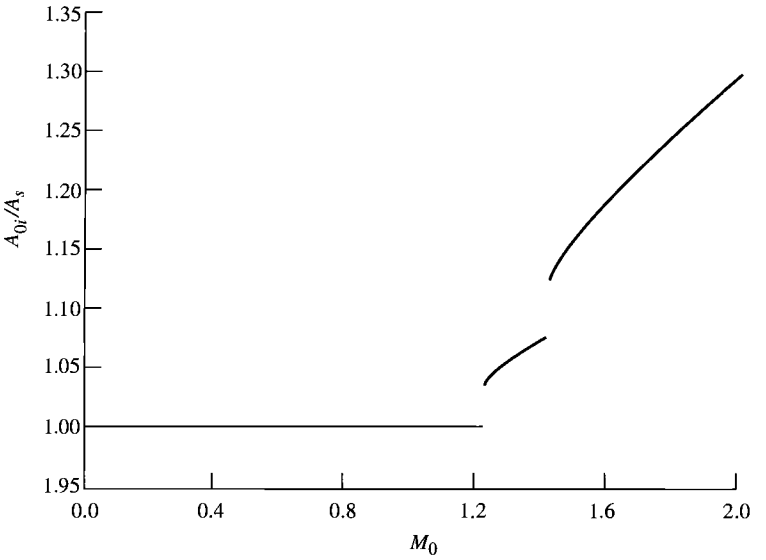

Fig. 10.45 Area ratio of Example 10.4 inlet (Fig. 10.34).

numbers are presented in Table 10.3. The flight condition at $M_0 = 1.42$ determines the inlet size as $A_1 = 1.425A^*_{0\text{ref}}$.

The resulting flow ratios of the sized inlet and its required performance are plotted for altitudes between 36 and 60 kft in Fig. 10.46. This plot shows the difference in flow behavior of the inlet between actual and required flows. As the flight Mach number increases above 1.5, the inlet mass flow rate A_{0i}/A_1

Table 10.2 Example 10.4 inlet performance

M_0	A_{0i}/A_1
0.9	0.7749
1.0	0.7681
1.1	0.7681
1.2	0.7681
1.3	0.8121
1.4	0.8259
1.5	0.8895
1.6	0.9151
1.7	0.9378
1.8	0.9592
1.9	0.9798
2.0	1.0

Table 10.3 Example 10.4 inlet sizing

M_0	$A_0/A_{0\,\text{ref}}^*$	$A_{0i\,\text{req}}/A_{0\,\text{ref}}^*$	A_{0i}/A_1	$A_{1\,\text{req}}/A_{0\,\text{ref}}^*$
1.23	1.0290	1.0854	0.7681	1.413
1.42	1.1004	1.1803	0.8283	1.425

increases while the required inlet mass flow rate $(A_{0i}/A_1)_{\text{req}}$ decreases. The difference between these mass flow rates is airflow that is accepted by the inlet and then bypassed about the engine back to the atmosphere, or spilled about the inlet, or is a combination of bypassed and spilled. The large quantity of excess air for this inlet will correspond to a high inlet installation loss at Mach numbers above 1.5. If a better match of inlet and engine is needed, the inlet will require variable geometry.

10.4.7 Examples of Existing Inlet Designs

Three examples of supersonic inlet designs are shown in Figs. 10.47a, 10.47b, 10.48, and 10.49. Figure 10.47a shows the fixed double-ramp (6-deg ramp followed by a 6.67-deg isentropic ramp) external compression inlet with a throat slot bleed system developed in the J-79 engine installation in the F-16 aircraft. The total pressure recovery of this inlet is shown in Fig. 10.47b.

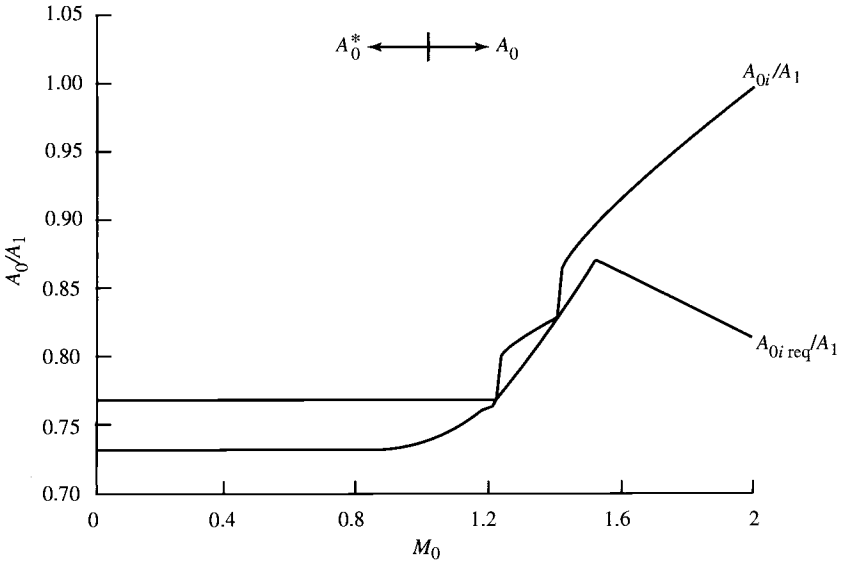

Fig. 10.46 Mass flow performance of sized Example 10.4 inlet at altitude and full engine throttle.

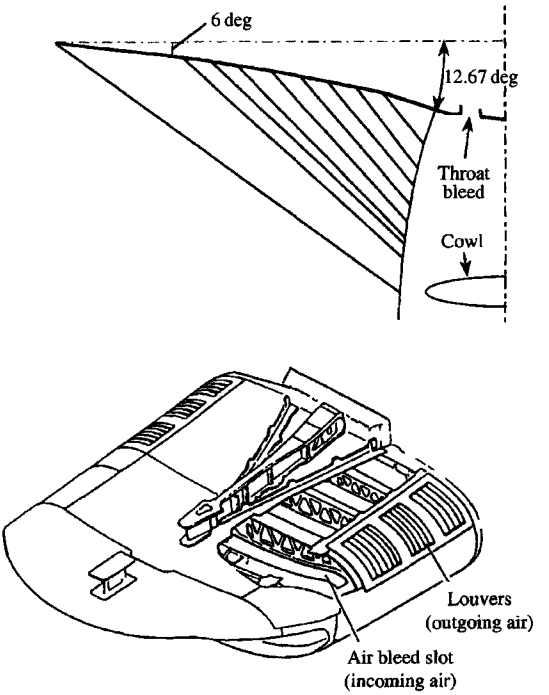

Fig. 10.47a The F-16/J-79 inlet: side and isometric views (Ref. 65).

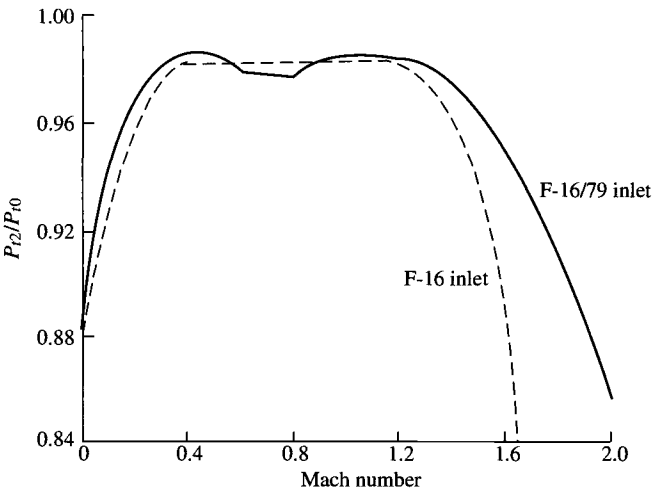

Fig. 10.47b The F-16/J-79 inlet: inlet pressure recovery comparison (Ref. 65).

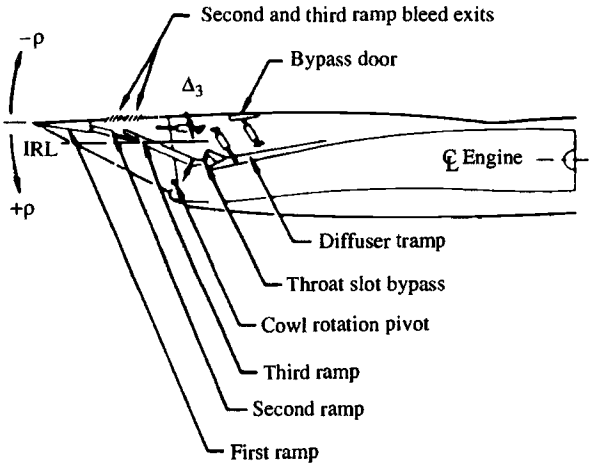

Note: Sideplate bleed not shown

Fig. 10.48 The F-15 inlet system (Ref. 66).

The variable triple-ramp external compression inlet of the F-15 aircraft is shown in Fig. 10.48. This side view of the inlet shows the ramps as they would be positioned when operating at the supersonic design point (ramp angles of 7, 8, and 8 deg for the first, second, and third ramps, respectively). The first ramp angle is fixed, and the second and third ramp angles are variable. The capture area of this inlet is variable with movement of the first ramp/top of inlet assembly from −4 to +11 deg (this assembly is shown at 0 deg).

The takeoff, transonic acceleration, and supersonic cruise modes of operation for the Concorde propulsion system are shown in Fig. 10.49. It has a complex variable-geometry inlet to satisfy the engine mass flow rate requirements at many diverse flight conditions. Note that the supersonic cruise dump control (3) is opened as an auxiliary inlet for takeoff.

10.5 Exhaust Nozzles

The purpose of the exhaust nozzle is to increase the velocity of the exhaust gas before discharge from the nozzle and to collect and straighten the gas flow. For large values of specific thrust, the kinetic energy of the exhaust gas must be high, which requires a high exhaust velocity. The pressure ratio across the nozzle controls the expansion process, and the maximum thrust for a given engine is obtained when the exit pressure P_e equals the ambient pressure P_0. Nozzles and their operation are discussed in many textbooks. The two basic types of nozzles used in jet engines are the *convergent* and *convergent-divergent* (C-D) nozzles.

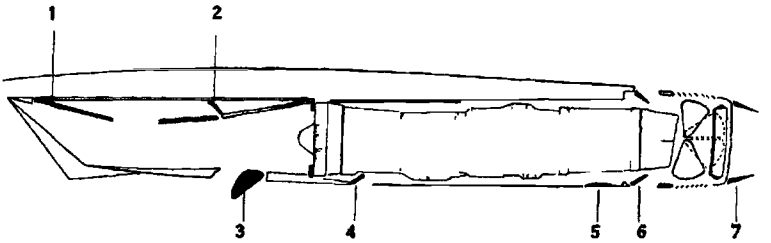

Engine variable geometry. The takeoff settings: 1-ramp sections retracted: 2-secondary control valve closed; 3-dump control open as auxiliary inlet; 4-engine bay cooling air flap open; 5-after spill flap closed; 6-tertiary doors open; 7-secondary nozzle in convergent position

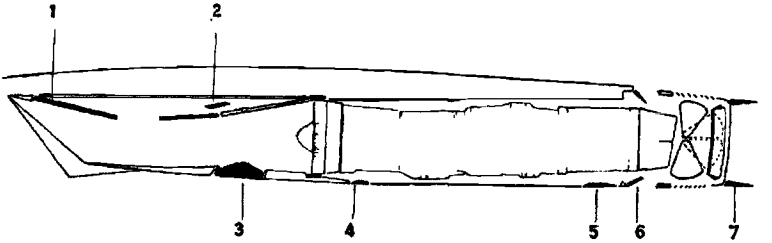

Transonic acceleration: 1-ramp section retracted; 2-secondary control valve open; 3-dump control closed; 4-cooling air flap closed; 5-spill flap closed; 6-tertiary doors open; 7-secondary nozzle trailing

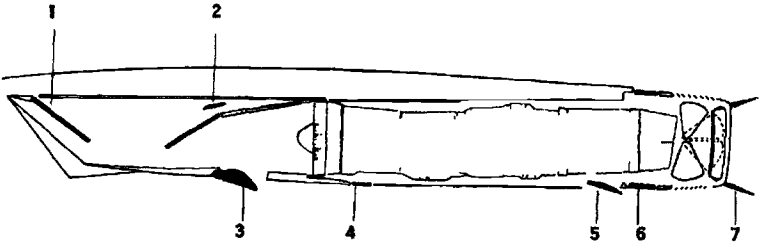

Cruise at Mach 2.2: 1-ramp sections extended; 2-secondary control valve open; 3-dump control open to dump; 4-cooling air flap closed; 5-spill flap open; 6-tertiary doors closed; 7-secondary nozzle divergent.

Fig. 10.49 Concorde propulsion system, modes of operation.

The functions of an exhaust nozzle may be summarized as follows:

1) Accelerate the flow to a high velocity with minimum total pressure loss.
2) Match exit and atmospheric pressures as closely as desired.
3) Permit afterburner operation without affecting main engine operation—this function requires a variable-area nozzle.

4) Allow for cooling of walls if necessary.
5) Mix core and bypass streams of turbofan if necessary.
6) Allow for thrust reversing if desired.
7) Suppress jet noise and infrared radiation (IR) if desired.
8) Thrust vector control if desired.

Do all of these with minimal cost, weight, and boattail drag while meeting life and reliability goals.

10.5.1 Nozzle Types

10.5.1.1 Convergent nozzle. The convergent nozzle is a simple convergent duct, as shown in Fig. 10.50. When the nozzle pressure ratio P_{te}/P_0 is low (less than about 4), the convergent nozzle is used. The convergent nozzle has generally been used in engines for subsonic aircraft.

10.5.1.2 Convergent-divergent (C-D) nozzle. The convergent-divergent nozzle is a convergent duct followed by a divergent duct. Where the cross-sectional area of the duct is at a minimum, the nozzle is said to have a *throat*. Most convergent-divergent nozzles used in aircraft are not simple ducts, but incorporate variable geometry and other aerodynamic features. The convergent-divergent nozzle is used if the nozzle pressure ratio P_{te}/P_0 is high (greater than about 6). High-performance engines in supersonic aircraft generally have some form of a convergent-divergent nozzle. If the engine incorporates an afterburner, the nozzle throat is usually scheduled to leave the operating conditions of the engine upstream of the afterburner unchanged (in other words, vary the exit nozzle area so that the engine does not know that the afterburner is operating). Also, the exit area must be varied to match the different flow conditions and to produce the maximum available thrust.

Earlier supersonic aircraft used ejector nozzles (Fig. 10.51) with their high-performance turbojets. Use of the ejector nozzle permitted bypassing varying amounts of inlet air around the engine, providing engine cooling, good inlet recovery, and reduced boattail drag. Ejector nozzles can also receive air from outside the nacelle directly into the nozzle for better overall nozzle matching—these are called *two-stage ejector nozzles*. For the modern high-performance afterburning turbofan engines, simple convergent-divergent nozzles are used without secondary air, as shown in Fig. 10.52 for the F100 engine.

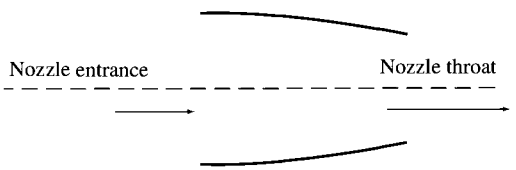

Fig. 10.50 Convergent exhaust nozzle.

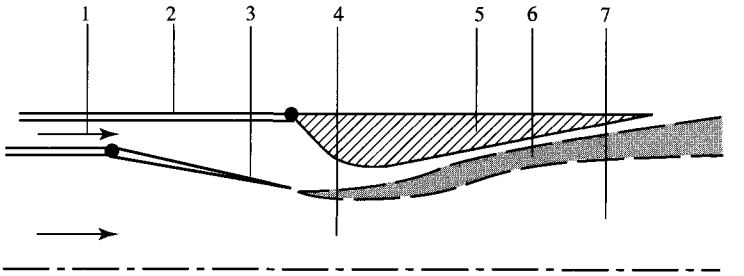

Supersonic nozzle configuration with afterburning: (1) secondary flow; (2) outer case engine; (3) movable primary nozzle shown at maximum area; (4) primary flow, effective throat; (5) movable secondary nozzle shown at maximum exit area; (6) mixing layer between primary and secondary streams; and (7) supersonic primary flow

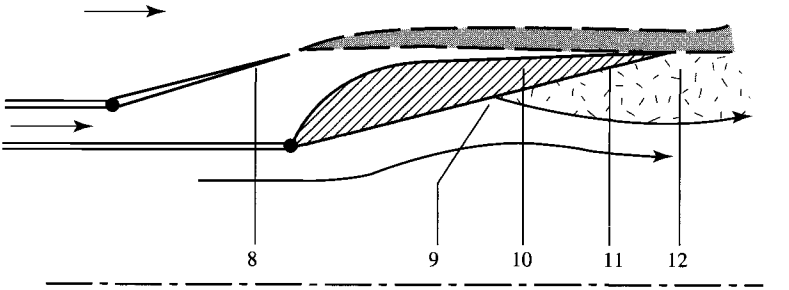

Subsonic nozzle configuration with no afterburning: (8) primary nozzle at minimum area; (9) separation point of external flow; (10) secondary nozzle at minimum area; (11) sonic primary stream; and (12) region of separated flow in external flow

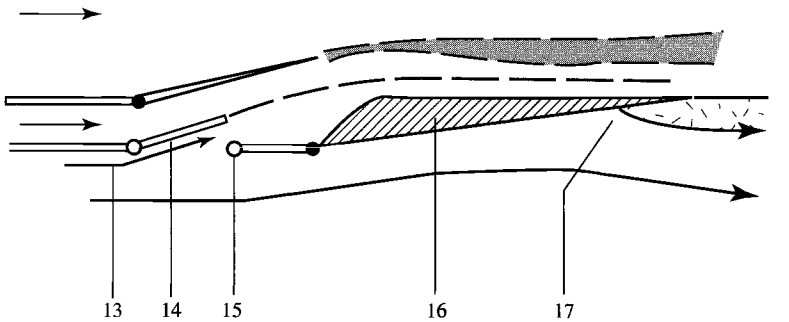

Subsonic nozzle configuration, not afterburning, and blow-in door in use: (13) tertiary flow of ambient gas into nozzle; (14) blow-in door and inflow configuration; (15) reversible hinge/latch; (16) movable secondary nozzle; and (17) separation point of external flow.

Fig. 10.51 Ejector nozzle configuration (Ref. 67).

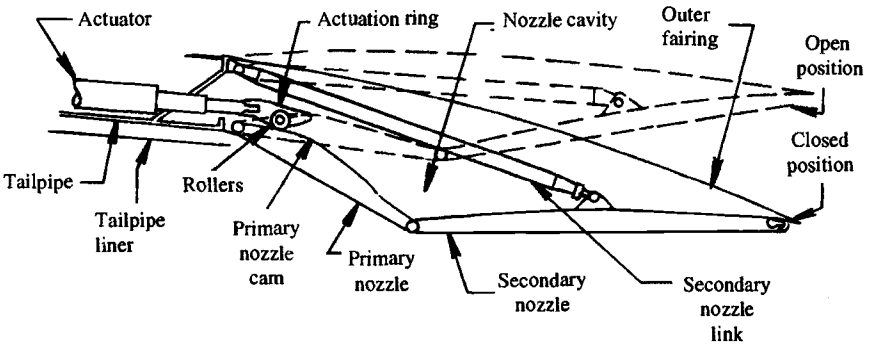

Fig. 10.52 Convergent-divergent exhaust nozzle schematic (Ref. 67).

10.5.2 Nozzle Functions

One can think of the exhaust nozzle as dividing the power available from the main burner exit gas between the requirements of the turbine and the jet power.[67] Thus the nozzle serves as a backpressure control for the engine and an acceleration device converting gas thermal energy to kinetic energy. A secondary function of the nozzle is to provide required thrust reversing and/or thrust vectoring.

10.5.2.1 Engine backpressure control. The throat area of the nozzle is one of the main means available to control the thrust and fuel consumption characteristics of an existing engine. In preliminary engine cycle analysis, selection of specific values for the engine design parameters and the design mass flow rate fixes the throat area of the nozzle. The engine performance methods of Chapter 8 assume that the nozzle throat area and the other internal flow areas of the engine remain constant. This assumption of constant areas establishes the off-design operating characteristics of the engine and the resulting operating lines for each major component. Changing the nozzle throat area from its original design value will change the engine design and the operating characteristics of the engine at both on- and off-design conditions.

At times, it is necessary to change the off-design operation of an engine in only a few operating regions, and variation of the throat area of the exhaust nozzle may provide the needed change. At reduced engine corrected mass flow rates (normally corresponding to reduced engine throttle settings), the operating line of a multistage compressor moves closer to the stall or surge line (see Fig. 10.53). Steady-state operation close to the stall or surge line is not desirable because transient operation may cause the compressor to stall or surge. The operating line can be moved away from the stall or surge line by increasing the exhaust nozzle throat area, as shown in Fig. 10.53. This increase in nozzle throat area reduces the engine backpressure and increases the corrected mass flow rate through the compressor (see Figs. 8.9 and 10.53).

Large changes in the exhaust nozzle throat area are required for afterburning engines to compensate for the large changes in total temperature leaving the

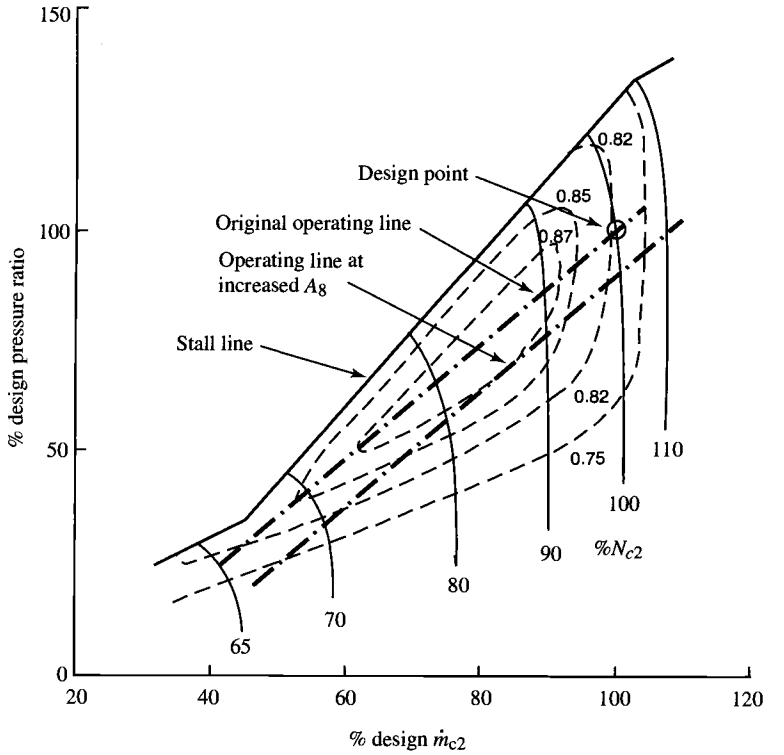

Fig. 10.53 Compressor map with exhaust nozzle area change.

afterburner. The variable-area nozzle required for an afterburning engine can also be used for back pressure control at its nonafterburning settings.

One advantage of the variable-area exhaust nozzle is that it improves the starting of the engine. Opening the nozzle throat area to its maximum value reduces the backpressure on the turbine and increases its expansion ratio. Thus the necessary turbine power for starting operation may be produced at a lower turbine inlet temperature. Also, because the backpressure on the gas generator is reduced, the compressor may be started at a lower engine speed, which reduces the required size of the engine starter.

10.5.2.2 Exhaust nozzle area ratio. Maximum engine thrust is realized for ideal flow when the exhaust nozzle flow is expanded to ambient pressure ($P_e = P_0$). When the nozzle pressure ratio is above choking, supersonic expansion occurs between aft-facing surfaces. A small amount of underexpansion is less harmful to aircraft and engine performance than overexpansion. Overexpansion can produce regions of separated flow in the nozzle and on the aft end of the aircraft, reducing aircraft performance.

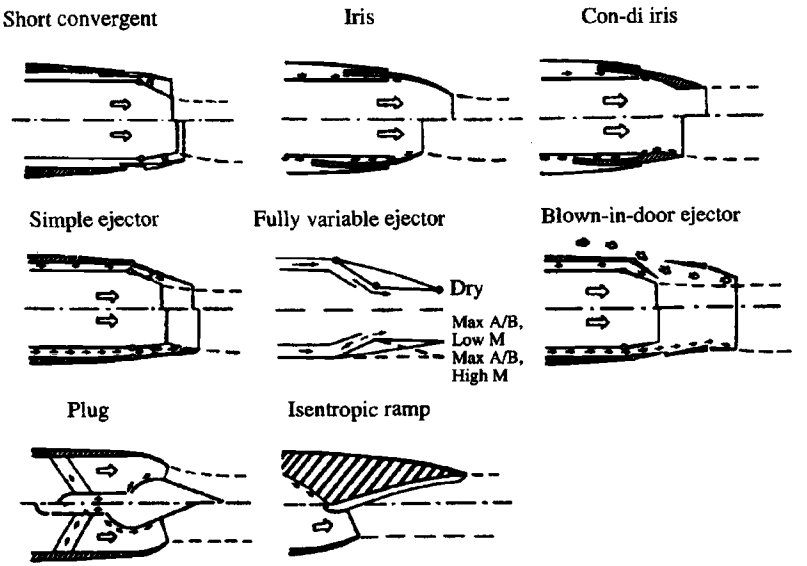

Fig. 10.54 Typical nozzle concepts for afterburning engines (Ref. 67).

The exhaust nozzle pressure ratio P_{te}/P_0 is a strong function of flight Mach number. Whereas convergent nozzles are usually used on subsonic aircraft, convergent-divergent nozzles are usually used for supersonic aircraft. When afterburning engine operation is required, complex variable-geometry nozzles must be used (see Fig. 10.52). Most of the nozzles shown in Fig. 10.54 are convergent-divergent nozzles with variable throat and exit areas. The throat area of the nozzle is controlled to satisfy engine backpressure requirements, and the exit area is scheduled with the throat area. The sophisticated nozzles of the F-15 and B-1 aircraft have two schedules: a low-speed mode and a high-speed mode.[67]

10.5.2.3 Thrust reversing and thrust vectoring. The need for thrust reversing and thrust vectoring is normally determined by the required aircraft and engine system performance. Thrust reversers are used on commercial transports to supplement the brakes. In-flight thrust reversal has been shown to enhance combat effectiveness of fighter aircraft.[67]

Two basic types of thrust reversers are used: the cascade-blocker type and the clamshell type (Fig. 10.55). In the cascade-blocker type, the primary nozzle exit is blocked off, and cascades are opened in the upstream portion of the nozzle duct to reverse the flow. In the clamshell type, the exhaust jet is split and reversed by the clamshell. Because both types usually provide a change in effective throat area during deployment or when deployed, most reversers are designed such that the effective nozzle throat area increases during the brief transitory period, thus preventing compressor stall. High bypass turbofan engines use cascade-blocker type thrust reverser in the fan nozzle.

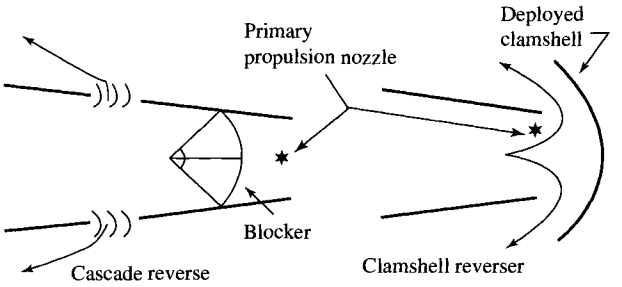

Fig. 10.55 Thrust reversers (Ref. 67).

The exhaust system for the Concorde is shown in Fig. 10.56a. There are two nozzles, a primary nozzle and a secondary nozzle. The secondary nozzle is positioned as a convergent nozzle for takeoff and as a divergent nozzle for supersonic cruise. The modes of operation for this exhaust system are shown in Fig. 10.49 along with the inlet.

Development of thrust vectoring nozzles for combat aircraft has increased in the last decade. Vectoring nozzles have been used on vertical takeoff and landing (VTOL) aircraft, such as the AV-8 Harrier and F-35 Joint Strike Fighter, and are proposed for future fighters to improve maneuvering and augment lift in combat.

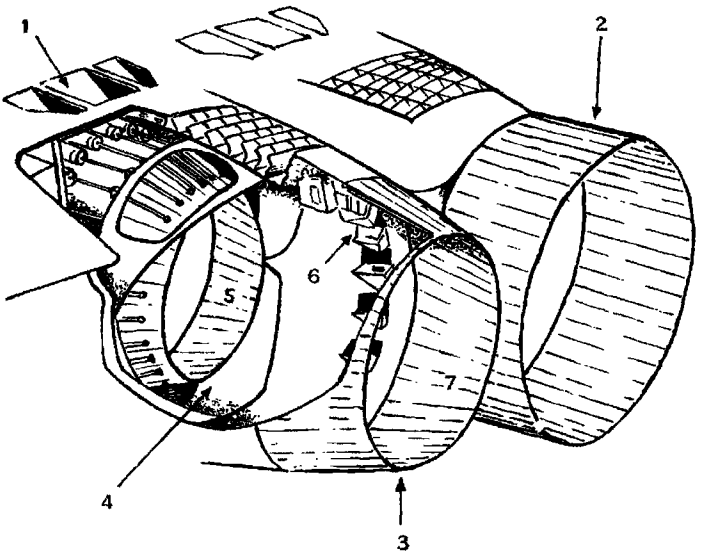

Details of the exhaust system: (1) tertiary doors; (2) nozzle in supersonic configuration; (3) subsonic configuration; (4) thrust reverse buckets; (5) primary nozzle; (6) silencer lobes; (7) secondary nozzle

Fig. 10.56a Concorde exhaust system.

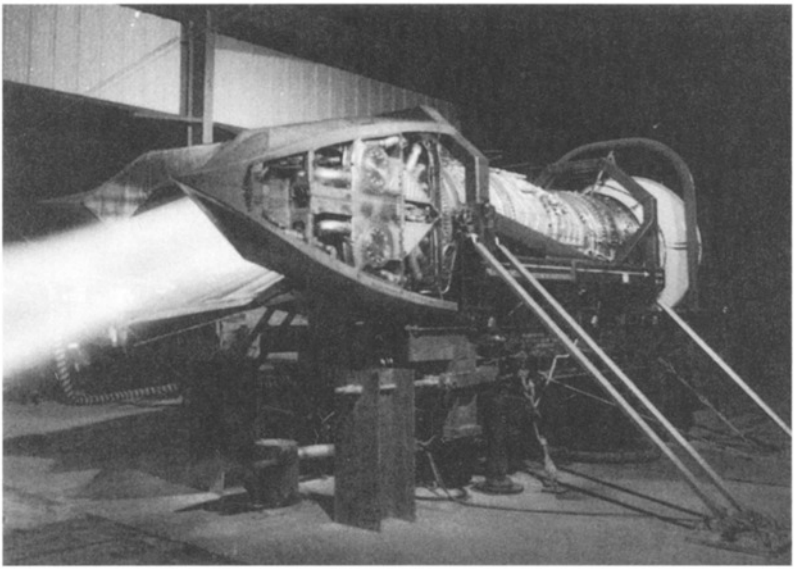

Fig. 10.56b Pratt & Whitney F119-PW-100 turbofan engine with two-dimensional thrust vectoring nozzle. (Courtesy of Pratt & Whitney.)

Thrust vectoring at augmented power settings is being developed for use in future fighters. However, cooling of the nozzle walls in contact with the hot turning or stagnating flows is very difficult and will require increased amounts of nozzle-cooling airflow. The operation of the Pratt & Whitney F119-PW-100 augmented turbofan engine's thrust vectoring nozzle is shown in Fig. 10.56b. This two-dimensional nozzle was developed for use in the F-22 Advanced Tactical Fighter.

Figure 10.57 shows the schematic of a two-dimensional convergent-divergent nozzle with thrust vectoring of ± 15 deg and thrust reversing. This is typical of the capabilities sought for use in future fighter aircraft.

10.5.2.4 Infrared signature. The rear of the engine is very hot and can produce a large infrared signature. Considerable effort is being used in modern military aircraft to reduce this signature. Most effective methods involve hiding the exit of the low-pressure turbine from direct view. Shown in Fig. 10.58 is a platypus exhaust duct used on the F-117A Nighthawk stealth fighter. This exhaust nozzle is canted up 10 deg to prevent ling-of-sight to the turbine face.[60,68] For afterburning engines, the nozzle in concert with the devices (e.g., flameholders) downstream of the turbine can hide the turbine exit and thus reduce high temperature signatures. Generally speaking, reduced engine performance is the cost of stealth.

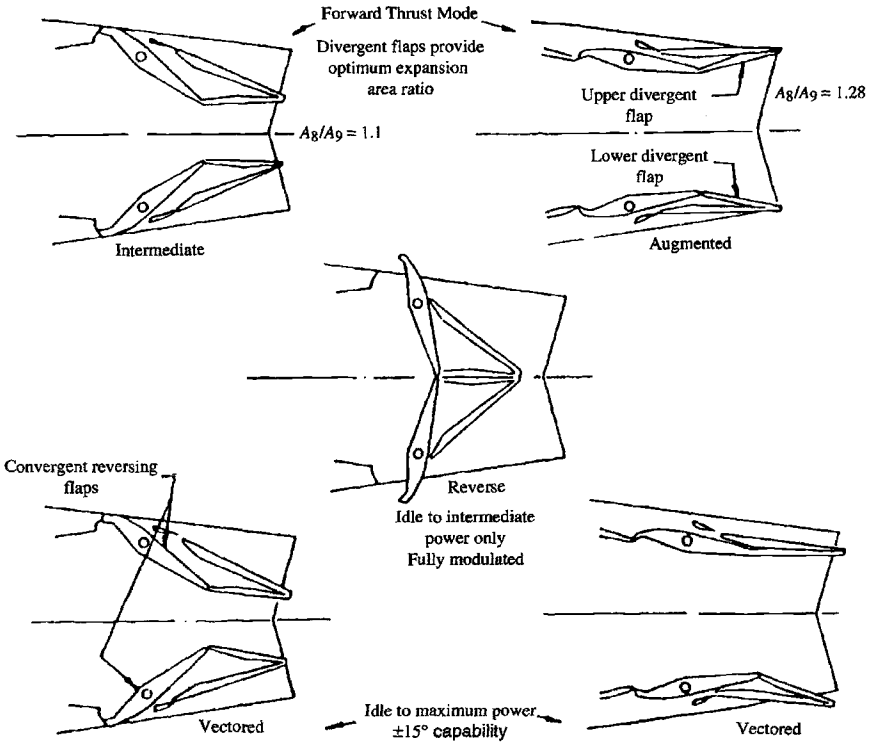

Fig. 10.57 Typical two-dimensional thrust vectoring nozzle with thrust reversing (Ref. 68).

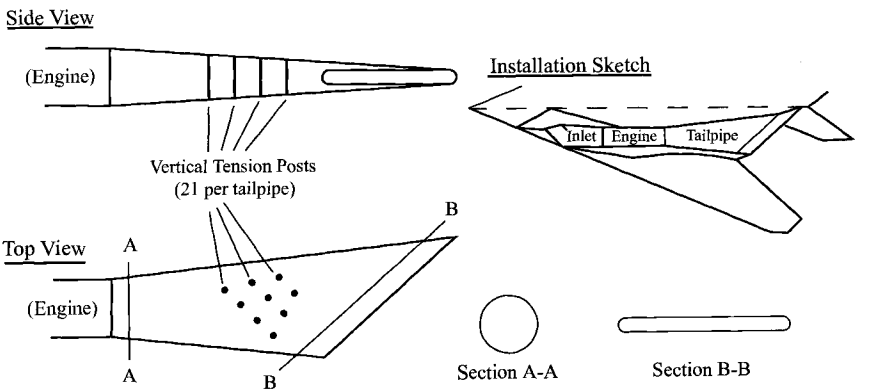

Fig. 10.58 Exhaust nozzle of F-117A (from Ref. 68).

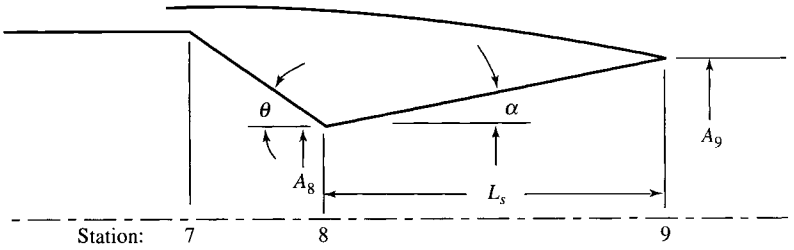

A_8 = Primary nozzle throat area
A_9 = Secondary nozzle exit area
α = Secondary nozzle half-angle
θ = Primary nozzle half-angle
L_s = Secondary nozzle length

Fig. 10.59 Nozzle geometric parameters.

10.5.3 Nozzle Coefficients

Nozzle performance is ordinarily evaluated by two dimensionless coefficients: the gross thrust coefficient and the discharge or flow coefficient. Figure 10.59 shows a convergent-divergent exhaust nozzle with the geometric parameters used in the following definitions of nozzle coefficients. Only total pressure losses downstream of station 8 are included in the gross thrust coefficient.

10.5.3.1 Gross thrust coefficient. The *gross thrust coefficient* C_{fg} is the ratio of the actual gross thrust $F_{g\,\text{actual}}$ to the ideal gross thrust $F_{g\,\text{ideal}}$, or

$$C_{fg} \equiv \frac{F_{g\,\text{actual}}}{F_{g\,\text{ideal}}} \tag{10.17}$$

Empirically derived coefficients are applied to Eq. (10.17) to account for the losses and directionality of the actual nozzle flow. Each engine organization uses somewhat different coefficients, but each of the following basic losses is accounted for:

1) Thrust loss due to exhaust velocity vector angularity
2) Thrust loss due to the reduction in velocity magnitude caused by friction in the boundary layers
3) Thrust loss due to loss of mass flow between stations 7 and 9 from leakage through the nozzle walls
4) Thrust loss due to flow nonuniformities

10.5.3.2 Discharge or flow coefficient. The ratio of the actual mass flow $\dot{m}_8$ to the ideal mass flow $\dot{m}_{8i}$ is called the *discharge coefficient* C_D:

$$C_D \equiv \frac{\dot{m}_8}{\dot{m}_{8i}} \tag{10.18}$$

This coefficient can be shown to be identically equal to the ratio of the effective one-dimensional flow area required to pass the total actual nozzle flow A_{8e} to the nozzle physical throat area A_8 as follows:

$$C_D = \frac{\dot{m}_8}{\dot{m}_{8i}} = \frac{\rho_8 V_8 A_{8e}}{\rho_8 V_8 A_8} = \frac{A_{8e}}{A_8}$$

The variation of the discharge coefficient with nozzle pressure ratio is shown in Fig. 10.60a for a conic convergent nozzle. When the nozzle is choked, the

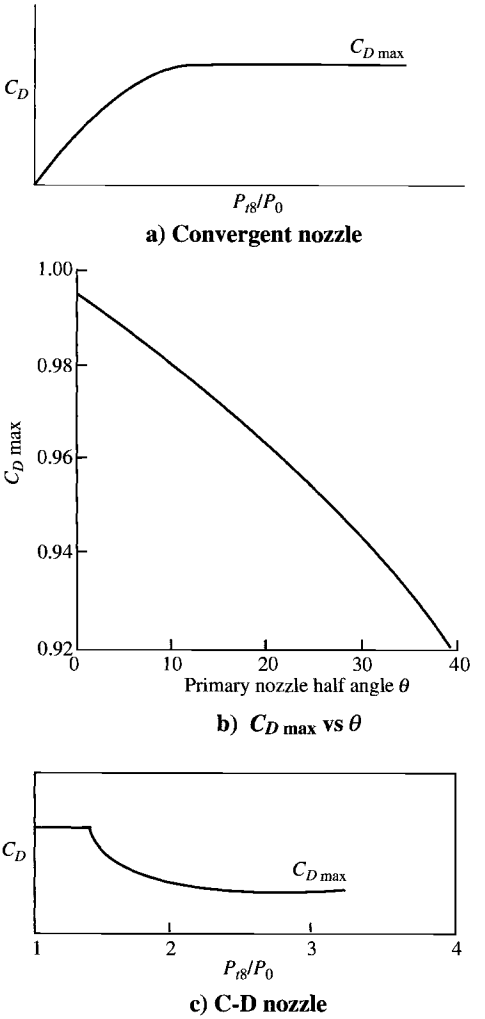

a) Convergent nozzle

b) $C_{D\,max}$ vs θ

c) C-D nozzle

Fig. 10.60 Nozzle discharge coefficient (Ref. 67).

discharge coefficient reaches a maximum value $C_{D\max}$. The value of $C_{D\max}$ is a function of the primary nozzle half-angle θ, as shown in Fig. 10.60b. Figure 10.60c shows the variation in discharge coefficient for a convergent-divergent nozzle with nozzle pressure ratio. Note the change in behavior of C_D between that of the convergent-divergent nozzle and that of the convergent nozzle as the nozzle pressure ratio drops below choking. This is due to the venturi behavior of the convergent-divergent nozzle.

The discharge coefficient is used to size the nozzle throat area to pass the desired mass flow rate. For example, consider a nozzle with

$$\dot{m}_8 = 200\,\text{lbm/s}, \quad P_{t8} = 30\,\text{psia}, \quad T_{t8} = 2000^\circ\text{R}, \quad \gamma = 1.33$$
$$R = 53.34\,\text{ft} \cdot \text{lbf/(lbm} \cdot {}^\circ\text{R)}, \quad \theta = 20\,\text{deg}$$

At $M_8 = 1$, GASTAB with $\gamma = 1.33$ and $\mathscr{M} = 28.97$, then MFP = 0.5224, and thus $A_{8e} = 570.7\,\text{in.}^2$. Figure 10.60b gives $C_{D\max} = 0.96$ for $\theta = 20\,\text{deg}$ and thus the required throat area is $594.5\,\text{in.}^2$.

10.5.3.3 Velocity coefficient. The *velocity coefficient* C_V is the ratio of the actual exit velocity V_9 to the ideal exit velocity V_{9i} corresponding to $P_{t9} = P_{t8}$, or

$$C_V \equiv \frac{V_9}{V_{9i}} \tag{10.19}$$

and represents the effect of frictional loss in the boundary layer of the nozzle. It is mainly a function of the nozzle ratio A_8/A_9 and the half-angle α, as shown in Fig. 10.61.

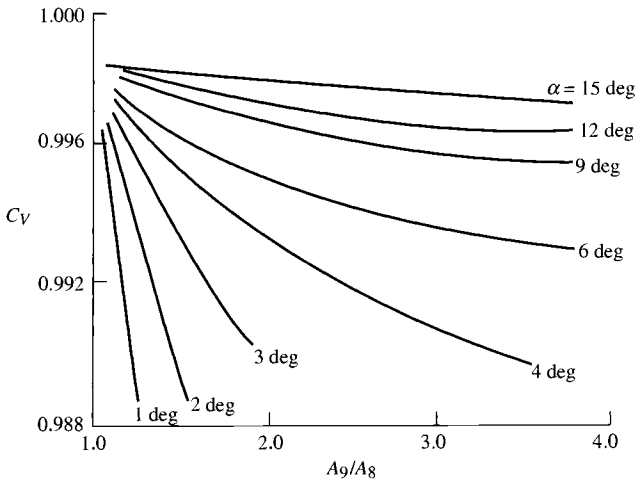

Fig. 10.61 C-D nozzle velocity coefficient (Ref. 67).

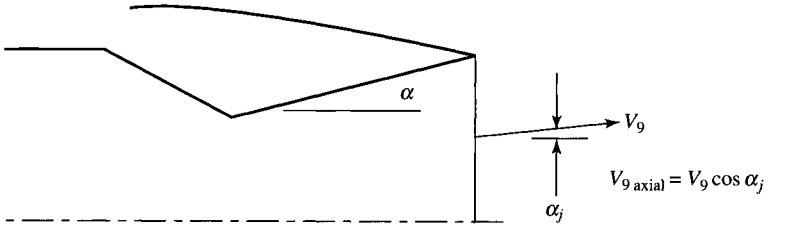

Fig. 10.62 Local angularity coefficient.

10.5.3.4 Angularity coefficient. The *angularity coefficient* C_A represents the axial friction of the nozzle momentum; thus it is proportional to the thrust loss due to the nonaxial exit of the exhaust gas (see Fig. 10.62). For a differential element of flow, this coefficient is the cosine of the local exit flow angle α_j.

The local flow angle α_j varies from zero at the centerline to α at the outer wall; thus, the nozzle angularity coefficient is the integral of α_j across the nozzle:

$$C_A \equiv \frac{1}{\dot{m}} \int \cos \alpha_j \, d\dot{m} \tag{10.20}$$

Figure 10.63 presents the correlation of the angularity coefficient with the nozzle area ratio A_8/A_9 and half-angle α. This figure is based on analytical evaluations of the inviscid flowfield in convergent-divergent nozzles for a range of practical nozzle geometries.

10.5.4 Nozzle Performance

Many nozzle coefficients simplify to algebraic expressions or become unity for the special case of *one-dimensional adiabatic flow*. This is a useful

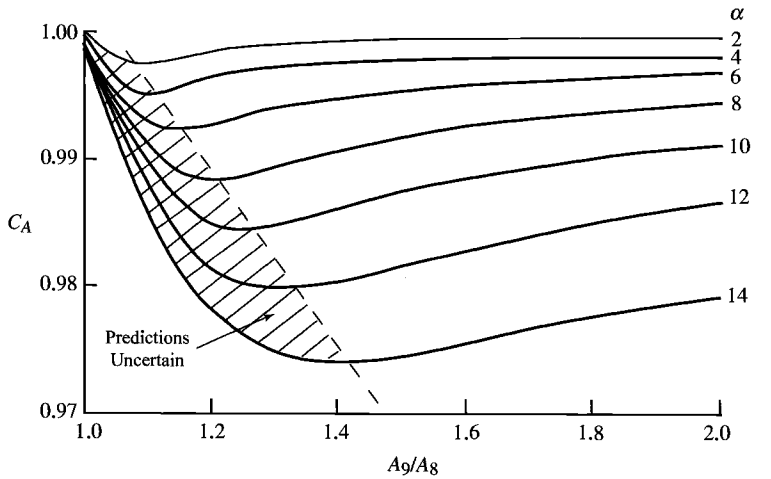

Fig. 10.63 C-D nozzle angularity coefficient (Ref. 67).

limit for understanding each coefficient and for preliminary analysis of nozzle performance using engine cycle performance data.

For one-dimensional adiabatic flow, $C_A = 1$,

$$C_D = \frac{\dot{m}_8}{\dot{m}_{8i}} = \frac{A_{8e}}{A_8} = \frac{P_{t8}}{P_{t7}}$$

and the velocity coefficient C_V is given by [Eq. (10.19)]

$$C_V \equiv \frac{V_9}{V_{9i}}$$

where V_9 is the exit velocity corresponding to T_{t8} and $(A/A^*)_9 = (P_{t9}/P_{t8}) \times [A_9/(C_D A_8)]$ and V_{9i} is the ideal exit velocity corresponding to T_{t8} and $(A/A^*)_{9i} = A_9/(C_D A_8)$.

The gross thrust for a one-dimensional flow can be expressed as

$$F_{g\,\text{actual}} = \frac{\dot{m}_8 V_9}{g_c} + (P_9 - P_0)A_9 \tag{10.21}$$

and the ideal gross thrust (corresponds to $P_9 = P_0$) as

$$F_{g\,\text{ideal}} = \frac{\dot{m}_{8i} V_s}{g_c} \tag{10.22}$$

where V_s is the isentropic exit velocity based on P_{t8}/P_0 and T_{t8}.

For one-dimensional flow of a calorically perfect gas, Eq. (10.21) can be written as

$$F_{g\,\text{actual}} = \frac{\dot{m}_8 V_9}{g_c}\left[1 + \frac{\gamma - 1}{2\gamma}\frac{1 - P_0/P_9}{(P_{t9}/P_9)^{(\gamma-1)/\gamma} - 1}\right] \tag{10.23}$$

The gross thrust coefficient for one-dimensional flow of a calorically perfect gas can be obtained by substituting Eqs. (10.22) and (10.23) into Eq. (10.17), giving

$$C_{fg} = C_D C_V \sqrt{\frac{1 - (P_{9i}/P_{t8})^{(\gamma-1)/\gamma}}{1 - (P_0/P_{t8})^{(\gamma-1)/\gamma}}}\left[1 + \frac{\gamma - 1}{2\gamma}\frac{1 - P_0/P_9}{(P_{t9}/P_9)^{(\gamma-1)/\gamma} - 1}\right] \tag{10.24}$$

This equation reduces to $C_{fg} = C_D C_V$ for the ideal expansion ($P_9 = P_{9i} = P_0$). For isentropic flow, $P_9 = P_{9i}$, $P_{t9} = P_{t8}$, $C_V = 1$, and $C_D = 1$.

Equation (10.24) is plotted in Fig. 10.64 for isentropic flow vs the nozzle area ratio A_9/A_8 for different nozzle pressure ratios P_{t8}/P_0. Note that ideal expansion ($P_9 = P_0$) gives a gross thrust coefficient of unity and that both underexpansion

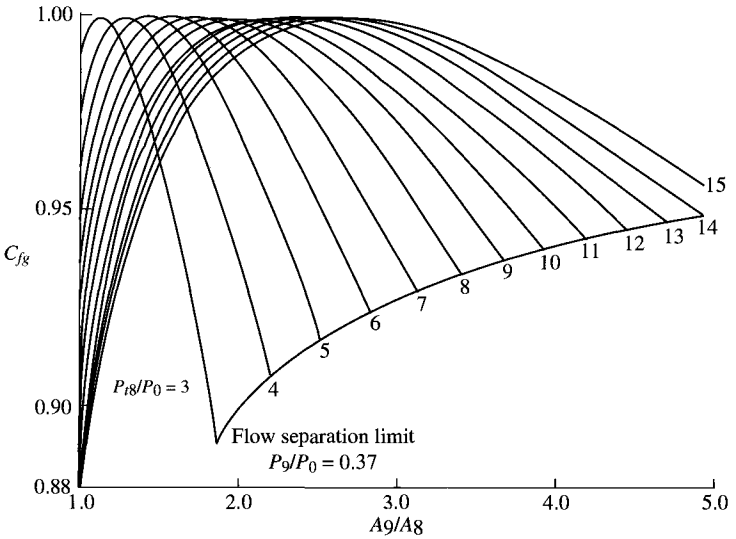

Fig. 10.64 Thrust coefficient for one-dimensional isentropic flow ($\gamma = 1.3$).

($P_9 > P_0$) and overexpansion ($P_9 < P_0$) reduces the gross thrust coefficient below unity.

The extent of overexpansion in nozzles is limited by flow separation resulting from the interaction of the nozzle boundary layer and the strong oblique shock waves at the exit of the nozzle. In extreme overexpansion, Summerfield et al.[20] noted that the oblique shock waves moved from the exit lip into the nozzle (see Fig. 3.17), the flow downstream of the shock waves was separated in the vicinity of the wall, and as a result, the wall static pressure downstream of the shock waves was nearly equal to the ambient pressure P_0. A simple estimate for the ratio of the pressure just preceding the shock waves P_s to the ambient pressure P_0, suggested by Summerfield et al.,[20] is given by

$$\frac{P_s}{P_0} \approx 0.37 \tag{10.25}$$

This flow separation limit can be included in the one-dimensional gross thrust coefficient of Eq. (10.24) for isentropic flow by considering the effective exit pressure ($P_9 = P_{9i}$) to be the pressure just preceding the shock wave (P_s). Equations (10.24) and (10.25) were used to obtain the flow separation limit shown in Fig. 10.64. The design area ratio A_9/A_8 of convergent-divergent nozzles is selected such that the nozzle flow does not separate due to overexpansion for most throttle settings. This is because the increase in gross thrust coefficient associated with flow separation does not normally offset the accompanying increase in installation loss.

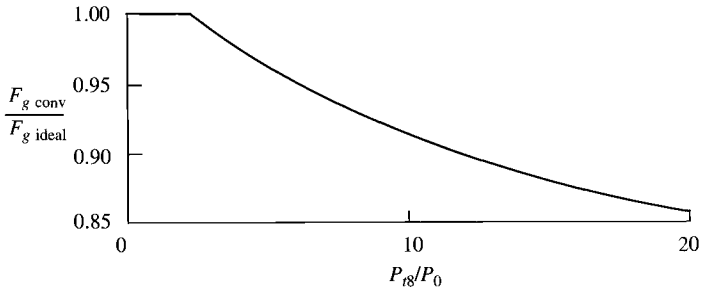

Fig. 10.65 Ratio of convergent nozzle gross thrust to ideal gross thrust vs pressure ratio ($\gamma = 1.3$).

Nozzle pressure ratios are 3 to 5 in the subsonic cruise speed range of turbofan and turbojet engines. Typically, a subsonic engine uses a convergent exhaust nozzle. This is because, in the nozzle pressure range of 3 to 5, the convergent gross thrust (interception of lines with vertical axis, $A_9/A_8 = 1$) is 1–3% below the peak gross thrust ($P_9 = P_0$). Consequently, there may be insufficient gross thrust increase available in going to a convergent-divergent nozzle on a subsonic cruise turbofan or turbojet engine to pay for the added drag and weight of such a nozzle. In some applications, this loss in gross thrust coefficient of a convergent nozzle is too much, and a C-D nozzle is used.

The design pressure ratio across the nozzle increases rapidly with supersonic flight Mach number. At Mach 2, a pressure ratio of about 12 is typical. At this pressure ratio, the convergent nozzle gross thrust penalty is about 9%, as shown in Fig. 10.65. This figure is a plot of the ratio of the gross thrust in Fig. 10.64 of a convergent nozzle ($A_9/A_8 = 1$) to the peak thrust ($P_9 = P_0$) vs P_{t8}/P_0. Substitution of convergent-divergent nozzles for convergent nozzles provides large thrust gains for supersonic aircraft.

Example 10.5

Consider the calculation based on one-dimensional flow.

Given:

$$\dot{m}_8 = 200 \text{ lbm/s} \quad P_{t8} = 30 \text{ psia} \quad T_{t8} = 2000^\circ\text{R}$$

$$\frac{A_9}{A_8} = 2.0 \quad \gamma = 1.33 \quad R = 53.34 \text{ ft} \cdot \text{lbf/(lbm} \cdot {}^\circ\text{R)}$$

$$\frac{P_{t9}}{P_{t8}} = 0.98 \quad C_D = 0.98 \quad P_0 = 5 \text{ psia}$$

Find the dimensions of an axisymmetric nozzle and the vaues of C_{fg}, F_g, and C_V.

Solution: At $M_8 = 1$ GASTAB with $\gamma = 1.33$ and $\mathscr{M} = 28.97$, then MFP = 0.5224, thus

$$A_{8e} = \frac{\dot{m}_8\sqrt{T_{t8}}}{P_{t8}\text{MFP}(M_8 = 1)} = \frac{200\sqrt{2000}}{30 \times 0.5224} = 570.7 \text{ in.}^2$$

With $C_D = 0.98$, thus $A_8 = 582.3$ in.^{2} and $r_8 = 13.61$ in. Since $A_9/A_8 = 2.0$, then $A_9 = 1165$ in.^{2} and $r_9 = 19.25$ in.:

$$\left(\frac{A}{A^*}\right)_{9i} = \frac{A_9}{C_D A_8} = \frac{2.0}{0.98} = 2.041 \longrightarrow M_{9i} = 2.168 \quad \text{and} \quad \frac{P_{9i}}{P_{t9i}} = 0.0990$$

Thus, $P_{9i} = (0.0990)(30 \text{ psia}) = 2.970$ psia,

$$V_{9i} = \sqrt{Rg_c T_{t8}}\sqrt{\frac{2\gamma}{\gamma - 1}\left[1 - \left(\frac{P_{9i}}{P_{t8}}\right)^{(\gamma-1)/\gamma}\right]}$$

$$V_{9i} = \sqrt{(1716)(2000)}\sqrt{\frac{2(1.33)}{0.33}[1 - (0.0990)^{0.33/1.33}]} = 3475 \text{ ft/s}$$

$$\left(\frac{A}{A^*}\right)_9 = \frac{P_{t9}}{P_{t8}}\frac{A_9}{C_D A_8} = \frac{0.98 \times 2.0}{0.98} = 2.0 \longrightarrow M_9 = 2.146 \quad \text{and} \quad \frac{P_9}{P_{t9}} = 0.1025$$

Thus, $P_9 = (0.1025)(0.98)(30 \text{ psia}) = 3.014$ psia,

$$V_9 = \sqrt{(1716)(2000)}\sqrt{\frac{2(1.33)}{0.33}[1 - (0.1025)^{0.33/1.33}]} = 3456 \text{ ft/s}$$

$$C_V = \frac{V_9}{V_{9_i}} = 0.9945$$

$$C_{fg} = (0.98)(0.9945)\sqrt{\frac{1 - (2.97/30)^{0.33/1.33}}{1 - (5.0/30)^{0.33/1.33}}} \times \left[1 + \frac{0.33}{2 \times 1.33}\frac{1 - 5.0/3.014}{(29.4/3.014)^{0.33/1.33} - 1}\right]$$

$$= 0.9593$$

Figure 10.3b gives $\theta = 10$ deg for $C_D = 0.98$. Likewise, Fig. 10.64 gives $\alpha = 6$ deg for $C_V = 0.9945$ and $A_9/A_8 = 2$. Thus $L_s = 54$ in. and the dimensions of the exhaust nozzle are shown in Fig. 10.66. The gross thrust can be calculated

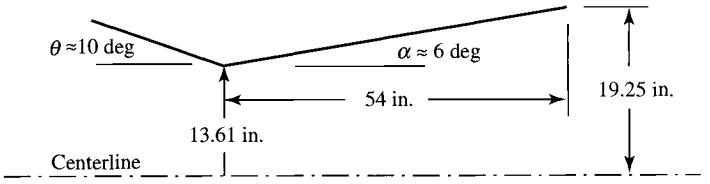

Fig. 10.66 Dimensions of Example 10.5 exhaust nozzle.

in several ways: directly from Eq. (10.23),

$$F_{g\,\text{actual}} = \frac{\dot{m}_8 V_9}{g_c} + (P_9 - P_0)A_9$$

$$= \frac{(200)(3456)}{32.174} + (3.014 - 5.0)(1165) = 19{,}170 \text{ lbf}$$

or from the ideal gross thrust and C_{fg} with

$$V_s = \sqrt{(1716)(2000)}\sqrt{\frac{2(1.33)}{0.33}\left[1 - \left(\frac{5}{30}\right)^{0.33/1.33}\right]} = 3151 \text{ ft/s}$$

then

$$F_{g\,\text{ideal}} = \frac{\dot{m}_{8t} V_s}{g_c} = \frac{(200/0.98)(3151)}{32.174} = 19{,}990 \text{ lbf}$$

$$F_{g\,\text{actual}} = C_{fg} F_{g\,\text{ideal}} = (0.9593)(19{,}990) = 19{,}170 \text{ lbf}$$

10.6 Introduction to Combustion Systems

Combustion systems of aircraft gas turbine engines largely encompass the main burners (also called *burners or combustors*) and afterburners (also called *augmenters or reheaters*). Both main burners and afterburners are covered in this section because they have many basic principles in common. The basic principles of the combustion process, combustion stability, total pressure ratio, length scaling, diffusers, and fuels are presented in the following sections and provide the means for understanding the design of the main burner and afterburner.

The thermal energy of the air/fuel mixture (reactants) flowing through an airbreathing engine is increased by the combustion process. The fuel must be vaporized and mixed with the air before this chemical reaction can occur. Once this is done, the combustion process can occur and thus increase the thermal energy of the mixture (products of combustion). All of this takes time and space.

The design of the main burner and afterburner of an airbreathing engine differs in many ways from that of conventional combustion devices. Space (especially length) is at a premium in aircraft applications, and the length of the combustion chamber is reduced by hastening completion of the combustion process. The combustion intensity (rate of energy released per unit volume) is much higher for the main burner of a turbojet [40,000 Btu/(s · ft^3) or 11,150 MW/m^3] compared to a typical steam power plant [10 Btu/(s · ft^3) or 2.8 MW/m^3]. The following properties of the combustion chambers are desired:

1) Complete combustion
2) Low total pressure loss
3) Stability of combustion process
4) Proper temperature distribution at exit with no "hot spots"
5) Short length and small cross section
6) Freedom from flameout
7) Relightability
8) Operation over a wide range of mass flow rates, pressures, and temperatures

However, many of these desirable properties are in competition. For example, both complete combustion and low total pressure loss are contrary to small size. Hence the design of a main burner or afterburner is a compromise. We examine many of these desirable combustion properties in order to understand the design and operation of main burners and afterburners, starting with the combustion process.

10.6.1 Combustion Process

The combustion processes occur with the vaporized fuel and air mixed on a molecular scale. The rate of this reaction depends on both the static pressure P and temperature T in a very complex way. For many situations, the reaction rate can be approximated by a form of the Arrhenius equation[67,69] written for the mass rate of reaction as

$$\text{Reaction rate} \propto P^n f(T) \exp \frac{-E}{\mathscr{R}T} \tag{10.26}$$

where n is an exponent that depends on the number of molecules involved in a reactive collision (for example, $n = 2$ for two molecules, $n = 3$ for three molecules); $f(T)$ is a function that relates the reaction rate to the forms of energy (translation, rotation, and vibration) the molecules have; the term $\exp[-E/(\mathscr{R}T)]$ accounts for the number of molecular collisions in which the energy of one molecule relative to another exceeds the activation energy E; and $\mathscr{R}$ is the universal gas constant.

For hydrocarbon-air combustion, $n = 1.8$. At low pressures, the reaction rate becomes slow and can become limiting for aircraft engines at very high altitudes. However, under most operating conditions, the rate of combustion is limited by the rate at which the fuel is vaporized and mixed with air. In most combustors, the fuel is injected as an atomized liquid-droplet spray into the hot reaction zone where it mixes with air and hot combustion gases. The atomized fuel vaporizes,

and then the vapor is mixed with air. If the temperature and pressure in the reaction zone are sufficiently high, the reaction rate will be fast and the fuel vapor will react as it comes in contact with sufficient oxygen.

The stoichiometric fuel/air ratio for the typical hydrocarbon fuel can be estimated by assuming octane as a representative hydrocarbon and writing the stoichiometric chemical reaction:

$$2C_8H_{18} + 25\left(O_2 + \frac{79}{21}N_2\right) \longrightarrow 16CO_2 + 18H_2O + 25\left(\frac{79}{21}\right)N_2$$

For this reason, the stoichiometric fuel/air ratio is found to be

$$f_{\text{stoich}} = \frac{2(96 + 18)}{25[32 + (79/21)28]} = 0.0664$$

The *equivalence ratio* ϕ is the actual fuel/air ratio divided by the fuel/air ratio required for complete combustion (stoichiometric fuel/air ratio), or

$$\phi \equiv \frac{f}{f_{\text{stoich}}} \tag{10.27}$$

The equivalence ratio ϕ is greater than 1.0 for rich fuel/air ratio and less than 1.0 for a lean fuel/air mixture. To prevent excessive temperatures at the exit of the main burner or afterburner and protect its walls, the overall fuel/air ratio must be much less than stoichiometric with $\phi < 1.0$.

As an example, an engine being flown at Mach 0.9, a 12-km altitude, and full throttle with a compressor pressure ratio of 20 and 85% isentropic efficiency will have a compressor pressure outlet temperature of about 653 K. If the turbine inlet temperature is limited to 1670 K, h_{PR} is 42,800 kJ/kg, and c_{pc} and c_{pt} are 1.004 and 1.235 kJ/(kg · K), then the fuel/air ratio for 100% efficient combustion in the main burner is, from Eq. (7.9),

$$f = \frac{1.235 \times 1670 - 1.004 \times 653}{42{,}800 - 1.235 \times 1670} = 0.0346$$

which corresponds to an overall equivalence ratio of 0.519 for a main burner using JP-8 fuel ($f_{\text{stoich}} = 0.0667$).

Figure 10.67 shows the flammability characteristics of a kerosene-type fuel. The 0.52 equivalence ratio of the preceding example is at the lower limit of flammability shown in Fig. 10.67. This presents a design problem at the full-throttle value of ϕ and at the engine's partial-throttle values of ϕ. The problem of lean mixtures in a burner can be overcome by mixing and burning a rich fuel/air mixture in a small region where the local equivalence ratio is near unity. By using only a portion of the total air in a region, a locally rich mixture can be efficiently burned and then the products of combustion diluted and cooled to an acceptable turbine inlet temperature by the remaining air (see Fig. 10.77).

At usual pressures and temperatures, hydrocarbon/air mixtures will react over only a rather narrow range of ϕ—from approximately 0.5 to 3 and not at all below

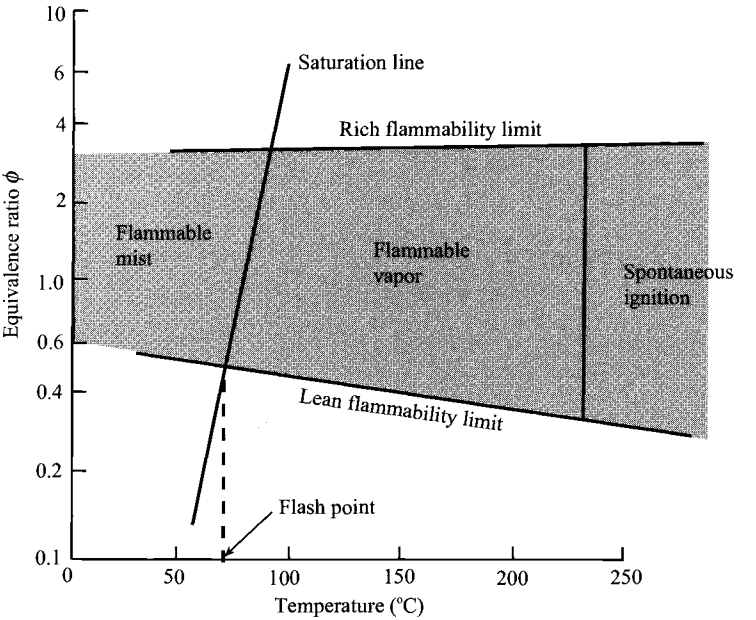

Fig. 10.67 Flammability characteristics for a kerosene type fuel in air at atmospheric pressure (Refs. 38 and 67).

0.2 atm at standard temperature. Hydrogen has much wider flammability limits than do hydrocarbons—approximately $0.25 < \phi < 6$ at standard temperature and 1 atm. Some special, rather expensive fuels have flammability limits intermediate between hydrogen and hydrocarbons. These special fuels have been used at times for testing and for extending the altitude limits of engines for special applications.

A limitation is imposed by the combustion because it is necessary to maintain a stationary flame within a high-velocity airstream. Imagine the flame as propagating through the combustible mixture at the flame speed, while the mixture is carried downstream. To have a stable flame, the velocity of the mixture must be maintained within certain limits: If the velocity is too high, the flame will be "blown out" the exit; if it is too low, the flame will travel upstream and be extinguished. This problem of holding the combustion flame within the combustion system is solved by establishing regions of recirculation at the front of the main burner (see Fig. 10.77) or behind a bluff body, called a *flame holder*, at the front of an afterburner (see Fig. 10.87). These regions of recirculation create areas of local low velocity that "hold" the flame, and at the same time, the resulting turbulence gently increases the rate of energy transfer from these regions.

Provided stable combustion is attained, complete combustion in the case of lean mixtures is virtually ensured since, with excess oxygen, local fuel-rich areas are unlikely. On the other hand, combustion of a near-stoichiometric

mixture requires an essentially uniform distribution of constituents to avoid wasting some fuel in local fuel-rich (oxygen-poor) regions.

10.6.2 Ignition

Ignition of a fuel/air mixture in a turbine engine combustion system requires inlet air and fuel conditions within flammability limits, sufficient residence time of a combustible mixture, and location of an effective ignition source in the vicinity of the combustible mixture. The flammability limits for a kerosene-type fuel are shown in Fig. 10.67. Note that the flammability region is further subdivided into two regions separated by the *spontaneous ignition temperature* (SIT). The spontaneous ignition temperature is the lowest temperature at which visible or audible evidence of combustion is observed. Typical values of SIT are presented in Table 10.4.

When the temperature in the combustion system is below the SIT, an ignition source is required to bring the local temperature above the spontaneous ignition temperature. The minimum amount of energy necessary to achieve ignition is shown in Fig. 10.68. Note that the minimum amount of energy is not always at a stoichiometric mixture ratio. For heavy fuels, such as C_7H_{16}, the minimum is nearer $\phi = 2$.

Once the flammability limits and SIT requirements are met, then the ignition delay time becomes the key combustion characteristic. The ignition delay time t_{ign} is related to the initial temperature T by

$$t_{ign} \propto \exp \frac{E}{\mathcal{R}T} \tag{10.28}$$

Table 10.4 Spontaneous-ignition temperatures

Fuel	SIT, K
Propane	767
Butane	678
Pentane	558
Hexane	534
Heptane	496
Octane	491
Nonane	479
Decane	481
Hexadecane	478
Isooctane	691
Kerosene (JP-8 or jet A)	501
JP-3	511
JP-4	515
JP-5	506

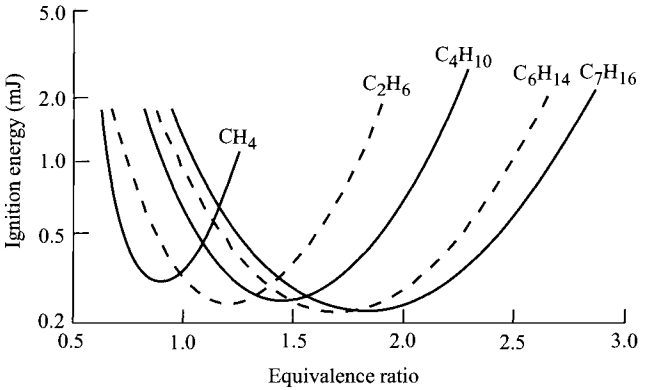

Fig. 10.68 Minimum ignition energies at standard temperature and pressure (Refs. 67 and 70).

The variation of ignition delay time with pressure has been experimentally observed to follow $t_{ign} \propto 1/P$. Ignition delay times for typical fuels are shown in Fig. 10.69.

10.6.3 Combustion Stability

The ability of the combustion process to sustain itself in a continuous manner is called *combustion stability*. Stable, efficient combustion can be upset by the fuel/air mixture becoming too lean or too rich such that the temperatures and reaction rates drop below the level necessary to effectively heat and vaporize the incoming fuel and air. Such a situation causes blowout of the combustion process. The effects of mass flow rate, combustion volume, and pressure on the stability of the combustion process are combined into the *combustor loading parameter* (CLP), defined as

$$\text{CLP} \equiv \frac{\dot{m}}{P^n(\text{combustion volume})} \tag{10.29}$$

Because the denominator of the combustor loading parameter is based on the rate of the combustion process, the pressure component n will correspond to 2 for a simple bimolecular reaction. Because of the complex set of reactions occurring when a hydrocarbon is burned in air, n has been experimentally determined to be about 1.8, and this value of n is applied for most situations. However, under high-pressure conditions, a value of 1 for n is more realistic because the chemical reaction rate is not the limiting factor and physical mixing processes play a more important role.

The method of presenting the stability characteristics of a combustion process for a gas turbine engine is based on stirred reactor theory[67,69,71,72] and shows the stable and unstable operation regions in a plot of the equivalence ratio vs the combustor loading parameter, as shown in Fig. 10.70. Spalding[72] reports

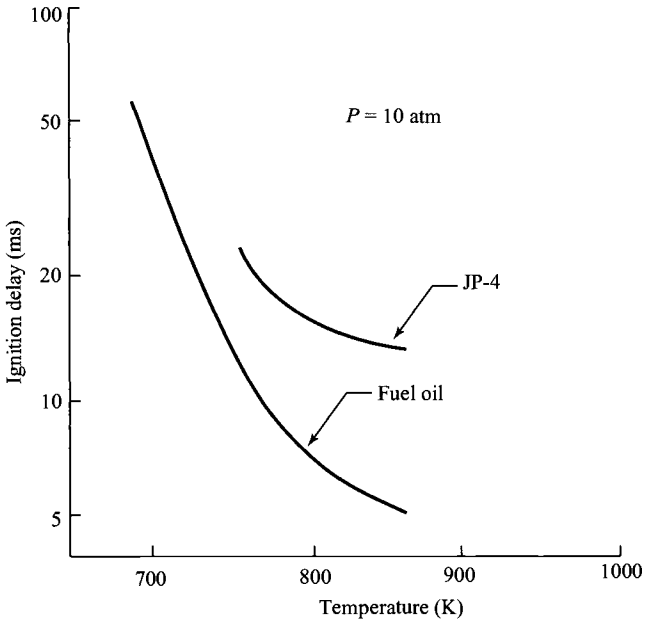

Fig. 10.69 Ignition delay times for practical fuels (Refs. 38 and 67).

the loading parameter stability limit of a stirred reactor with $n = 1.8$ as 90 lbm/$(s \cdot atm^{1.8} \cdot ft^3)$ at $\phi = 1$ and 10 lbm/$(s \cdot atm^{1.8} \cdot ft^3$ at $\phi = 0.5$ and 1.7.

10.6.4 Length Scaling

An estimate of the size of the main burner and/or afterburner is required during the engine's preliminary design. The cross-sectional area can be easily

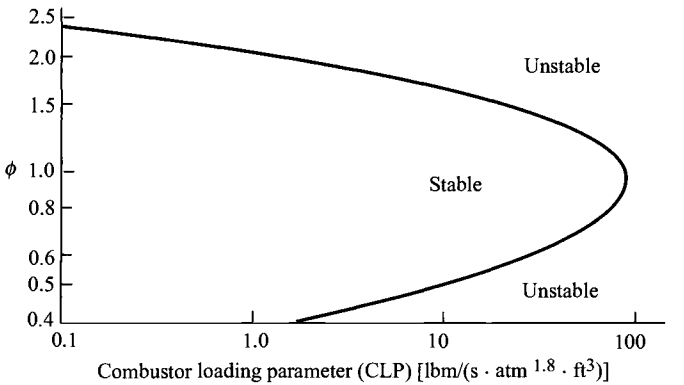

Fig. 10.70 Combustion stability characteristics (Refs. 67 and 73).

determined based on one-dimensional gas dynamics, but the length requires scaling laws. The length of a main burner is primarily based on the distance required for combustion to come to near completion. Equation (10.26) gives the reaction rate in terms of pressure and temperature and will be used to develop the length-scaling equation for main burners.

The residence time t_{res} in the main burner is given by

$$t_{\text{res}} = \frac{L}{V_{\text{av}}} \approx \frac{L}{V_{\text{ref}}} = \frac{\rho_{t3} A_{\text{ref}} L}{\dot{m}_3} \tag{10.30}$$

where V_{ref} is based on the air mass flow rate entering the combustor; A_{ref} is the cross-sectional area normal to the airflow (case to case) of the combustion chamber; L is the length of the main burner; the density of the air entering the combustion chamber is approximated by ρ_{t3}; and the other variables have their normal meanings. Assuming an isentropic compression process, the total density at state 3 is proportional to the total pressure at this state as given by

$$\rho_{t3} \propto P_{t3}^{1/\gamma_c}$$

Substituting the preceding relationship into Eq. (10.30) and solving for the main burner length yield

$$L \propto \frac{\dot{m}_3}{A_{\text{ref}}} \frac{t_{\text{res}}}{P_{t3}^{1/\gamma_c}}$$

Noting that

$$\frac{\dot{m}_3}{A_{\text{ref}}} = \frac{\dot{m}_3 A_4}{A_4 A_{\text{ref}}} = \frac{P_{t4}}{\sqrt{T_{t4}}} \frac{A_4}{A_{\text{ref}}} \frac{\text{MFP}(M_4 = 1, \gamma_4)}{1 + f}$$

(where station 4 is in the high-pressure turbine inlet stators and this flow is choked) and P_{t4} is approximately equal to P_{t3}, we see that the preceding equation for L becomes

$$L \propto \frac{P_{t3}^{(\gamma_c - 1)/\gamma_c}}{\sqrt{T_{t4}}} \frac{A_4}{A_{\text{ref}}} t_{\text{res}} \tag{10.31}$$

The reaction time t_{rea} is inversely proportional to the reaction rate. Thus from Eq. (10.26)

$$t_{\text{rea}} \propto P_{t3}^{-n} \tag{10.32}$$

Table 10.5 Contemporary main burners

Engine type	TF39 Annular	TF41 Cannular	J79 Cannular	JT9D Annular	F100 Annular	T63 Can
Mass flow						
Air, lb/s	178	135	162	242	135	3.3
Fuel, lb/h	12,850	9965	8350	16,100	10,580	235
Size						
Length, in.	20.7	16.6	19.0	17.3	18.5	9.5
Diameter, in.	33.3	5.3/24.1[a]	6.5/32.0[a]	38.0	25.0	5.4
P_{t3}, psia	382	314	198	316	366	92
$T_{t4\ \max}$, °R	2915	2620	2160	2865	3025	1840

[a]Can diameter/annulus diameter.

For the main burner, the residence time t_{res} is proportional to the reaction time t_{rea}. Thus t_{res} in Eq. (10.31) can be replaced by Eq. (10.32), giving

$$L \propto \frac{A_4}{A_{ref}\sqrt{T_{t4}}} P_{t3}^{-[n-(\gamma_c-1)/\gamma_c]} \tag{10.33}$$

For the main burners of similar design, the area ratio A_4/A_{ref} is constant and

$$L \propto P_{t3}^{-r}/\sqrt{T_{t4}} \tag{10.34}$$

where $r = 1.51$ for $n = 1.8$ and $r = 0.714$ for $n = 1$. Thus the length of main burners having similar design varies with the pressure and temperature and is unaffected by the size of the engine. This explains both the shortening of the main burner length with increases in compressor pressure ratio and the reduction in the ratio of the main burner length to engine diameter as engine size increases.

Equation (10.34) can be used to obtain a preliminary estimate of the main burner length based on a known-reference similar design. The size and sea-level operating conditions for contemporary main burners are provided in Table 10.5, and this information may be used as a reference in estimating main burner length.

As an example of estimating main burner length, consider a design similar to the JT9D but with $P_{t3} = 350$ psia at sea level and $T_{t4} = 2900$°R. Use of Eq. (10.34) with $n = 1$ ($r = 0.714$) gives a length that is 92.4% of the JT9D, or 16.0 in.

10.6.5 Combustion System Total Pressure Ratio

An estimate of the total pressure loss resulting from increasing the gas total temperature and frictional loss of a combustion system can be obtained by modeling the combustion system as a constant-area duct (Fig. 10.71) with simple heating (increase in total temperature) and internal drag proportional to

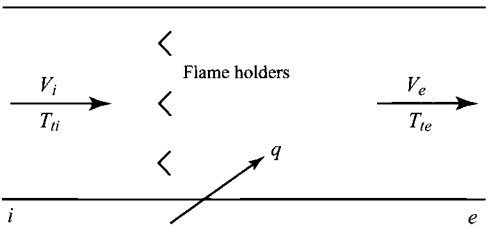

Fig. 10.71 Model of combustion system.

the incoming dynamic pressure (drag $= 0.5\rho_i V_i^2 C_D A$). The gas is assumed to be calorically perfect at inlet i and exit e, and the mass addition of fuel neglected in comparison to the air mass flow.

The basic conservation equations are the following.

Mass:

$$\rho_i V_i = \rho_e V_e$$

Momentum:

$$P_i + \frac{\rho_i V_i^2}{g_c} = P_e + \frac{\rho_e V_e^2}{g_c} + C_D\left(\frac{1}{2}\rho_i V_i^2\right)$$

Energy:

$$q = c_{pe}T_{te} - c_{pi}T_{ti}$$

Solution of these equations[4] gives

$$\frac{T_{te}}{T_{ti}} = \frac{q + c_{pi}T_{ti}}{c_{pe}T_{ti}}$$

$$\Phi = \frac{\gamma_i}{\gamma_e}\frac{M_i^2\{1 + [(\gamma_i - 1)/2]M_i^2\}}{[1 + \gamma_i M_i^2(1 - C_D/2)]^2}\frac{T_{te}}{T_{ti}} \tag{10.35}$$

$$M_e^2 = \frac{2\Phi}{1 - 2\gamma_e\Phi + \sqrt{1 - 2(\gamma_e + 1)\Phi}} \tag{10.36}$$

$$\frac{P_e}{P_i} = \frac{1 + \gamma_i M_i^2(1 - C_D/2)}{1 + \gamma_e M_e^2} \tag{10.37}$$

$$\frac{P_{te}}{P_{ti}} = \frac{P_e}{P_i}\frac{\{1 + [(\gamma_e - 1)/2]M_e^2\}^{\gamma_e/(\gamma_e - 1)}}{\{1 + [(\gamma_i - 1)/2]M_i^2\}^{\gamma_i/(\gamma_i - 1)}} < 1 \tag{10.38}$$

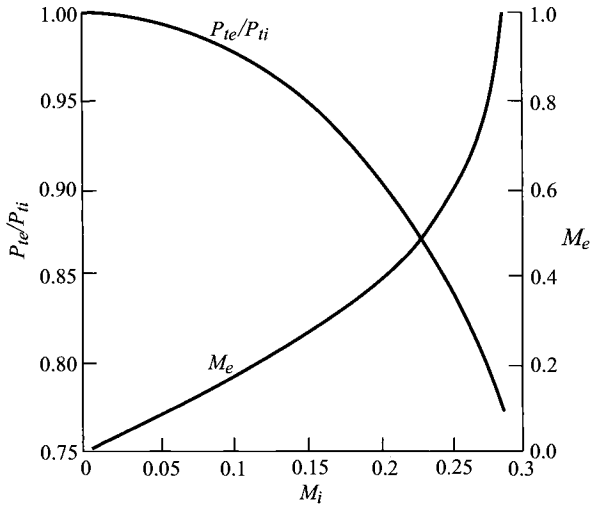

Fig. 10.72 Main burner total pressure loss.

Example 10.6

Consider the following data for a turbojet's main burner:

$$T_{t4} = 3000^\circ\text{R} \quad \gamma_t = 1.3 \quad C_D = 1.5 \quad \tau_r = 1.162\,(M_0 = 0.9)$$

$$T_0 = 540^\circ\text{R} \quad \gamma_c = 1.4 \quad \tau_c = 1.92 \quad (\pi_c = 7.55 \text{ and } \eta_c = 0.85)$$

For convenience, the equation for the total temperature ratio can be written in terms of engine temperature ratios as

$$\frac{T_{te}}{T_{ti}} = \frac{T_{t4}}{T_{t3}} = \frac{T_{t4}/T_0}{(T_{t2}/T_0)(T_{t3}/T_{t_2})} = \frac{T_{t_4}/T_0}{\tau_r \tau_c} = \frac{3000/540}{1.162 \times 1.92} = 2.49$$

Thus $T_{t4}/T_{t3} = 2.49$ and calculations using Eqs. (10.35–10.38) yield the results of Fig. 10.72. These results show that the inlet Mach number to the combustion zone of a main burner must be kept below 0.10 to achieve a reasonable total pressure ratio ($P_{te}/P_{ti} > 0.975$) resulting from increasing gas total temperature and frictional loss.

10.6.6 Diffusers

Many instances arise in the design of engine components when the flow velocity must be decreased; a diffuser is used to perform this important function. One such instance is the flow entering the main burner where the flow leaving the

compressor must be slowed from a high subsonic Mach number to a very low Mach number.[72] Another instance is the flow entering the afterburner where the flow leaving the turbine must be slowed from a high subsonic Mach number to a Mach number of about 0.2.

Because the flow is being slowed in the diffuser, an adverse pressure exists and flow separation from the walls is possible. Figure 10.12 presents the standard diffuser flow regimes. Main burner and afterburner diffusers are designed to fall below the flow separation boundary line.

The pressure recovery coefficient C_P and the pressure recovery effectiveness η are two performance parameters used to describe diffuser performance. The *pressure recovery coefficient* C_P is a measure of the diffuser's ability to recover dynamic pressure and is defined by

$$C_P \equiv \frac{P_e - P_i}{\rho V_i^2/2} \tag{10.39}$$

where P_i and P_e are the static pressure at the inlet and exit, respectively, and $\rho V_i^2/2$ is the inlet dynamic pressure. For the ideal diffuser (incompressible flow with constant total pressure), C_P can be expressed in terms of the area ratio

$$C_{P\,\text{ideal}} \equiv 1 - \left(\frac{A_i}{A_e}\right)^2 \tag{10.40}$$

where A_i and A_e are the inlet and exit areas, respectively. The *pressure recovery effectiveness* η of the diffuser is the ratio of the actual pressure recovery coefficient to the ideal pressure recovery coefficient:

$$\eta \equiv \frac{C_P}{C_{P\,\text{ideal}}} \equiv \frac{P_e - P_i}{(\rho V_i^2/2)[1 - (A_i/A_e)^2]} \tag{10.41}$$

The total pressure ratio of the diffuser can, therefore, be expressed in terms of the pressure recovery effectiveness η and other convenient flow properties as

$$\frac{P_{te}}{P_{ti}} = 1 - \frac{\rho V_i^2}{2P_{ti}}(1 - \eta)\left[1 - \left(\frac{A_i}{A_e}\right)^2\right] \tag{10.42a}$$

or

$$\frac{P_{te}}{P_{ti}} = 1 - \frac{(\gamma/2)M_i^2(1 - \eta)[1 - (A_i/A_e)^2]}{\{1 + [(\gamma - 1)/2]M_i^2\}^{\gamma/(\gamma-1)}} \tag{10.42b}$$

The diffuser performance characteristics for preliminary design are presented in Fig. 10.73. This figure relates diffuser area ratio A_e/A_i and length/height ratio L/H to the pressure recovery effectiveness η. Maintaining high pressure recovery effectiveness often leads to long diffusers that are undesirable.

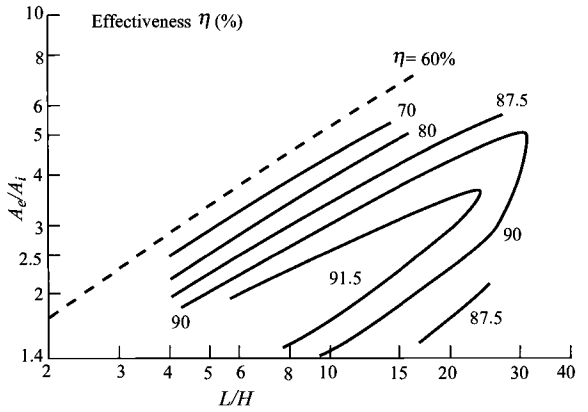

Fig. 10.73 Straight-wall diffuser performance (Ref. 67).

Dump diffusers are often used in conjunction with straight-walled diffusers to meet design goals. The pressure loss for a dump diffuser, as depicted in Fig. 10.74, was investigated by Barclay[74] and can be estimated in the range $0.2 < A_i/A_e < 1$ by

$$\frac{P_{te}}{P_{ti}} = \exp\left\{-\frac{\gamma}{2}M_i^2\left[\left(1-\frac{A_i}{A_e}\right)^2+\left(1-\frac{A_i}{A_e}\right)^6\right]\right\} \tag{10.43}$$

Example 10.7

Find the total pressure ratio of a straight wall diffuser with the following data: $A_e/A_i = 4.0$, $M_i = 0.5$, $\gamma = 1.4$, and $L/H = 15$. Using Fig. 10.73 and Eq. (10.42b) gives $\eta = 0.9$ and $P_{te}/P_{ti} = 0.9858$.

Example 10.8

Find the total pressure ratio for a dump diffuser with the following data: $A_e/A_i = 5.0$, $M_i = 0.5$, and $\gamma = 1.4$. Using Eq. (10.43) gives $P_{te}/P_{ti} = 0.8540$.

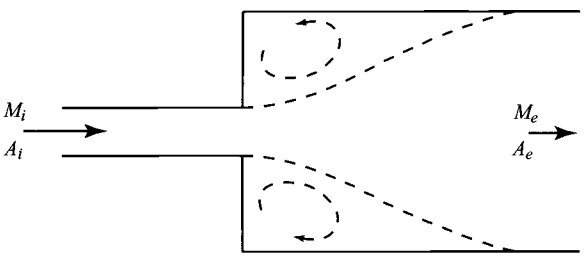

Fig. 10.74 Model dump diffuser.

10.6.7 Fuels

In the early development of the gas turbine engine, it was common belief that this engine could use any fuel that would burn. This is true in theory, but not in practice. The modern turbojet engine is quite particular about the fuel used due to the high rate of fuel flow and wide temperature and pressure variations.

Jet fuel is refined from crude oil petroleum. A typical pound of jet fuel might be composed of 16% hydrogen atoms, 84% carbon atoms, and a small amount of impurities, such as sulfur, nitrogen, water, and sediment. Various grades of jet fuel have evolved during the development of jet engines in an effort to ensure both satisfactory performance and adequate supply. JP-8 is the most commonly used fuel for U.S. Air Force jet engines. The U.S. Navy uses JP-5, a denser, less volatile fuel than JP-8, which allows it to be safely stored in the skin tanks of ships. The most common commercial aircraft fuels are Jet A and Jet A-1. They are alike except Jet A has a freezing point below $-40°$F and Jet A-1 has a freezing point below $-58°$F. Table 10.6 gives specifications for some of the most commonly used jet fuels. The heating value h_{PR} used for most jet fuels is 18,400 Btu/lbm or 42,800 kJ/kg (=10,222 cal/g).

Many aircraft engines are built to operate on any of these fuels. To do so, they must have a special switch on the fuel control to allow it to compensate for differences in specific gravity that is used in fuel metering calculations.

There are many other fuels of interest for use in aircraft gas turbine engines. High-Mach-number aircraft like the SR-71 uses JP-7, a fuel with a very high boiling point. Hydrogen is often considered a fuel because of its very high heating value (h_{PR} of approximately 49,900 Btu/lb or 116,000 kJ/kg) and its capacity to absorb the thermal loads of high-Mach-number flight.

10.7 Main Burners

10.7.1 Types

Turbine engine burners have undergone continuing development over the past 50 years, resulting in the evolution of a variety of basic combustor configurations. Contemporary main burner systems may be broadly classified into one of the three types schematically illustrated in Fig. 10.75: can, cannular, or annular.

A can system consists of one or more cylindrical burners, each contained in a burner case. Because of its modular design, the can system was used during the early development of the turbojet engine. The cannular system consists of a series of cylindrical burners arranged within a common annulus—hence, the name *cannular*. This burner type was the most common in the aircraft turbine engine population, but has been replaced with the annular type in most modern engines. Most modern main burner systems employ the annular design wherein a single burner having an annular cross section supplies gas to the turbine. The improved combustion zone uniformity, design simplicity, reduced linear surface area, and shorter system length provided by the common combustion annulus have made the annular burner the leading contender for all future propulsion systems.

Table 10.6 Jet engine fuels[a]

Property	JP-4		JP-5		JP-8 (Jet A-1)	
	Specification requirement	Typical value	Specification requirement	Typical value	Specification requirement	Typical value
Vapor pressure, atm @ 38°C (100°F)	0.13–0.2	0.18	—	0.003	—	0.007
Initial boiling point, °C	—	60	—	182	—	169
Endpoint, °C	—	246	288	260	288	265
Flash point, °C	—	−25	>63	65	>49	52
Aromatic content, % vol.	<25	12	<25	16	<20	16
Olefinic content, % vol.	<5	1	—	1	—	1
Saturates content, % vol.	—	87	—	83	—	83
Net heat of combustion, cal/g	>10,222	10,388	>10,166	10,277	>10,222	10,333
Specific gravity	0.751	0.758	0.788	0.818	0.755	0.810
U.S. yearly consumption, 10^9 gal		5		1		12

[a]Source: Refs. 12, 15.

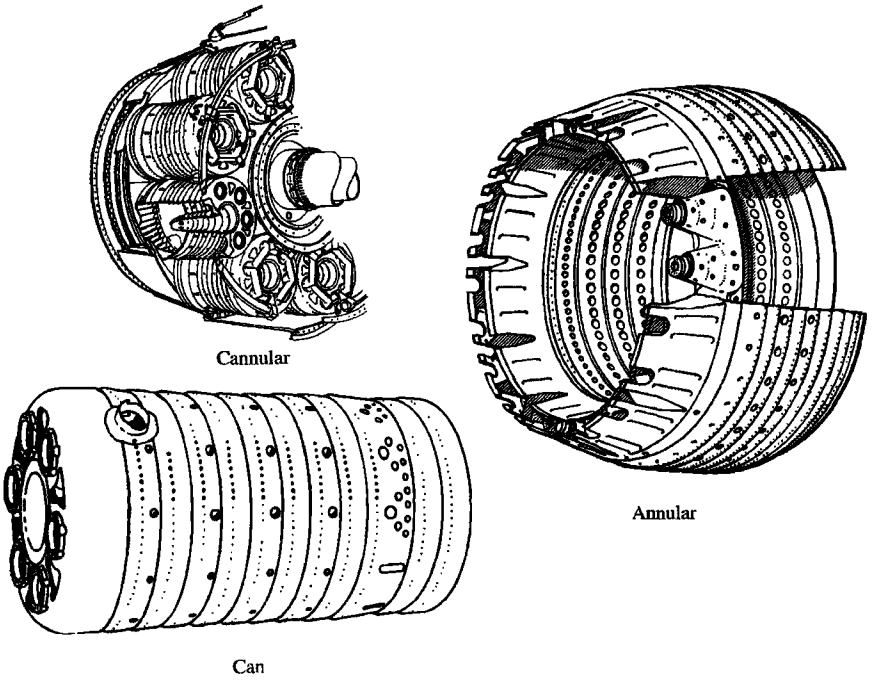

Fig. 10.75 Main burner type. (Courtesy of Pratt & Whitney.)

10.7.2 Main Burner Components

The turbine engine main burner system consists of three principal elements: the inlet diffuser, the dome and snout or cowl, and the liner. In addition, important subcomponents are necessary: the fuel injector, igniter, burner case, and primary swirler, if used. The term *combustion zone* is used to designate that portion of the main burner within the dome and liner. These elements are illustrated in Fig. 10.76.

The purpose of the inlet diffuser is to reduce the velocity of the air exiting the compressor and deliver the air to the combustion zone as a stable, uniform flowfield while recovering as much of the dynamic pressure as possible. The inlet diffuser represents a design and performance compromise relative to required compactness, low-pressure loss, and good flow uniformity. Early inlet diffuser designs were of the smooth curved wall or contoured wall type. Because of the wide variations in the characteristics of the flowfield exiting the compressor, however, the curved wall diffuser cannot always provide uniform, nonseparated flow at all operating conditions. This can become a critical problem in the short-length diffusers required of many current systems. Consequently, a trend toward dump, or combination curved wall and dump, diffuser designs is occurring. Although this design results in somewhat higher total pressure losses, it provides a known and constant point of flow separation at the dump plane, which prevents stalled operation at all diffuser entrance conditions.

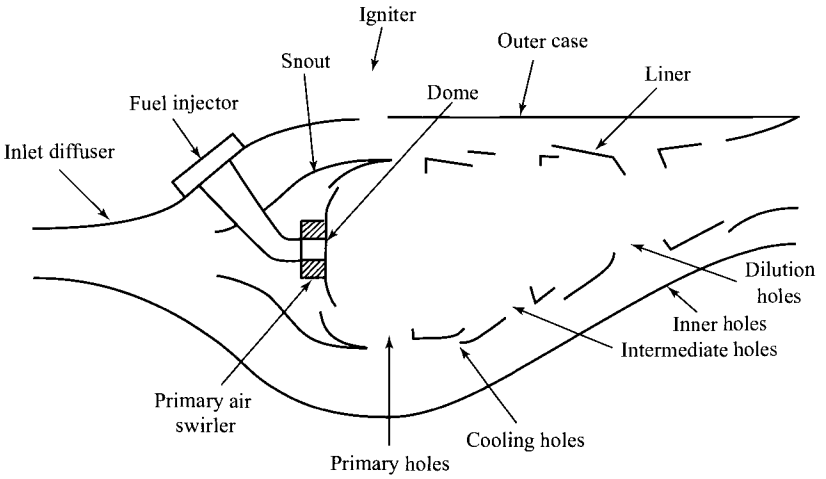

Fig. 10.76 Main burner components (Ref. 67).

The snout divides the incoming air into two streams: primary air and the other airflows (intermediate, dilution, and cooling air). The snout streamlines the combustor dome and permits a larger diffuser divergence angle and reduced overall diffuser length.

The combustor dome is designed to produce an area of high turbulence and flow shear in the vicinity of the fuel nozzle to finely atomize the fuel spray and promote rapid fuel/air mixing. There are two basic types of combustor domes: bluff body and swirl-stabilized. The bluff-body domes were used in early main burners, but swirl-stabilized domes are used in most modern main burners.

The combustion process is contained by the liner. The liner also allows introduction of intermediate and dilution airflow and the liner's cooling airflow. The liner must be designed to support forces resulting from pressure drop and must have high thermal resistance capable of continuous and cyclic high-temperature operation. This requires use of high-strength, high-temperature, oxidation-resistant materials (e.g., Hastalloy X) and cooling air.

Fuel injectors can be classified into four basic types according to the injection method utilized: pressure-atomizing, air blast, vaporizing, and premix/prevaporizing. The first two methods are the most common and are described next, but the reader is directed to other references (e.g., Ref. 38) for a description of the other two methods. In past main burner designs, the most common method of fuel injection was pressure atomizing, which can provide a large flow range with excellent fuel atomization when fuel system pressures are high (500 psi above main burner pressure). The pressure-atomized system is susceptible to fuel leaks (due to high fuel pressures) and plugging of orifices from fuel contaminants. Most modern main burner designs incorporate the air-blast atomizing fuel injector, which achieves fuel atomization and mixing through the use of primary air momentum with strong swirling motion. The air-blast atomizing fuel injector requires lower fuel pressures (50–200 psi above main burner pressure) than the pressure-atomizing type.

Spark igniters, similar to automotive spark plugs, are used to ignite the cold, flowing fuel/air mixture in main burners. These spark igniters produce 4–12 J of ignition energy and require several thousand volts at the plug tip. Main burner starting redundancy is typically provided by use of at least two spark lighters.

10.7.3 Airflow Distribution and Cooling Air

This section identifies and briefly describes the airflow distribution terminology in, around, and through the main burner, resulting in the four basic airflow regions illustrated in Fig. 10.77. Effective control of this air distribution is vital to the attainment of complete combustion, stable operation, correct burner exit temperature profile, and acceptable liner temperatures for long life.

Primary air is the combustion air introduced through the dome or head plate of the burner and through the first row of liner airholes. This air mixes with the incoming fuel, producing the locally near-stoichiometric mixture necessary for optimum stabilization and operation. To complete the reaction process and consume the high levels of primary zone CO, H^-, and unburned fuel, intermediate air is introduced through a second row of liner holes. The reduced temperature and excess oxygen cause CO and H^- concentrations to decrease. In contemporary systems, the dilution air is introduced at the rear of the burner to reduce the high temperature of the combustion gases. The dilution air is used to carefully tailor exit temperature radial and circumferential profiles to ensure acceptable turbine durability and performance. This requires minimum temperatures at the turbine root (where stresses are highest) and at the turbine tip (to protect seal materials). However, modern and future main burner exit temperature requirements are necessitating increased combustion air in the primary and intermediate zones; thus, dilution zone airflow is necessarily reduced or eliminated to permit these increases.

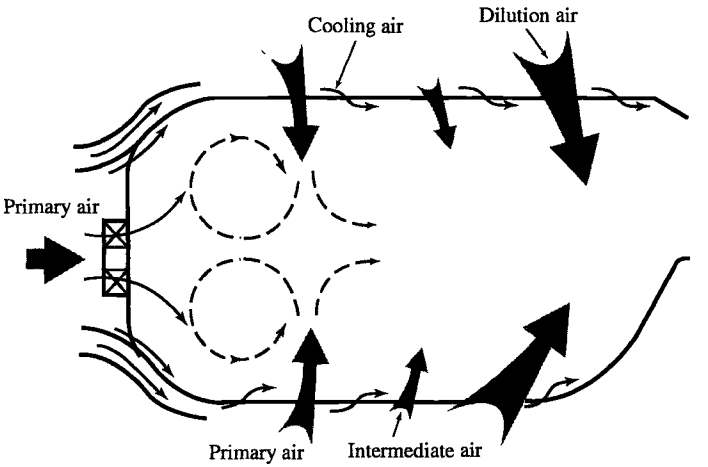

Fig. 10.77 Main burner airflow distribution (Ref. 67).

Cooling air must be used to protect the burner liner and dome from the high radiative and convective heat loads produced within the burner. This air is normally introduced through the liner such that a protective blanket or film of air is formed between the combustion gases and the liner hardware (see Fig. 10.78).

The effectiveness of the cooling technique is quantified by the *cooling effectiveness* Φ, defined by

$$\Phi \equiv \frac{T_g - T_m}{T_g - T_c} \tag{10.44}$$

where T_g, T_m, and T_c, are the mainstream gas, average metal, and cooling air temperatures, respectively.

Figure 10.79 provides design data for the amount of coolant flow required to achieve the desired cooling effectiveness and, thus, desired metal temperature of a combustor liner. Hastalloy X[12,22,38,47] and similar materials are generally used for the main burner liner with a useful upper-limit metal temperature of 1800°F. If film cooling is considered with $T_g = 2400$°F, $T_c = 1200$°F, and $T_m = 1800$°F, then Φ must be at least 0.5, which requires a coolant flow of at least 17% of the combustor flow. Transpiration cooling, using advanced liner construction (e.g., Lamilloy, Ref. 75), can obtain a cooling effectiveness of about 0.8 with 17% cooling air, which can be used to obtain lower average metal temperatures (longer life) or higher gas temperatures (improved performance). As future combustor exit temperature requirements increase, the percentage of combustor air available for cooling decreases and increased cooling effectiveness will be required.

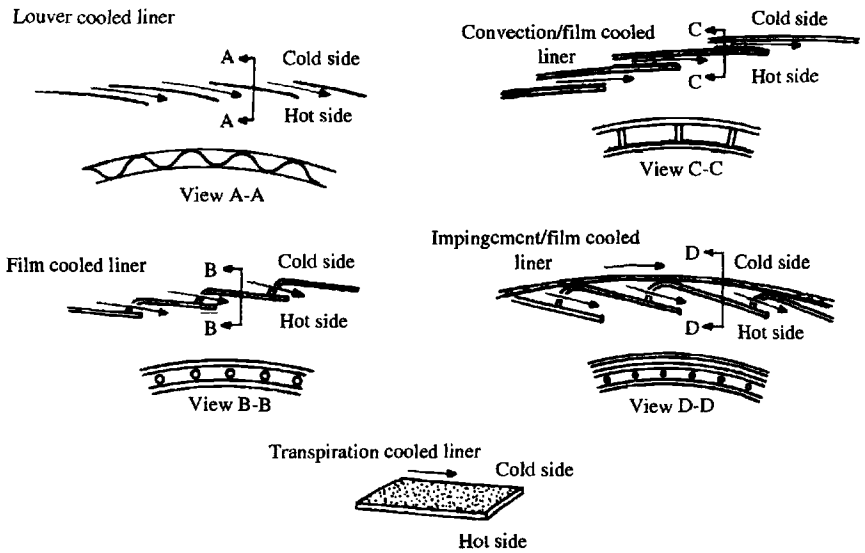

Fig. 10.78 Liner cooling techniques (Ref. 67).

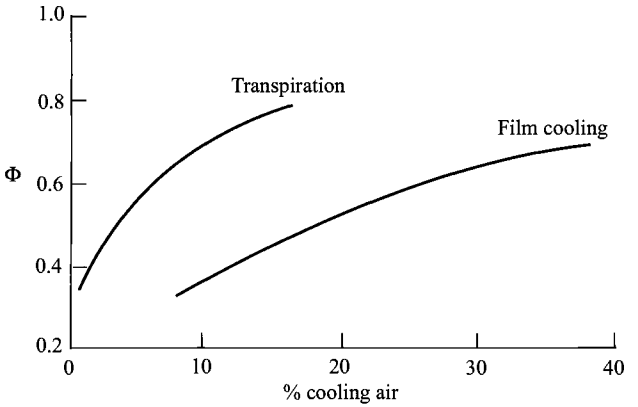

Fig. 10.79 Linear cooling effectiveness (Refs. 75–77).

10.7.4 Performance Parameters

10.7.4.1 Combustion efficiency. Because propulsion system fuel consumption has a direct effect on aircraft system range, payload, and operating cost, it is imperative that design-point combustion efficiency be as close to 100% as possible. By design, combustion efficiency at the high power/fuel consumption conditions of takeoff and cruise is near 100% (usually greater than 99.5%). However, off-design efficiency, particularly at idle, can be in the low 90s. With the advent of chemical emission controls and limitations, this parameter has particular significance during low-power operation because inefficiency and pollution are inextricably linked. For example, combustion efficiency at off-design conditions, such as idle, must now exceed 98.5% to satisfy regulations on exhaust carbon monoxide and unburned hydrocarbons.

One empirical model of combustion efficiency η_b is based on the reaction rate parameter θ and is plotted in Fig. 10.80. The *reaction rate parameter* θ is defined[38,67] as

$$\theta = \frac{P_{t3}^{1.75} A_{\text{ref}} H \exp(T_{t3}/b)}{\dot{m}_3} \times 10^{-5} \tag{10.45}$$

where

P_{t3} = main burner inlet pressure, psi
A_{ref} = main burner, reference area, in.^{2}
H = height of main burner, in.
T_{t3} = main burner inlet temperature, °R
$\dot{m}_3$ = main burner inlet airflow, lbm/s
b = function of local equivalence ratio ϕ and b, given by Herbert[70] as

$$b = 382\left(\sqrt{2} \pm \ell n \frac{\phi}{1.03}\right) \tag{10.46}$$

where plus is used when $\phi < 1.03$ and minus when $\phi > 1.03$.

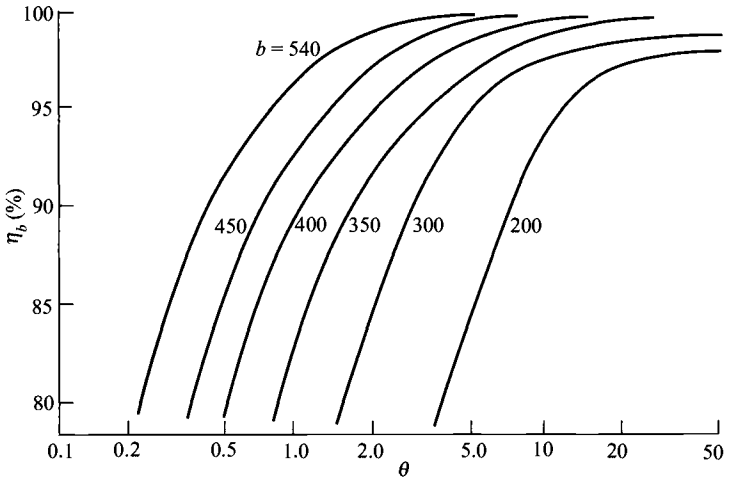

Fig. 10.80 Combustion efficiency vs reaction rate parameter (Ref. 67).

Example 10.9

Determine the combustion efficiency of a main burner with the following data:

$$P_{t3} = 300\,\text{psia}, \quad T_{t3} = 1500^\circ\text{R}, \quad \dot{m}_3 = 60\,\text{lbm/s}, \quad \phi = 0.8$$
$$A_{\text{ref}} = 1.0\,\text{ft}^2, \quad H = 2\,\text{in.}$$

Equation (10.46) gives $b = 444$, Eq. (10.45) gives $\theta = 30$, and Fig. 10.80 gives $\eta_b > 0.995$. For another example, consider the following main burner data:

$$P_{t3} = 2.4\,\text{MPa}, \quad T_{t3} = 800\,\text{K}, \quad \dot{m}_3 = 200\,\text{kg/s}, \quad \phi = 0.9$$
$$A_{\text{ref}} = 0.2\,\text{m}^2, \quad H = 6\,\text{cm}$$

Equation (10.46) gives $b = 488$, Eq. (10.45) gives $\theta = 43.2$, and Fig. 10.80 gives $\eta_b > 0.995$.

10.7.4.2 Overall total pressure loss. The overall total pressure loss of the main burner is the sum of inlet diffuser loss, burner dome and liner loss, and momentum loss resulting from main burner flow acceleration attendant with increased gas total temperature. It is normally expressed as a percentage of the compressor discharge pressure. Total pressure losses of 4–5% are typically encountered in current systems. Main burner system pressure loss is recognized as necessary to achieve certain design objectives (pattern factor, effective turbine cooling, etc.), and it can also provide a stabilizing effect of main burner aerodynamics. However, total pressure loss also impacts engine thrust and thrust

specific fuel consumption. Consequently, design goals for main burner total pressure loss represent a compromise among the preceding factors.

Equation (10.38) may be used to obtain a preliminary estimate of the main burner total pressure losses excluding the inlet diffuser and liner. Equation (10.42b), in combination with Fig. 10.73 and/or Eq. (10.43), may be used to obtain a preliminary estimate of the inlet diffuser total pressure ratio. Liner total pressure loss can be approximated as the dynamic pressure of the passage air.

10.7.4.3 Exit temperature profile. Two performance parameters are related to the temperature uniformity of the combustion gases as they enter the turbine. To ensure that the proper temperature profile has been established at the main burner exit, combustion gas temperatures are often measured by means of high-temperature thermocouples or via gas-sampling techniques employed at the main burner exit plane. A detailed description of the thermal field entering the turbine both radially and circumferentially can be determined from these data. A simplified expression called the *pattern factor* or *peak temperature factor* may be calculated from these exit temperature data. The *pattern factor* PF is defined as

$$\text{PF} \equiv \frac{T_{t\,\max\,\text{av}} - T_{t\,\text{av}}}{T_{t\,\text{av}} - T_{t\,\text{in}}} \tag{10.47}$$

where

$T_{t\,\max}$ = maximum measured exit temperature (local)
$T_{t\,\text{av}}$ = average of all temperatures at exit plane
$T_{t\,\text{in}}$ = average of all temperatures at inlet plane

Contemporary main burners exhibit pattern factors ranging from 0.25 to 0.45. Pattern factor goals are based primarily on the design requirements of the turbine first-stage stationary airfoils. Thus a pattern factor of 0.0 is not required. Durability considerations require the new high-temperature-rise main burners to have exit temperature profiles corresponding to pattern factors in the range of 0.15 to 0.25.

The *profile factor* P_f characterizes the main burner average exit temperature profile and is defined by

$$P_f \equiv \frac{T_{t\,\max\,\text{av}} - T_{t\,\text{in}}}{T_{t\,\text{av}} - T_{t\,\text{in}}} \tag{10.48}$$

where $T_{t\,\max\,\text{av}}$ is the maximum circumferential average temperature. Main burners exhibit profile factors ranging from 1.04 to 1.08, with 1.06 being the common design goal. Profile factor goals are based primarily on the design requirements of the turbine first-stage rotating airfoils, which are exposed to average gas temperature leaving the first-stage stationary airfoils.

Pattern factor and profile factor are important main burner design parameters. They describe the possible thermal impact on the turbine and are critical factors

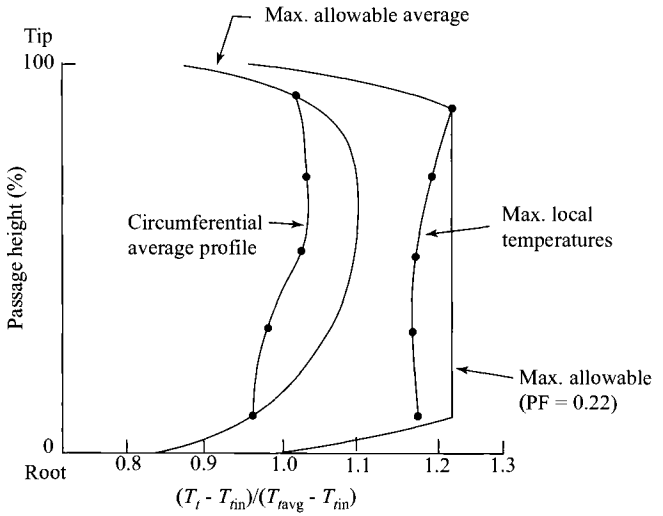

Fig. 10.81 Radial temperature profile at main burner exit (Ref. 67).

in matching the main burner and turbine components. Failure to achieve the required pattern factor and/or profile factor will normally result in shorter turbine life and may require redesign of the main burner and/or turbine.

Although the pattern factor and profile factor define the peak and average turbine airfoil gas temperatures, the shape of the burner exit temperature radial profile is the critical factor controlling turbine airfoil life. Figure 10.81 illustrates typical radial profile characteristics and their attendant relationship with the pattern factor. By proper control of dilution air, the burner exit temperature field is tailored to give the design pattern factor and radial profile consistent with turbine requirements.

10.7.4.4 Ignition. Reliable ignition in the main burner system is required during ground-level startup and for relighting during altitude windmilling. The broad range of main burner inlet temperature and pressure conditions encompassed by a typical ignition/relight envelope is illustrated in Fig. 10.82. It is well known that ignition performance is improved by increases in main burner pressure, temperature, fuel/air ratio, and ignition source energy. In general, ignition is impaired by increases in reference velocity, poor fuel atomization, and low fuel volatility.

Development work[78] in the application of the double-annular combustor design (Fig. 10.83) to main burners having a high temperature rise ($T_{t4} - T_{t3} =$ 1000–1400°C or 1800–2500°F) has shown very good low-throttle operation when the outer annulus is designed to operate as the pilot stage with lower airflows than the inner annulus. Only the pilot stage of this double-annular combustor is fueled at starting, altitude relight, and idle conditions. This pilot-stage design attains the desired low air velocities and rich fuel/air ratios at low-temperature-rise conditions of starting, altitude relight, and idle.

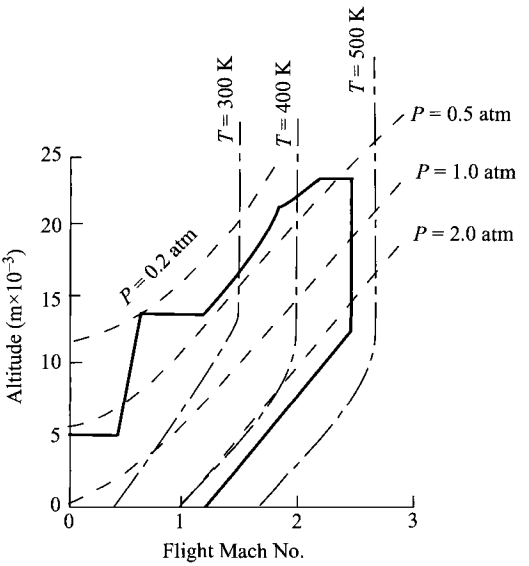

Fig. 10.82 Ignition/relight envelope (Ref. 67).

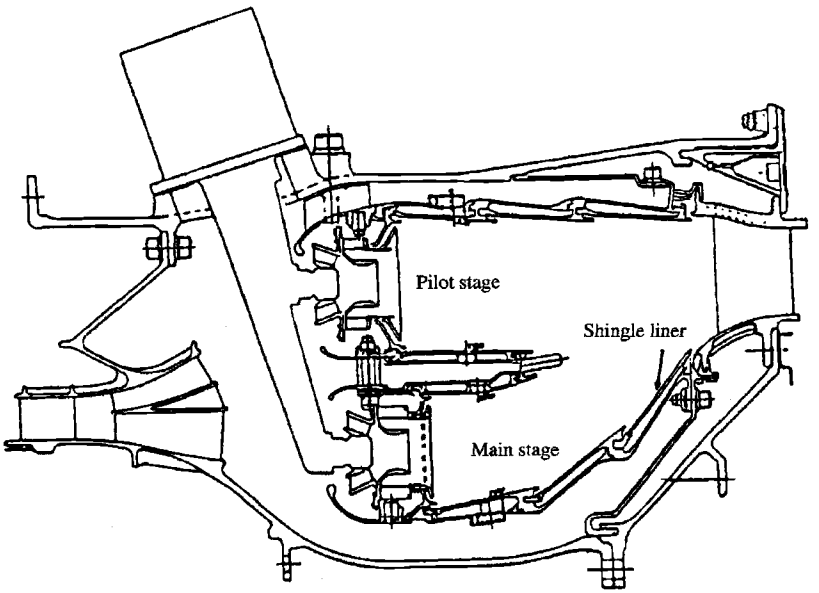

Fig. 10.83 Double-annular main burner (Ref. 78).

10.7.5 Main Burner Design Parameters

The design of main burner systems for aircraft gas turbine engines is a complex and difficult problem that is usually solved by reaching a reasonable compromise between the conflicting requirements. Design involves a broad range of technical disciplines including combustion chemistry, fluid dynamics, heat transfer, stress analysis, and metallurgy. Although there are many design parameters for a main burner, most experts would include the following in their list of most critical design parameters:

1) Equivalence ratio ϕ
2) Combustor loading parameter (CLP)
3) Space heat release rate (SR)
4) Reference velocity V_{ref}
5) Main burner dome height H_d
6) Main burner length/dome height ratio L_{mb}/H_d
7) Main burner dome velocity
8) Passage velocity V_{pass}
9) Number and spacing of fuel injectors
10) Pattern factor correlation parameters (PF)
11) Profile factor correlation parameters P_f

The *space heat release rate or space rate* (SR) is

$$\text{SR} \equiv \frac{f\dot{m}_3 h_{PR}(3600)}{P_{t3}(\text{volume})} \tag{10.49}$$

and generally is between 5×10^6 and 10×10^6 Btu/(h · ft^3 · atm) [0.5 and 1.0 W/(m^3 · Pa)]. The reference velocity is defined as

$$V_{\text{ref}} \equiv \frac{\dot{m}_3}{\rho_{t3} A_{\text{ref}}} \tag{10.50}$$

where A_{ref} is the cross-sectional area across the whole main burner at the primary combustion zone.

Taylor[79] gives the following typical values of design parameters: The reference velocity is typically from 60 to 100 ft/s (18–30 m/s); the ratio of main burner length to dome height L_{mb}/H_d is 2.73–3.5; velocities in the main burner dome are generally around 30 ft/s (9 m/s) and in the passages 120–200 ft/s (36–60 m/s); fuel injectors are typically spaced about one dome height apart in the circumferential direction; and fuel injectors require at least 25% of their design fuel rate to obtain good fuel atomization.

The use of selective fuel injection is a method of modulating primary zone equivalence ratio at very low engine throttle settings. Tests were reported in Ref. 78 on the minimum fuel/air ratio f for the CF6-50 main burner with selective fuel injection patterns, and these results are presented in Fig. 10.84. In addition to low engine throttle operation, use of a selective fuel injection pattern can improve engine starting and relight.

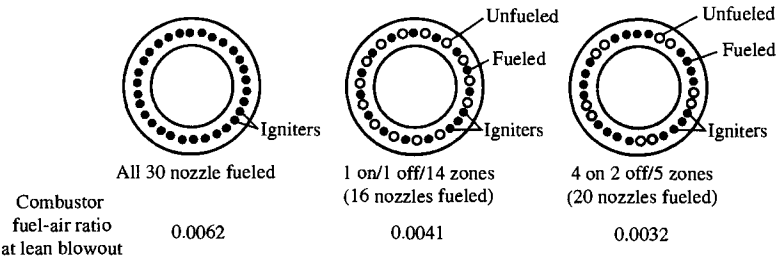

Fig. 10.84 Lean blowout characteristics of CF6-50 main burner with selective fuel injection patterns (Ref. 78).

10.8 Afterburners

Afterburning or reheating is one method of augmenting (increasing) the basic thrust of the turbojet engine or the turbofan engine, when required, without having to use a larger engine with its concurrent penalties of increased frontal area and weight. The afterburner increases thrust by adding thermal energy to the entering gas stream. For a turbojet engine, this gas stream corresponds to the exhaust gases of the turbine. However, for the augmented turbofan engine, this gas stream may be a mixture of the bypass air and the turbine exhaust gases. At the afterburner inlet, there is still much uncombined oxygen in the gas stream. The higher inlet temperatures and near-stoichiometric fuel/air ratio of the afterburners enable them to operate with a simpler configuration (see Figs. 10.85a and 10.85b) than the main burner can. The resultant increase in temperature raises the exhaust velocity of the exiting gases and, therefore, boosts engine thrust. Most afterburners will produce an approximate 50% thrust increase, but with a corresponding threefold increase in fuel flow.

Because the specific and actual fuel consumptions are considerably higher during the time the engine is in the afterburning or *hot* (also called *wet*) operation, as compared to the nonafterburning or *cold* (also called *dry*) mode of operation, afterburning is used typically for the time-limited operation of takeoff, climb, and maximum bursts of speed.

For a turbofan engine, augmentation can be used in both fan and core streams. Afterburning in a separate fan stream is normally referred to as *duct burning*, and this alone or in combination with afterburning in the core stream may be advantageous for certain flight conditions.

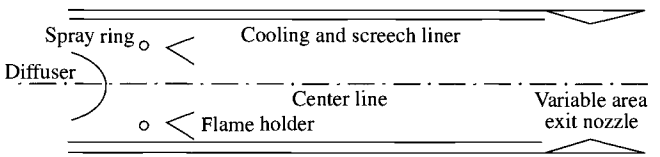

Fig. 10.85a Typical afterburner components.

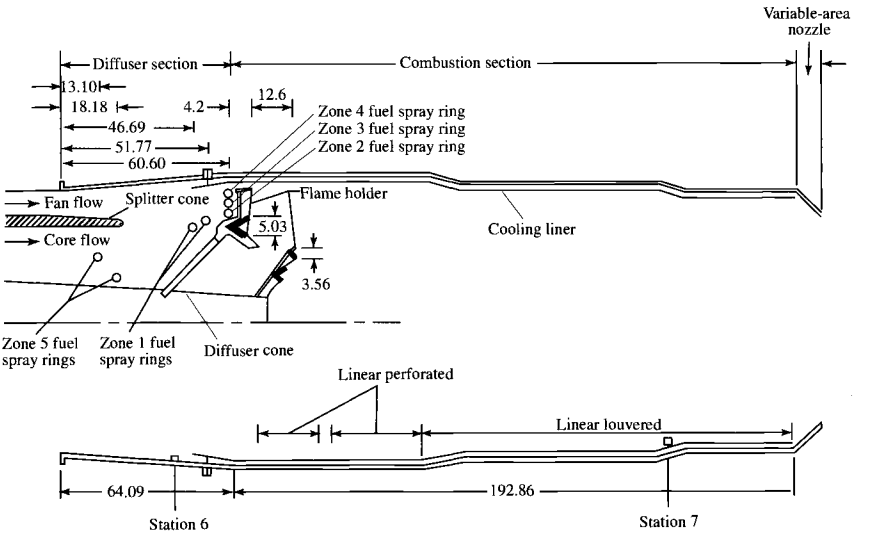

Fig. 10.85b Afterburner for TF30-P-3 augmented turbofan engine (all dimensions are in centimeters) (from Ref. 80).

The major components of an afterburner are shown in Figs. 10.85a and 10.85b. Gas leaving the turbine is deswirled and diffused, fuel is added by fuel spray bars (tubes) or rings, the combustion process is initiated by igniter or pilot burner in the wake of a number of flame-stabilizing devices (flame holders), and the thermal energy of combustion is mixed along flame surfaces spreading downstream from the stabilizing devices. Also, a liner is used in afterburners as both a cooling liner and a screech or antihowl liner (*screech* and *howl* are acoustic combustion instabilities). This liner can also serve as a passage for the cooling air required by the exhaust nozzle. All engines incorporating an afterburner must also be equipped with a variable-area throat exhaust nozzle to provide for proper operation under afterburning and nonafterburning conditions. In addition to these components, an afterburner will require the following components:

1) Afterburner fuel pump
2) Afterburner fuel control
3) Pressurizing valve, if multistage operation is required
4) Connections (mechanical and pressure) from the main fuel control, throttle, and engine

Specific design requirements for an afterburner are as follows:

1) Large temperature rise. The afterburner does not have to provide for the physical and temperature limits of the turbine. The temperature rise is limited mainly by the amount of oxygen that is available for combustion and the liner and nozzle cooling air requirements.

2) Low dry loss. The engine suffers a very slight penalty in thrust during cold operation due principally to the drag caused by the flame holders, fuel spray bars, and walls of the afterburner.

3) Wide temperature modulation. This is necessary to obtain *degrees* (also called *zones* or *stages*) of afterburning for better control of thrust.
4) High combustion efficiency.
5) Short length; light weight.
6) Altitude light-off capability.
7) No acoustic combustion instabilities.
8) Long life, low cost, easy repair.

10.8.1 Afterburner Components

This section covers the major afterburner components associated with the flow passage and combustion process. Although it is brief, the major features affecting preliminary engine design are addressed. The open literature contains a wealth of information on each individual component, and the interested reader may want to research a particular component further.

10.8.2 Diffuser

The flow entering the afterburner is first slowed to a Mach number that provides a balance between the total pressure loss and the afterburner cross-sectional area. The minimum Mach number entering the combustion zone of the afterburner is usually fixed by a requirement that the diameter of the afterburner section not exceed that of the engine components located upstream. A short diffuser length is desired without producing flow separation to reduce engine weight and length. In augmented turbofan engines, the diffuser may be combined with a mixer so that a mixed stream enters the combustion section.

10.8.3 Fuel Injection, Atomization, and Vaporization

This subject area is best summarized by Zukoski[67,70] and is quoted here:

> The goal of the fuel injection stream is to produce a specified distribution of fuel vapor in the gas stream entering the afterburner. In most engines, fuel is introduced in a staged manner so that heat addition rate can be increased gradually from zero to the desired value. Because ignition, flame stabilization, and flame spreading are easiest to achieve when the fuel/air ratio is close to the stoichiometric value, staging is usually produced by adding fuel to successive annular stream tubes so that the mixture ratio in each tube is nearly stoichiometric. Each stream tube has its own set of fuel injectors and control system which can be activated independently. For example, see the two sets of injectors used in the F100 engine shown as items 6 and 7 in [Fig. 10.86].
>
> The most remarkable fact concerning the fuel system for afterburners is their simplicity. In many engine systems, fuel is supplied to a circular tube which lies with its axis perpendicular to the gas stream. Fuel is injected into the gas through small diameter holes located in the sides of the tubes such that the liquid jet enters the gas stream in a direction perpendicular to the undisturbed flow direction. The liquid jet penetrates some distance into the gas stream before its momentum is dissipated. During this penetration process, the air stream tears the jet apart and produces droplets with diameters of micron size. Heat transfers from the hot gas stream then vaporizes the droplets.
>
> Given the wide range of values of mass flow of fuel required, it is remarkable that reasonably thorough mixing of the fuel with the air can be achieved with this simple

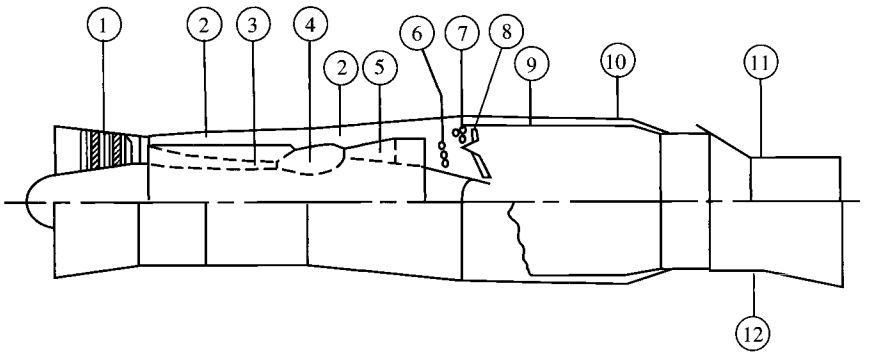

Fig. 10.86 Pratt & Whitney F100-PW-100 augmented turbofan engine (Ref. 67): 1) three-stage fan; 2) bypass duct; 3) core engine compressor; 4) main burner; 5) turbine; 6) fuel injectors for core engine gas stream; 7) fuel injections for bypass airsteam; 8) flame stabilizer for afterburner; 9) perforated afterburner linear; 10) afterburner case; 11) nozzle closed to minimum area; and 12) nozzle opened to maximum area.

injection system. In some recent engines, efforts are being made to use simple variable area injector ports which may possibly give better preparation of the fuel/air mixture.

The whole area of fuel penetration, atomization, and vaporization is not well understood from first principles and one of the time-consuming parts of an afterburner development program is to determine the optimum distribution of locations for injector tubes, injector parts, and port diameters.

10.8.4 Ignition

Ignition of the fuel/air mixture in the afterburner is usually accomplished by using a spark or arc igniter or a pilot burner. Once initiated in the primary stream tube, combustion continues in the wake of a flame stabilizer (a bluff body) and the process will spread to the rest of the flame stabilizers if the wakes of the stabilizers overlap.

The spark or arc igniter uses a high-energy electric arc to initiate combustion of the primary stream tube. The igniter is usually placed in the wake of a sheltered flame stabilizer having its own fuel supply. A stable flame results, and combustion is initiated behind other flame stabilizers by the mechanism mentioned previously.

As described earlier, ignition in an afterburner system will be easiest to achieve in gas having a local equivalence ratio near unity, in a region of the stabilization system where the residence times are longest, and where the pressures and temperatures are highest. When such a region is not available, a pilot burner can be used to locally create this region.

The pilot burner consists of a pilot zone where a small portion of the inlet air (usually 10% or less) is burned to stoichiometric temperatures in an enclosed protected region. The hot gases generated by the pilot burner are used as an ignition and stabilizing source for the main fuel injection system.

Afterburning for turbofan engines such as the Pratt & Whitney F100 is accomplished by adding fuel first to the core flow near the interface between the core and fan streams, then to the fan stream, and finally to the rest of the core flow. Afterburning in the fan stream produces the largest performance gain because of the low temperature of this stream. However, the fan stream's low temperature makes the fuel vaporization and afterburning very difficult. By adding fuel first to the core flow near its interface with the fan stream, the resulting afterburning stream can act as a pilot for the combustion process in the fan stream.

10.8.5 Flame Stabilization

Two general types of flame-stabilizing devices that have been used in afterburners are shown in Fig. 10.87: bluff-body vee-gutter flame holders and piloted burners where a small piloting heat source is used to ignite the main fuel flow. The bluff-body vee-gutter flame holders have the advantage of low flow blockage and low total pressure loss. They are simple and lightweight and have a good development history.

The wake of a flame holder, shown in Fig. 10.88, is divided into two regions: a recirculation zone and mixing zones. The recirculation zone is characterized by a strong circulating flow, very low reaction rates, and a temperature that is nearly equal to the adiabatic flame temperature corresponding to the fuel/air mixture ratio of the approaching stream. The mixing zones are characterized as turbulent regions of very strong shear, steep temperature gradients, and vigorous chemical reaction.

A stable flame is established in the mixing zones by a balance of the continuing entrainment of cool unburned gas and the heat and species transfer from the hot burned gases. The residence time of the gas in the mixing zone establishes whether a stable flame is established or the flame is blown off. Flame stabilization is characterized by the values of the velocity at the edge of the mixing zones V_2, the length of the recirculation zone L, and the characteristic ignition time t_c. This

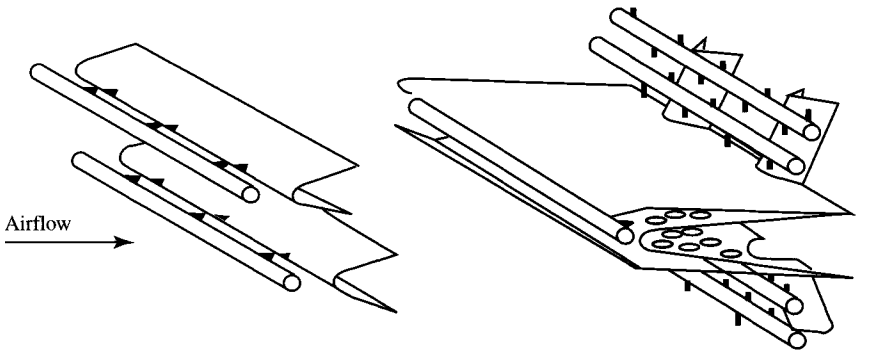

a) Vee-gutter flame holders **b) Piloted burner**

Fig. 10.87 Common afterburner flame holders (Ref. 81).

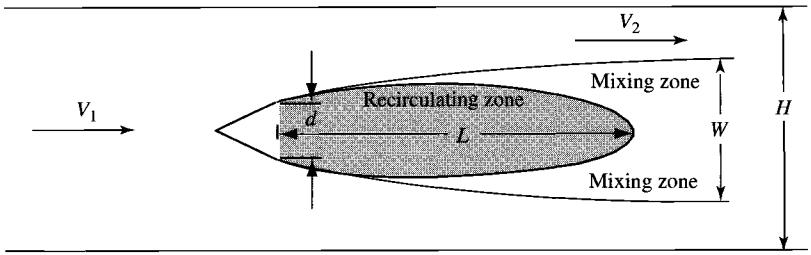

Fig. 10.88 Typical flame holder used in analysis of stabilization: V_1 = velocity of approaching steam, V_2 = velocity of flow at edge of mixing zone, d = width of flame holder, L = length of recirculation zone, W = width of wake, and H = height of the duct.

ignition time is determined experimentally at conditions that result in flame extinction or blowoff and the definition

$$t_c \equiv \frac{L}{V_{2c}} \tag{10.51}$$

where the subscript c denotes values corresponding to flame extinction or blowoff. Thus the flame extinction or blowoff criteria can be expressed as

$$\left(\frac{V_{2c}t_c}{L}\right)_{\text{blowoff}} = 1 \tag{10.52}$$

Numerous experiments with a wide range of flame holder and duct configurations have shown that the ignition time is essentially independent of the geometry and velocity as long as the flow is turbulent. The ignition time depends on a number of chemical parameters such as fuel type, fuel/air ratio, gas temperatures and pressures, and degree of vitiation.

The variation of the characteristic ignition time t_c with equivalence ratio ϕ is shown in Fig. 10.89 for a hydrocarbon fuel with a molecular weight of about 100. Note that t_c increases very rapidly for both high and low values of ϕ. In general, t_c decreases rapidly as the static temperature of the approach stream increases and varies inversely with static pressure for hydrocarbon fuels like JP-8. This variation with temperature and pressure can be approximated by

$$t_c \propto \frac{1}{PT^{2.5}} \tag{10.53}$$

Flame holder stability calculations using Eq. (10.52) required values of t_c,, V_2, and L. The characteristic ignition time can be obtained from Fig. 10.89. However, V_2 and L are not simply related to the size of the flame holder d and the velocity of the approach stream V_1. Rewriting Eq. (10.52) in a more

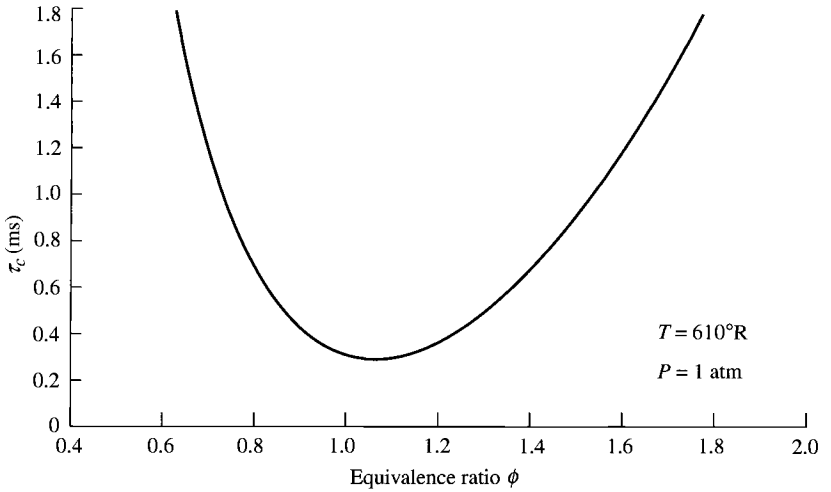

Fig. 10.89 Variation of characteristic ignition time with equivalence ratio (Ref. 67).

convenient form gives

$$\left(\frac{V_{1c}t_c}{H}\right)_{\text{blowoff}} = \frac{V_1}{V_2}\frac{L}{W}\frac{W}{H} \tag{10.54}$$

To apply this criterion, values of V_1/V_2, L/W, and W/H are needed as functions of flame holder geometry, fluid dynamic parameters, and the blockage ratio B, where

$$B \equiv \frac{d}{H} \tag{10.55}$$

Calculations by Cornell[82] yielded relationships between the blockage ratio B and values of V_2/V_1 and W/d for wedge half-angles of 15–90 deg (a flat plate) and are presented in Table 10.7. Tests of a variety of bluff-bodies show that the length/width ratio of the recirculation zone L/W depends only on the geometry of the bluff-body, and the majority of the data lie in the range of 3.6 to 4.0. For the preliminary design, this ratio can be approximated[67] by

$$\frac{L}{W} \approx 4 \tag{10.56}$$

Now, all of the parameters of Eq. (10.54) can be determined for a given flame holder shape and blockage ratio.

Example 10.10

Consider a flame holder stability calculation.

Given:

$$T = 1000°\text{R}, P = 0.2 \text{ atm}, M_1 = 0.25, \gamma = 1.3$$

$$\phi = 0.8, H = 1 \text{ ft}, B = 0.2$$

and a 15-deg half-angle flame holder. Table 10.7 gives $W/d = 1.5$ and $V_2/V_1 = 1.42$. Then $W/H = (W/d)(d/H) = (1.5)(0.2) = 0.3$. Thus, with $L/W = 4$, Eq. (10.54) gives

$$\left(\frac{V_{1c}t_c}{H}\right)_{\text{blowoff}} = \left(\frac{1}{1.42}\right)(4)(0.3) = 0.845$$

Figure 10.89 gives $t_c = 0.7$ ms at 610°R, $\phi = 0.8$, and 1 atm. Thus, at 1000°R, $\phi = 0.8$, and 0.2 atm, Eq. (10.53) gives $t_c = 1.017$ ms. Using this value of t_c and $H = 1$ ft, we get $V_{1c} = H/t_c = 983.3$ ft/s. For $T = 1000°\text{R}$, $M_1 = 0.25$, and $\gamma = 1.3$, then $V_1 = 373$ ft/s and $V_2 = 530$ ft/s. Since $V_1 < V_{1c}$, flame stabilization will occur at the given conditions.

10.8.6 Multiple-Flame-Holder Arrays

The material just presented on flame holder stabilization was restricted to a single flame holder located on the centerline of a constant-area duct. When multiple flame holders are positioned in a single plane perpendicular to the approaching flow and spaced so that each lies on the centerline of equivalent ducts of equal height, then the preceding analysis can be used directly to estimate the stability characteristics. When flame holders are spaced irregularly, the analysis just presented does not directly apply. However, this analysis is useful in a qualitative manner.

10.8.7 Flame Spread

To achieve maximum combustion efficiency, the afterburner length needs to be longer than the burning length. The complex flame holder shape and

Table 10.7 Dependence of wake width W and edge velocity V_2 on blockage ratio B and wedge half-angle α[a]

	$\alpha = 15$ deg		$\alpha = 90$ deg	
$B = d/H$	W/d	V_2/V_1	W/d	V_2/V_1
0.05	2.6	1.15	4.0	1.25
0.10	1.9	1.23	3.0	1.43
0.20	1.5	1.42	2.2	1.75
0.30	1.3	1.62	1.7	2.09
0.40	1.2	1.90	1.6	2.50
0.50	1.2	2.30	1.4	3.16

[a]Source: Ref. 12.

interactions do not permit determination of afterburner length from the burning length measurements of basic flame holder experiments. However, most modern afterburners use 17 deg total angle for estimating spread.

10.8.8 Afterburner Liner

The afterburner liner is used as a cooling liner and to improve combustion stability. As a cooling liner, it isolates the very high temperatures from the outer casing (similar to the liner of the main burner). A film of cooler air is distributed along the length of the cooling liner, which reduces the metal temperature of this liner and subjects the outer casing of the afterburner to the afterburner pressure and temperature of the cooling flow.

The liner is also used as a screech or antihowl liner to prevent extreme high frequency and amplitude pressure fluctuations resulting from combustion instability or the unsteady state of thermal energy. This function is accomplished by use of multiple holes along the initial length of the liner. Selective frequencies can be dampened by the selection of the proper size hole.

10.8.9 Total Pressure Loss

The total pressure loss of the afterburner is mainly composed of that due to the diffuser, to the drag of the flame holders, and to the combustion process. The total pressure ratio of the diffuser can be estimated by the methods presented earlier. The total pressure ratio due to the friction of the flame holders and combustion process can be estimated, by using Eqs. (10.35–10.38), provided that C_D of the flame holders, based on the duct area and upstream velocity V_1, is known. The drag coefficient of a bluff-body is about 1.0 (Ref. 83) based on the frontal area and the edge velocity (V_2 of Fig. 10.88). This drag coefficient can be expressed in terms of a C_D based on the duct area and upstream velocity V_1 by

$$C_D \approx B\left(\frac{V_2}{V_1}\right)^2 \tag{10.57}$$

where B is the blockage ratio [see Eq. (10.55)].

10.8.10 Afterburner Design Parameters

The design of the afterburner system for aircraft gas turbine engines is a difficult problem and involves compromise similar to the complexity of the main burner system. The major design parameters for the afterburner include: 1) equivalence ratio ϕ, 2) reference Mach number M_{ref}, 3) flame holder blockage B, 4) flame holder width d, 5) flame holder edge Mach number, 6) afterburner burning length, 7) spray bar spacing, and 8) space heat release rate (SR).

The reference Mach number is at the entrance to the afterburner and ranges from 0.20 to 0.25. Flame holder blockage is normally 30–40% with an edge Mach number of about 0.30. The burning length is 35–50 in. (0.9–1.3 m), and the spray bar spacing is about 3 in. (8 cm) at the outer flame holder position.[79]

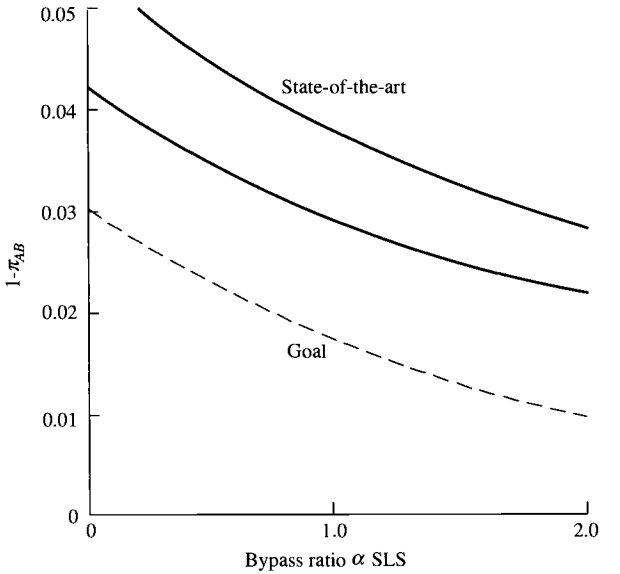

Fig. 10.90 Afterburner total pressure loss (Ref. 84).

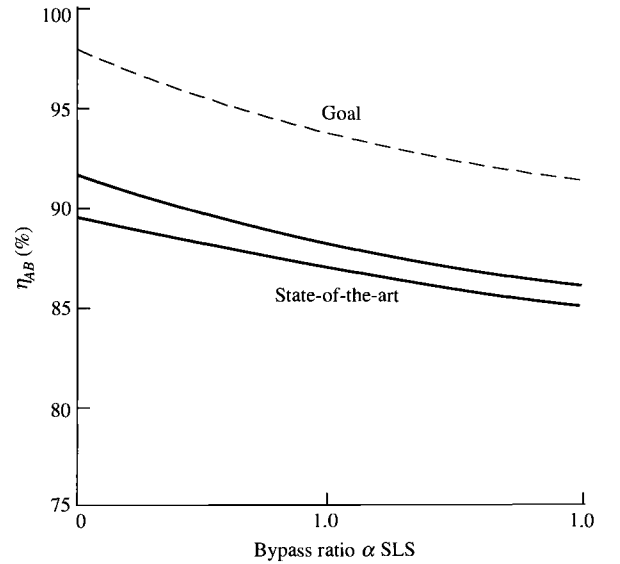

Fig. 10.91 Afterburner combustion efficiency (Ref. 84).

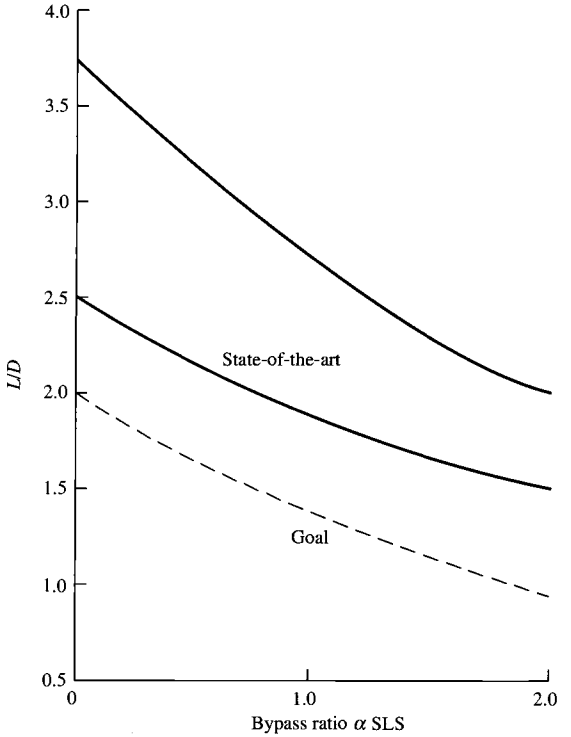

Fig. 10.92 Afterburner size (Ref. 84).

A space heat release rate [Eq. (10.49)] near 8×10^6 Btu/(h · ft^3 · atm) [0.8 W/(m^3 · Pa)] is desired.[81]

The performance and size of the afterburner of an augmented turbofan engine depend on the bypass ratio,[84] as shown in Figs. 10.90, 10.91, and 10.92. Both the current state-of-the-art and the goal of future afterburner development are shown.

Problems

10.1 Develop Eq. (10.1) in SI units.

10.2 Determine the throat diameter of an inlet for the turbojet engine of Example 8.4 for subsonic operation ($M_0 < 0.8$).

10.3 Determine the throat diameter of an inlet for the turbofan engine of Example 8.9 for subsonic operation ($M_0 < 0.8$).

10.4 Determine the throat diameter of an inlet for the turboprop engine of Example 8.11 for subsonic operation ($M_0 < 0.8$).

10.5 A fixed-area internal compression inlet has a capture/throat area ratio A_c/A_t of 1.2. Determine the following:
(a) The Mach number at which the inlet will start.
(b) The Mach number at the throat after starting.
(c) The π_d of the inlet after starting with the shock at the throat.
(d) The Mach number at which the inlet will unstart.

10.6 A ramjet is to fly at 9-km altitude and Mach 2.3. Determine the following:
(a) The inlet contraction ratio A_c/A_t of a fixed-area internal compression inlet for this ramjet and its maximum pressure recovery when operated at the preceding conditions.
(b) Maximum pressure recovery of the inlet of part a when operated at Mach 2.7.

10.7 A ramjet is to fly at 30-kft altitude and a speed of 2388 ft/s. Determine the following:
(a) The inlet contraction ratio A_c/A_t of a fixed-area internal compression inlet for this ramjet and its maximum pressure recovery when operated at the preceding conditions.
(b) Maximum pressure recovery of the inlet of part a when operated at a flight velocity of 2786 ft/s.

10.8 A ramjet that is to cruise at 20-km altitude and 767.2 m/s has the ability to overspeed to 914.7 m/s prior to attaining its final cruise condition. Determine the best inlet contraction ratio A_c/A_t of a fixed-area internal compression inlet for this ramjet and its maximum pressure recovery when operated at cruise conditions.

10.9 A ramjet that is to cruise at 60-kft altitude and Mach 2.5 has the ability to overspeed to Mach 3.0 prior to attaining its final cruise condition. Determine the best inlet contraction ratio A_c/A_t of a fixed-area internal compression inlet for this ramjet and its maximum pressure recovery when operated at cruise conditions.

10.10 You are required to design an internal compression inlet with a fixed capture area A_c of 14 ft^2 (1.3 m^2) that will operate for a cruise Mach number M_0 of 2.5 with an inlet throat Mach number M_t of 1.2.
(a) Determine A_t and A_c/A_t for cruise.
(b) If the throat area is held constant, can this inlet be started for M_0 of 4.0 or less?
(c) If it is desired to start the inlet at $M_0 = 2.0$, find the required values of A_c/A_t and A_t.

10.11 An aircraft with a turbojet engine uses a fixed contraction ratio, internal compression inlet designed for $M_0 = 3.0$. The aircraft is flying at $M_0 = 2.0$ with the inlet started, and the shock is optimally positioned when the inlet suddenly unstarts, popping the shock.
(a) Find the maximum pressure recovery for the started and unstarted conditions.

(b) Find the ratio of the unstarted inlet mass flow rate to the started inlet mass flow rate.

10.12 For supersonic flight conditions, a conservative estimate of the inlet drag is the momentum loss of the bleed and bypass air. Variable A_1 is the capture area of an inlet, and A_0 is the freestream area for the engine mass flow rate (see Fig. 10.36).

(a) Show that the inlet drag coefficient can be written as

$$\phi_{\text{inlet}} = \frac{\rho_0 V_0 (A_1 - A_0)(V_0 - V_e)}{F g_c}$$

where V_e is the axial velocity with which the bypass and bleed flows leave the inlet.

(b) For adiabatic flow with $M_e = 1$, show that the preceding equation becomes

$$\phi_{\text{inlet}} = \frac{(A_1/A_0 - 1)\{M_0 - \sqrt{2/(\gamma+1) + [(\gamma-1)/(\gamma+1)]M_0^2}\}}{F g_c/(\dot{m}_0 a_0)}$$

(c) Using the A_{0i}/A_1, results of Fig. 10.46, calculate and plot ϕ_{inlet} for $F g_c/(\dot{m}_0 a_0) = 3.0$.

10.13 Determine the total pressure recovery η_r and area ratio A_{0i}/A_s of a pitot inlet with a normal shock over the range of Mach numbers from 1 to 2. Compare this inlet's performance to that of Examples 10.3 and 10.4.

10.14 Determine the total pressure recovery η_r and area ratio A_{0i}/A_s of an external compression inlet with a single 10-deg ramp over the range of Mach numbers from 1 to 2. Compare this inlet's performance to that of Examples 10.3 and 10.4.

10.15 Determine the total pressure recovery η_r and area ratio A_{0i}/A_s of an external compression inlet with a single 8-deg ramp over the range of Mach numbers from 1 to 2. Compare this inlet's performance to that of Examples 10.3 and 10.4.

10.16 Calculate the dimensions and values of C_{fg}, F_g, and C_V, for an axisymmetric exhaust nozzle with a mass flow rate of 150 lbm/s and the following data:

$$P_{t8} = 25\,\text{psia}, \quad T_{t8} = 3600°\text{R}, \quad A_9/A_8 = 1.8, \quad \gamma = 1.3$$

$$R = 53.4\,\text{ft}\cdot\text{lbf}/(\text{lbm}\cdot°\text{R}), \quad P_{t9}/P_{t8} = 0.98, \quad C_D = 0.98, \quad P_0 = 3\,\text{psia}$$

10.17 Calculate the dimensions and values of C_{fg}, F_g, and C_V for an axisymmetric exhaust nozzle with a mass flow rate of 75 kg/s and the

following data:

$$P_{t8} = 350\,\text{kPa}, \quad T_{t8} = 1600\ \text{K}, \quad A_9/A_8 = 1.8, \quad \gamma = 1.33$$
$$R = 0.287\,\text{kJ(kg}\cdot\text{K)}, \quad P_{t9}/P_{t8} = 0.98, \quad C_D = 0.98, \quad P_0 = 40\,\text{kPa}$$

10.18 Determine the fuel/air ratios of the main burners listed in Table 10.5.

10.19 Estimate the length of a main burner similar to the JT9D but with $P_{t3} =$ 2.5 MPa at sea level and $T_{t4} = 1500$ K.

10.20 Estimate the length of a main burner similar to the F100 but with $P_{t3} = 300$ psia at sea level and $T_{t4} = 3200°$R.

10.21 Estimate the total pressure ratio P_{te}/P_{ti} and exit Mach number M_e of a main burner with $T_{te}/T_{ti} = 3$, $M_i = 0.05$, $C_D = 2$, $\gamma_i = 1.38$, and $\gamma_e = 1.3$.

10.22 Estimate the total pressure ratio P_{te}/P_{ti} and exit Mach number M_e of an afterburner with $T_{te}/T_{ti} = 2$, $M_i = 0.3$, $C_D = 1.5$, $\gamma_i = 1.33$, and $\gamma_e = 1.3$.

10.23 Estimate the total pressure ratio P_{te}/P_{ti} and exit Mach number M_e of a straight wall diffuser with an area ratio $A_e/A_i = 4$ and $L/H = 10$ for a gas with $\gamma = 1.38$ at $M_i = 0.1$.

10.24 Estimate the total pressure ratio P_{te}/P_{ti} and exit Mach number M_e of a dump diffuser with an area ratio $A_e/A_i = 4$ for a gas with $\gamma = 1.38$ at $M_i = 0.1$, 0.2, and 0.3.

10.25 Find the shortest L/H of a straight wall diffuser that gives a total pressure ratio P_{te}/P_{ti} of 0.999 with an area ratio $A_e/A_i = 4$ for a gas with $\gamma = 1.38$ at $M_i = 0.1$.

10.26 Determine the combustion efficiency of a main burner with the following data:

$$P_{t3} = 200\ \text{psia}, \quad T_{t3} = 1000°\text{R}, \quad \dot{m}_3 = 100\ \text{lbm/s}$$
$$\phi = 0.6, \quad A_{\text{ref}} = 1.5\,\text{ft}^2, \quad H = 2\,\text{in.}$$

10.27 Determine the combustion efficiency of a main burner with the following data:

$$P_{t3} = 1.8\,\text{MPa}, \quad T_{t3} = 600\,\text{K}, \quad \dot{m}_3 = 100\,\text{kg/s}$$
$$\phi = 1.3, \quad A_{\text{ref}} = 0.1\ \text{m}^2, \quad H = 6\,\text{cm}$$

10.28 Estimate the volume of the F100 main burner (see data in Table 10.5) if its space rate SR is in the range 5×10^6 to 10×10^6 Btu/(h · ft^3 · atm).

10.29 Determine the characteristic ignition time t_c, the blowoff velocity V_{1c}, and the flame holder stability for the following data: $T = 800°$R, $M_1 = 0.5$, $\gamma = 1.33$, $\phi = 1.4$, $H = 10$ in., $B = 0.3$, a 15-deg half-angle flame holder, and pressures P of 0.4 and 0.1 atm.